



**POLITECNICO**  
**MILANO 1863**

SCUOLA DI INGEGNERIA INDUSTRIALE  
E DELL'INFORMAZIONE

# Real-time estimation of power system inertia

TESI DI LAUREA MAGISTRALE IN  
ELECTRICAL ENGINEERING - INGEGNERIA ELETTRICA

Author: **Marco Migliaretti**

Student ID: 987279

Advisor: Prof. Alberto Berizzi

Co-advisors: Andrea Vicario, Edoardo Daccò

Academic Year: 2022-2023



# Abstract

In recent years, in order to reduce the environmental impact of fossil fuel power plants, in most electrical systems in the world, there has been a massive penetration of renewable energy. This phenomenon has allowed a reduction in the amount of  $CO_2$  released into the atmosphere, but has also highlighted a number of new issues never addressed before.

One of the most significant is certainly the increase in frequency excursions as a result of power imbalances on the network. These become more and more intense and dangerous because generators based on renewable energy sources do not contribute to the equivalent inertia of the system.

In this context a method to estimate system inertia in real time is increasingly important to ensure system security. An important help to this end has been provided by the development of Phasor Measurement Units (PMUs), which are devices able to acquire measurements from the network and provide phasors synchronized through Global Positioning System (GPS) in real time with high sampling rates, every 20-100 ms. This technology has allowed to have a large amount of measurements with a high sampling frequency, creating an environment suitable for the application of specific algorithms for data manipulation called "Data-driven algorithm".

The purpose of this thesis is to verify if there is the possibility to estimate, in real time, the equivalent inertia of a system using only the measurements of electric power and frequency. To this end, several perturbations have been simulated to verify the effectiveness of the proposed inertia estimation methods.

In addition, other comparative tests were also addressed regarding different topics such as: the choice of the most performant algorithm, the exclusive use of frequency and power variables and the sensibility of the PMUs. In particular, 7 tests were carried out, most of them consisting of two simulations each, in which the proposed methods are studied considering the same perturbation but located at different points of the system. Or in the comparative test, the same perturbation is considered, but the number of PMUs available and sample rates change.

**Keywords:** inertia estimation, data-drive algorithm, Phasor Measurement Units



## Abstract in lingua italiana

Negli ultimi anni per ridurre l'impatto ambientale delle centrali elettriche a combustibile fossile, nella maggior parte dei sistemi elettrici nel mondo, vi è stata una massiccia penetrazione delle energie rinnovabili. Questo fenomeno ha bensì permesso una riduzione della quantità di  $CO_2$  immessa nell'atmosfera, ma ha anche evidenziato una serie di nuove problematiche. Una di quelle più rilevanti è sicuramente l'incremento delle escursioni di frequenza a seguito di squilibri di potenza sulla rete. Le quali diventano sempre più pericolose poiché i generatori basati su fonti di energia rinnovabile non contribuiscono all'inerzia equivalente del sistema. In questo contesto un metodo per stimare in tempo reale l'inerzia del sistema è sempre più importante per garantire la sicurezza del sistema. Un importante aiuto a tal fine è stato fornito dallo sviluppo delle Phasor Measurement Units (PMUs), le quali sono dei dispositivi in grado di acquisire misure in tempo reale con alte frequenze di campionamento, ogni 20-100 ms. Questa tecnologia ha permesso di avere a disposizione una grande quantità di misure con un'elevata frequenza di campionamento creando un ambiente adatto all'applicazioni di specifici algoritmi chiamati "Data-driven algorithm". Lo scopo di questa tesi è verificare se vi è la possibilità di stimare, in tempo reale, l'inerzia equivalente di un sistema utilizzando solamente le misure di potenza elettrica e frequenza. A questo fine sono state simulate diverse perturbazioni per verificare l'efficacia dei metodi proposti per la stima dell'inerzia. Inoltre, sono stati affrontati anche altri test di confronto riguardo diversi temi come: la scelta dell'algoritmo più performante, l'uso esclusivo delle variabili di frequenza e potenza elettrica e la sensibilità delle PMU. In particolare, sono stati effettuati 7 test, la maggior parte composta da due simulazioni ciascuno, in cui i metodi proposti vengono studiati considerando la stessa perturbazione ma situata in punti diversi del sistema. Oppure nei test di confronto viene considerata la stessa perturbazione, ma cambiano il numero delle PMU disponibili e la frequenza di campionamento.

**Parole chiave:** stima dell'inerzia, algoritmi "data-driven", Phasor Measurement Units



# Contents

<b>Abstract</b>	<b>i</b>
<b>Abstract in lingua italiana</b>	<b>iii</b>
<b>Contents</b>	<b>v</b>
<b>Introduction</b>	<b>1</b>
<b>1 Power system stability</b>	<b>7</b>
1.1 Stability in Power Systems . . . . .	8
1.2 Swing equation . . . . .	10
1.3 Swing equation in multi-machine systems . . . . .	13
<b>2 Determination of the Power System Inertia</b>	<b>15</b>
2.1 Sparse identification of nonlinear dynamics (SINDy) . . . . .	15
2.1.1 Application of SINDy to a generic nonlinear dynamic system . . . . .	15
2.1.2 Sequentially thresholded least-squares algorithm (STLS) . . . . .	18
2.1.3 Application of SINDy for the estimation of the power system inertia	19
2.2 Division of the machine dynamics . . . . .	25
2.3 Moving window method for a real time estimation . . . . .	28
<b>3 Performed tests and Numerical results</b>	<b>31</b>
3.1 Test 1: Application of SINDy . . . . .	32
3.1.1 Simulation 1 . . . . .	32
3.1.2 Simulation 2 . . . . .	35
3.1.3 Conclusion of test 1 . . . . .	38
3.2 Test 2: Removal of mechanical power . . . . .	40
3.2.1 Simulation 1 . . . . .	40

3.2.2	Simulation 2 . . . . .	43
3.2.3	Conclusion of test 2 . . . . .	45
3.3	Test 3: MATLAB algorithms comparison . . . . .	46
3.3.1	Simulation 1 . . . . .	46
3.3.2	Simulation 2 . . . . .	48
3.3.3	Conclusion of test 3 . . . . .	51
3.4	Test 4: Opening of a line . . . . .	52
3.4.1	Simulation 1 . . . . .	52
3.4.2	Simulation 2 . . . . .	57
3.4.3	Conclusion of test 4 . . . . .	59
3.5	Test 5: Trig of a load . . . . .	60
3.5.1	Simulation 1 . . . . .	60
3.5.2	Simulation 2 . . . . .	63
3.5.3	Conclusion of test 5 . . . . .	65
3.6	Test 6: Short-circuit at a bus . . . . .	66
3.6.1	Simulation 1 . . . . .	66
3.6.2	Simulation 2 . . . . .	69
3.6.3	Conclusion of test 6 . . . . .	71
3.7	Test 7: Increased sensitivity of the PMUs . . . . .	72
3.7.1	Conclusion of test 7 . . . . .	75
<b>4</b>	<b>Conclusions and future developments</b>	<b>77</b>
4.1	Conclusion . . . . .	77
4.2	Future development . . . . .	78
	<b>Bibliography</b>	<b>81</b>
<b>A</b>	<b>Appendix A</b>	<b>85</b>
A.1	Numerical differentiation: finite differences . . . . .	85
<b>B</b>	<b>Appendix B</b>	<b>87</b>
B.1	STLS code . . . . .	87
B.2	Parsimonious modelling . . . . .	87
<b>C</b>	<b>Appendix C</b>	<b>91</b>
C.1	Test-system . . . . .	91



<b>List of Figures</b>	<b>93</b>
<b>List of Tables</b>	<b>97</b>
<b>List of Symbols</b>	<b>100</b>
<b>Acknowledgements</b>	<b>103</b>



# Introduction

In the last years, renewable energy has spread more and more inside the grids of every country. Their huge increase is expected to mitigate many important problems of our society like climate change, energy security and environmental sustainability. For 10 years, the growth rate of renewable energy in the World was positive every year as shown in Figure 1 and Figure 2 [23].

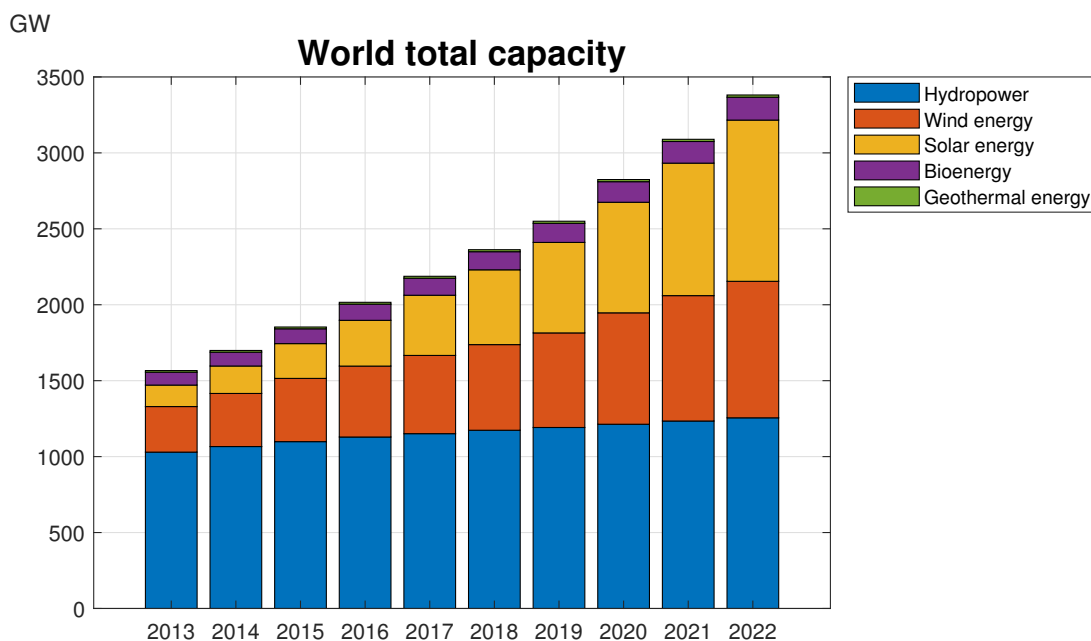


Figure 1: World total capacity.

The World total capacity is almost composed of hydropower, solar energy and wind energy which are the most spread renewable technologies. Hydropower is a well-established renewable power technology, in which the main developments in this field are focused on increasing the flexibility of plants. Flexibility is one of the most important features of modern power plants due to the increasing penetration of intermittent renewables [16].

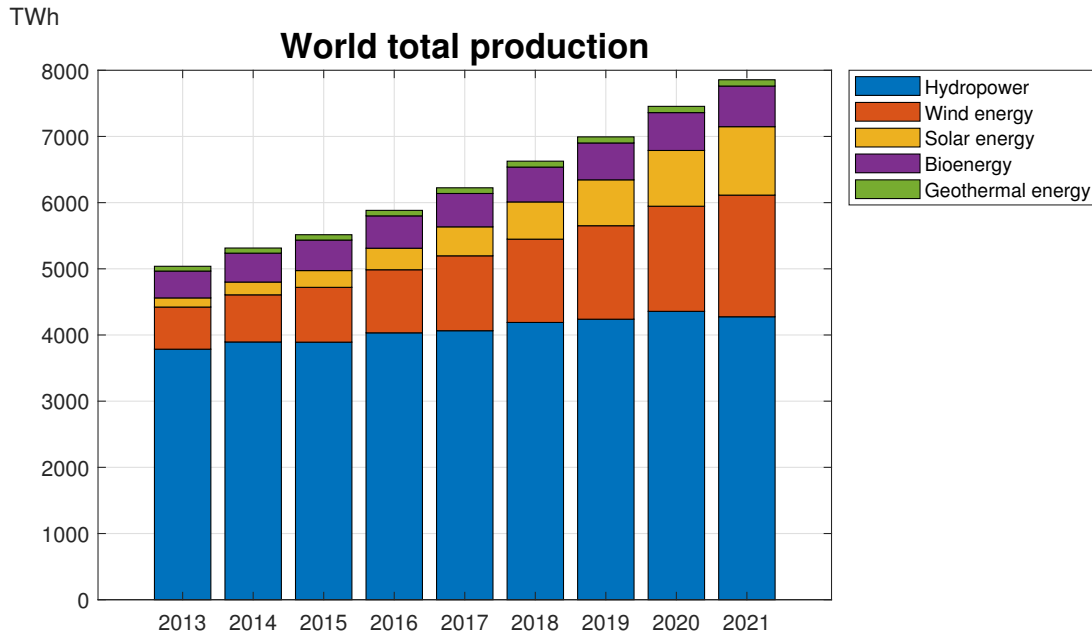


Figure 2: World total production.

In the past two decades, the policy attention was focused on the spread of the wind and solar PV technology (and lowering their cost). Short- and long-term targets and financial incentives have been introduced by more than 100 countries for wind and solar PV. Indeed, in Figure 1 and Figure 2 we can see that the capacity of the solar and wind energy increase much more than hydropower. This phenomenon is largely justified by the absence of large spaces suitable for the construction of these type of plants, high-risk investments, specific policy instruments and incentives a longer-term policy in relation to other installations. Moreover, the slowdown in hydropower growth is due to the delays in development of the new projects in China, Latin America and Europe and due to the increasingly erratic rainfall due to climate change that disrupting hydro production in many parts of the world.

Instead, solar energy experienced a record increase of 270 TWh (up 26%) in 2022, surpassing wind for the first time in history. The capacity of solar PV is set to increase by almost 1500 GW between 2023 and 2027 exceeding the installed capacity of natural gas and coal.

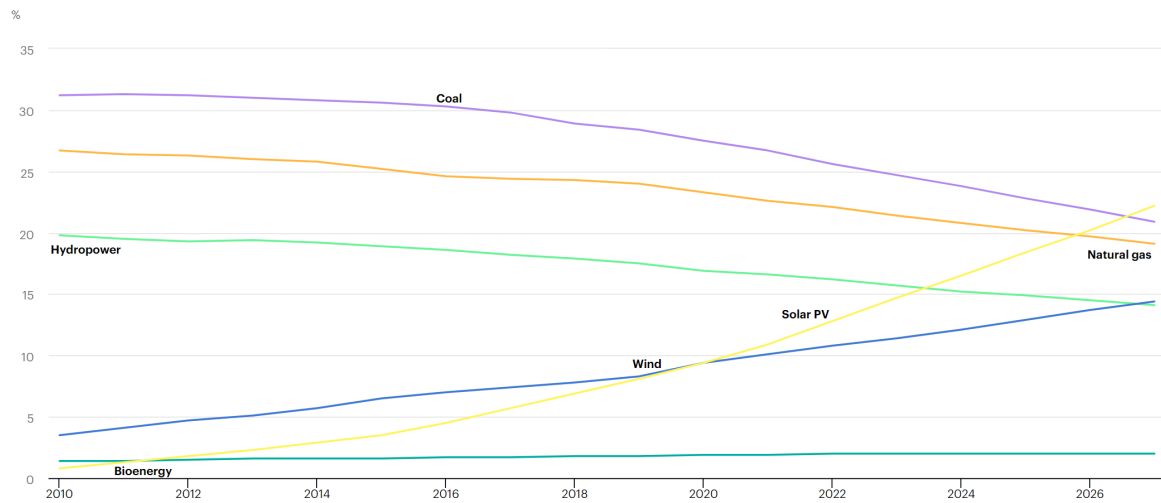


Figure 3: Share of cumulative power capacity by technology, 2010-2027 [17].

The record increase of solar energy is due to the spread of distributed solar PV which result a good choice for consumers thanks to the policy support and high retail electricity prices. The last of the three most popular renewable energy is wind energy which is the second highest growth among all renewable power technologies, behind solar PV. The expected increase of this technology is not as high as the record increase of 2021 due to the low volume of projects under construction outside China [16].

While the increase in the use of renewable energy contributes to reducing greenhouse gas emissions and thus mitigating climate change, the increasing penetration of renewable energy in the national electric systems has brought many challenges to be addressed in the future:

- **Voltage Control**

The RES can be installed only where the natural resources, exploited for energy production, are available. In this condition, the main demanding centre could be far from the renewable generating units and this could lead to the inversion of the power flow in some lines of the distribution network causing congestion and voltage control issues.

- **Flexibility of the plants**

Most of the RES generation are characterized by uncertainty, unpredictability and variability; therefore, the flexibility of the plants becomes one of the most important features of the modern power plants. An increase in the flexibility of the plant means that they must be able to follow the network requirement and keep the frequency inside the security limit of the system, avoiding the risk of undergeneration

or overgeneration.

To increase the flexibility of the system, many solutions can be put in place. A list of technical measures to increase system flexibility is illustrated in Figure 4

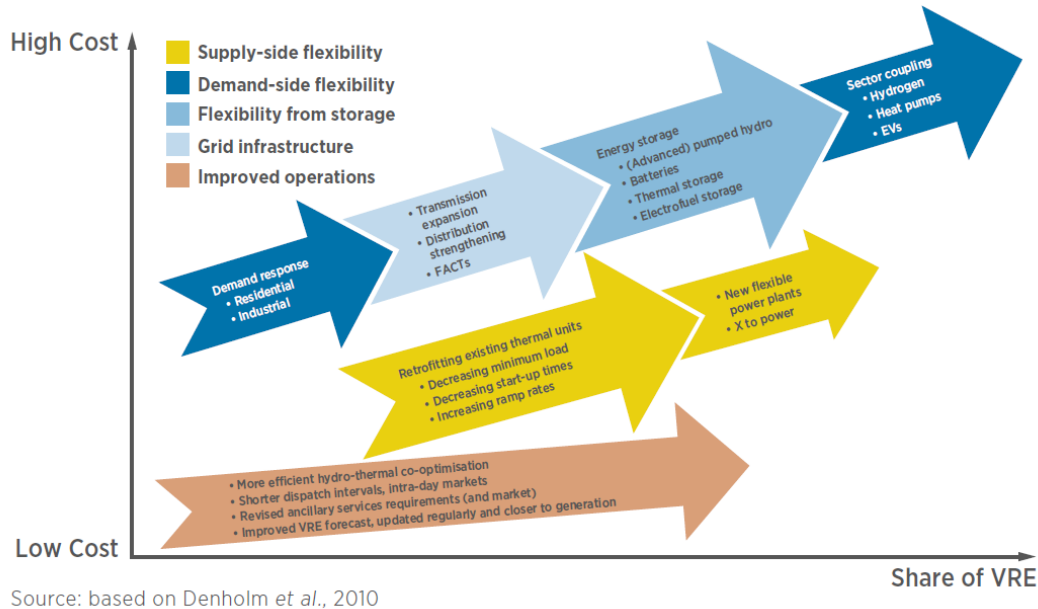


Figure 4: Technical options to increase system flexibility [15].

### • System security

Any power imbalance in the grid involves dangerous frequency excursion that, without any security systems, could be catastrophic for the entire grid. Usually, the power imbalances are damped by the inertia of the rotary machines connected to the grid, but it decreases when wind and photovoltaic generators are connected to the grid. This is because RES are decoupled from the grid by converters and do not provide directly rotational inertia.

The main aim of this work is focused on this last problem related to the diffusion of the RES generation. Different methods permit to increase the inertia level when it goes down such as the synthetic inertia and synchronous condensers, but a method able to detect when the inertia level of the system is too low is necessary.

With a continuous monitoring of the inertia level of the system, it is possible to understand when the system is in a dangerous situation and to start compensate it.

The continuous monitoring of the value of the inertia is a problem for the Transmission System Operator (TSO) or a Distribution System Operator (DSO) since there is not a precise method to define in real-time the level of the inertia. In the past, the complexity of this goal was greater, since the only instrument used to monitor the grid was the Supervi-

sory Control and Data Acquisition (SCADA) system that collected data from substations. The data available from SCADA systems are not suitable for dynamic analysis, since the resolution of the measure was limited and the phase angles were not monitored.

Nowadays, we can exploit a very competitive alternative which is the Phasor Measurement Unit (PMU). PMUs are devices able to acquire measurements voltages and current phasors of a three-phase network in a synchronized way with a reporting maximum frequency of typically 30–60 samples per seconds [22]. About 10 years ago the commercial PMUs were very expensive (reported as costing \$40000 to \$180000 in 2014, [18]) and this aspect was very limiting for a real application, but the continuous development of this technology has led to a sensible reduction of the PMUs's price. In the last years, low-cost PMU are being developed and the cost of developed prototypes is very low about 110 €[6].

The new features in real-time measurements of the PMUs merged with the huge decrease in the price of this technology open the possibility of a true application of the methods exposed in this work.

In a way proportional to the increasing spread of PMUs there is also a considerable increasing interest in the data-driven parameter estimation algorithms [12].

Data-driven algorithms that utilize PMUs measurements have recently been utilized in innovative applications like power grid parameter estimation. One of the first approach in the estimation of the power grid parameter was through the application of the Kalman filter and its variants [26]. This approach is followed by several works, such as the Unscented Kalman Filter (UKF) based approach to estimate the transient reactance and inertia of the generator.

The main drawback of the KF-based techniques is that it cannot perform well in the presence of strong nonlinearity and for low-inertia systems that exhibit very fast dynamics [9]. The disadvantages of the approaches based on the Kalman Filter are overcome by a data-driven approach for power grid parameter estimation based on the technique of Physics-Informed Neural Networks (PINNs). Although this method can handle strong non-linearity, its main drawbacks are:

- **High computational burden:** The computational complexity makes it time-consuming, especially for large power grids. Therefore, use this method for the real-time parameter estimation may not be the best fit for it.
- **Difficulties with high-inertia systems:** the PINNs method does not perform well when the system exhibit very slow dynamics.

To overcome these limitations, an algorithm for data-driven power grid parameter estimation based on the Sparse Identification of Nonlinear Dynamics (SINDy) was development

[4]. The idea of SINDy was derived from the Least Absolute Shrinkage and Selection Operator (LASSO), that is an algorithm used to promote sparsity using the L1-norm for the identification of linear systems [19]. Another techniques studied for the estimation of the power grid parameter are:

- **Koopman theory**: used to estimate generator-inertia constants, but it is restricted to transient event measurements only [14].
- **Artificial Neural-Networks (ANN)** [21].

Moreover, there are some interesting data-driven algorithms used for the discovery of governing physical laws that can be applied for the estimation of the power grid parameter such as the threshold sparse Bayesian regression algorithm [25] and the Sparse Relaxed Regularized Regression (SR3) [27].



# 1 | Power system stability

A power system is an electrical network whose main function is to supply the loads through the energy that is transmitted and distributed from the generation units. Every power system has three major components:

- **Generation:** that is the source of power, ideally with a specified voltage and frequency
- **Loads:** which consumes power; ideally with a constant resistive value or constant power.
- **Grid:** that transfer power allowing the connection between generators and loads creating a network.

The grid of a power system is more complex and divided in different voltage levels to guarantee the minimum operational cost and minimum environmental impact. Its main parts are:

- **Transmission grid 400-230 kV:** This part is a meshed grid in which the load or the generator must be rated more than 200 MW each to be connected. The reliability of this grid is very high since possible failure could interrupt the supply of a huge part of the power system.
- **Subtransmission grid 132-150 kV:** In this part of the system, partially meshed, can be connected load or generator in the range of 8-200 MW. The reliability is lower than the Transmission grid to reduce the initial costs.
- **Primary distribution grid 10-60 kV:** The usual topology of this grid is radial or ring normally open, while the installed capacity must be in the range of 4-8 MW.
- **Secondary distribution grid 400-230 V:** This part of this grid could be a radial grid or a pure radial system, in which the installed capacity must be up to some hundreds of kW.

Traditionally, the power was produced by big thermal or hydraulic generation units and then was converted and carried directly to the load sites. In this condition the power flow

was unidirectional from the generator to the load and the system was defined *centralized*. In the last 15 year, the massive increase of the installed capacity of RES has modified the operation of the transmission and distribution grid. In particular, the distribution system is designed to distribute energy from upstream to downstream. With the advent of the RES, the distribution network reaches not only loads but also generators, which means that power flows in this new scenario are bidirectional and no longer unidirectional. The bi-directionality of power flows has changed many of the logic initially used to operate the distribution networks. This change is due not only to the single big renewable generation units but also to the overall effect of all small renewable generation units of individual users. This new concept of the system is called *distributed* system and a graphical comparison with respect to the centralized system can be seen in Figure 1.1

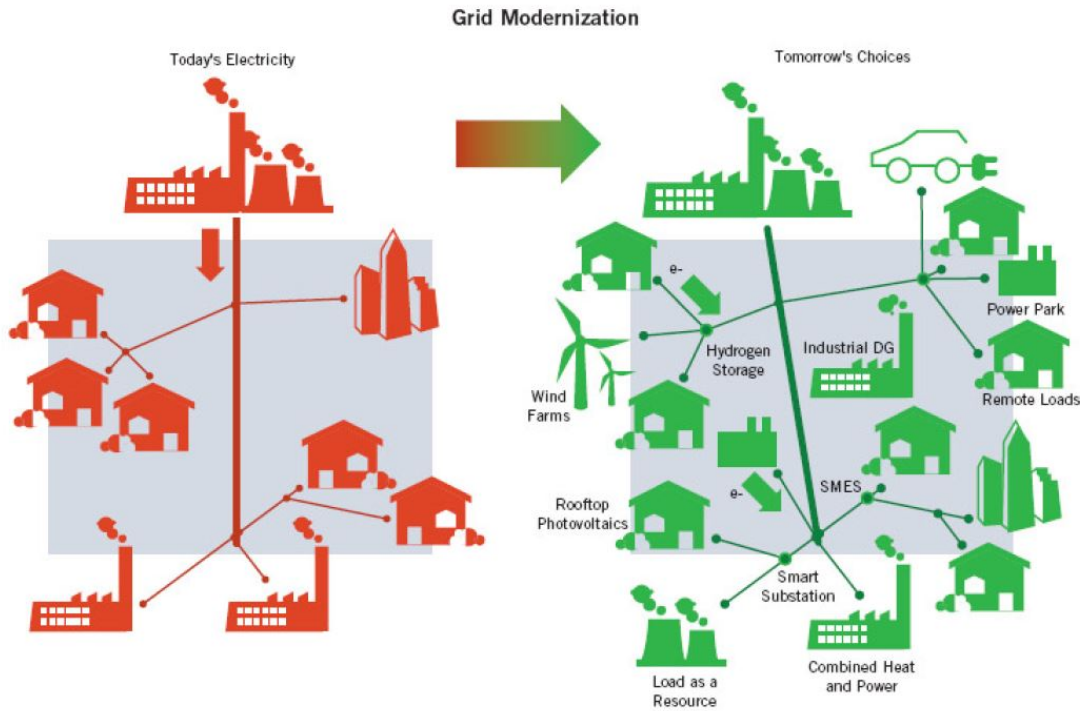


Figure 1.1: Schematic of centralized and distributed systems [2].

## 1.1. Stability in Power Systems

The traditional power systems were based on operating at synchronous speed. Any time in the system there is a power imbalance between the mechanical power of the generating unit's shaft and the electrical power absorbed by the loads the system experiences a perturbation of the synchronous speed. The relationship between the power imbalance and the changing of the synchronous speed can be described by the *equation of motion* for a

generator [11]

$$J \frac{d\omega_m}{dt} = T_a = T_m - T_e \quad (N \cdot m) \quad (1.1)$$

where

- $T_a$  = accelerating torque in  $N \cdot m$
- $T_m$  = mechanical torque in  $N \cdot m$
- $T_e$  = electromagnetic torque in  $N \cdot m$
- $J$  = combined moment of inertia of the generator and turbine in  $kg \cdot m^2$
- $\omega_m$  = angular velocity of the rotor in mech.  $rad/s$
- $t$  = time in  $s$

The power imbalance could be an undergeneration in which the electric power exceeds the mechanical power and the frequency decreases with respect to the nominal value or an overgeneration in which the system experiences the opposite phenomenon.

One of the main goals of the TSO is to keep the frequency around its nominal value and so operate the system at synchronous speed. This goal is much more challenging considering all the possible disturbances which may occur during the operation of the system. Regarding this subject, a fundamental property for the power systems is the *stability*, which can be stated as *"the ability of an electric power system, for a given initial operating condition, to regain a state of operating equilibrium after being subjected to a physical disturbance, with most system variables bounded so that practically the entire system remains intact"* [8].

The power system stability can be classified by considering [8]:

- Physical nature of the resulting mode of instability
- Size of the disturbance
- Devices, processes, and the time span considered to assess the stability

An overall description of the power system stability problem with its categories and sub-categories is given by the Figure 1.2

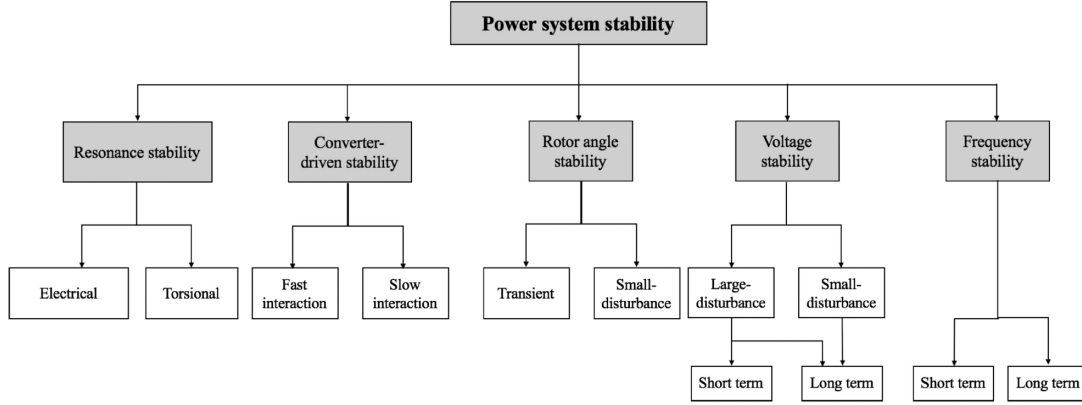


Figure 1.2: Classification of power system stability [8].

The category of the power system stability problem studied in this work is the Frequency Stability. The continuous reduction of the system inertia due to the diffusion of the RES inside the grid increases the excursions of frequency in case of perturbation. A real-time estimation of the inertia level of the system will permit us to avoid dangerous situations that could easily degenerate into large excursions of frequency.

## 1.2. Swing equation

To obtain the swing equation we have to start from the *equation of motion* for a generator [11]

$$J \frac{d\omega_m}{dt} = T_a = T_m - T_e \quad (N \cdot m) \quad (1.2)$$

In the above equation, if we suppose that the machine works as a motor we need to consider the right side of the equation with opposite sign as  $T_e - T_m$

If we consider a fixed reference that rotates at the synchronous speed  $\omega_{sm}$  it is possible define an angle  $\theta_m$  that is at the angular position  $\delta_m$  with respect to the reference, such that

$$\theta_m = \omega_{sm} t + \delta_m \quad (mech. \text{ rad}) \quad (1.3)$$

$$\frac{d\theta_m}{dt} = \omega_m = \omega_{sm} + \frac{d\delta_m}{dt} \quad (rad/s) \quad (1.4)$$

By computing the second derivative with respect to the time of this expression, it results

in

$$\frac{d^2\theta_m}{dt^2} = \frac{d\omega_m}{dt} = \frac{d^2\delta_m}{dt^2} \quad (\text{rad/s}^2) \quad (1.5)$$

The time derivative of the term  $\omega_{sm}$  is equal to zero since the speed of the reference axis is constant.

Substitute this result in Equation 1.2

$$J \frac{d^2\delta_m}{dt^2} = T_a = T_m - T_e \quad (N \cdot m) \quad (1.6)$$

By multiplying both sides for the mechanical speed of the rotor it is possible to move from torque to power

$$\omega_m J \frac{d^2\delta_m}{dt^2} = (T_m - T_e) \omega_m = P_m - P_e \quad (W) \quad (1.7)$$

where:

- $P_m$  = mechanical power in  $W$
- $P_e$  = electromagnetic power in  $W$

If we introduce a constant called *angular momentum* defined as

$$M \triangleq J\omega_{sm} \quad (\text{kg} \cdot \text{m}^2 \cdot \frac{\text{rad}}{\text{s}}) \quad (1.8)$$

Then we consider the following simplification

$$M \triangleq J\omega_{sm} \cong J\omega_m \quad (\text{kg} \cdot \text{m}^2 \cdot \frac{\text{rad}}{\text{s}}) \quad (1.9)$$

and we replace the angular momentum of the rotor in Equation 1.7 the result is

$$M \frac{d^2\delta_m}{dt^2} \cong P_m - P_e \quad (W) \quad (1.10)$$

However,  $M$  can assume values very different numerically, depending on the size of the machine. For this reason, another constant, called *inertia constant*, is used. The inertia constant is denoted by  $H$  and defined as

$$H \triangleq \frac{\frac{1}{2} J \omega_{sm}^2}{A_{nom}} = \frac{\frac{1}{2} M \omega_{sm}}{A_{nom}} \quad \left( \frac{W s}{VA} \right) \quad (1.11)$$

where  $A_{nom}$  is the nominal power of the synchronous machine in  $VA$ . The inertia constant defines how many seconds are needed to discharge the kinetic energy of the machine when it rotating at a synchronous speed if you supply a load with rated power equal to the rated power of the synchronous machine. This is the physical meaning of the inertia constant. Expressing the angular momentum of the rotor respect to the value of the inertia constant it results in

$$M = \frac{2H}{\omega_{sm}} A_{nom} \quad \left( kg \cdot m^2 \cdot \frac{rad}{s} \right) \quad (1.12)$$

If we replace this result in Equation 1.10 we obtain

$$\frac{2H}{\omega_{sm}} A_{nom} \frac{d^2 \delta_m}{dt^2} \cong P_m - P_e \quad (W) \quad (1.13)$$

Losses can be considered if we subtract to the right side of the Equation 1.13 a *damping term*  $D$  which is multiplied by the time derivative of the angular position of the rotor in mech. radians [11]

$$\frac{2H}{\omega_{sm}} A_{nom} \frac{d^2 \delta_m}{dt^2} \cong P_m - P_e - D \frac{d\delta_m}{dt} \quad (W) \quad (1.14)$$

By replacing the result in Equation 1.4 it is possible to express the Equation 1.14 with respect to the mechanical speed of the rotor

$$\frac{2H}{\omega_{sm}} A_{nom} \frac{d\omega_m}{dt} \cong P_m - P_e - D(\omega_m - \omega_{sm}) \quad (W) \quad (1.15)$$

If we divide both sides by the term  $A_{nom}$  the Equation 1.15 results in

$$\begin{aligned} \frac{2H}{\omega_{sm}} \frac{d\omega_m}{dt} &\cong (P_m - P_e - D(\omega_m - \omega_{sm})) \frac{1}{A_{nom}} \quad (W) \\ \frac{2H}{\omega_s} \frac{d\omega}{dt} &\cong p_m - p_e - \frac{D}{A_{nom}} (\omega - \omega_s) \quad (p.u.) \end{aligned} \quad (1.16)$$

The Equation 2.16 is commonly referred to as the *swing equation* because it represents swings in rotor angle  $\delta_m$  during disturbances.

The swing equation is the basic equation that drives the motion of the rotor of a generator and links its dynamic behaviour with the working frequency of a synchronous machine.

### 1.3. Swing equation in multi-machine systems

Systems in which many generators and loads are interconnected by tie-lines are called *multi-machine systems*. In these systems, the Equation 2.16 can be used to describe the dynamic of each one of the  $k$  machines of the system [1]. The general set of the  $k$  equation, neglecting the damping for the sake of simplicity, appears as

$$\begin{cases} \frac{2}{\omega_s} H_1 A_{nom,1} \frac{d\omega_1}{dt} \cong P_{1,m} - P_{1,e} & (W) \\ \frac{2}{\omega_s} H_2 A_{nom,2} \frac{d\omega_2}{dt} \cong P_{2,m} - P_{2,e} & (W) \\ \vdots \\ \frac{2}{\omega_s} H_k A_{nom,k} \frac{d\omega_k}{dt} \cong P_{k,m} - P_{k,e} & (W) \end{cases} \quad (1.17)$$

A common transformation used to study the multi-machine dynamic models is the center-of-inertia (COI) reference.

To obtain the COI reference of a multi-machine system we need to start from the generic expression of a  $i$ -th machine

$$\frac{2}{\omega_s} H_i A_{nom,i} \frac{d\omega_i}{dt} \cong P_{i,m} - P_{i,e} \quad (W) \quad (1.18)$$

Then, is possible to describe the dynamic of the system using a single equivalent machine defined in the Equation 1.19

$$\sum_{i=1}^k \frac{2}{\omega_s} H_i A_{nom,i} \frac{d \frac{\sum_{i=1}^k H_i A_{nom,i} \omega_i}{\sum_{i=1}^k H_i A_{nom,i}}}{dt} = \frac{2}{\omega_s} \sum_{i=1}^k H_i A_{nom,i} \frac{d \frac{\sum_{i=1}^k H_i A_{nom,i} \omega_i}{\sum_{i=1}^k H_i A_{nom,i}}}{dt} \cong \sum_{i=1}^k P_{i,m} - \sum_{i=1}^k P_{i,e} \quad (W) \quad (1.19)$$

Fixing the base power as  $A_{nom,tot} = \sum_{i=1}^k A_i$ , is possible to express the Equation 1.19 in per unit as

$$\frac{2}{\omega_s} \sum_{i=1}^k \frac{H_i A_{nom,i}}{A_{nom,tot}} \frac{d \frac{\sum_{i=1}^k H_i A_{nom,i} \omega_i}{\sum_{i=1}^k H_i A_{nom,i}}}{dt} \cong \sum_{i=1}^k \frac{P_{i,m}}{A_{nom,tot}} - \sum_{i=1}^k \frac{P_{i,e}}{A_{nom,tot}} \quad (p.u.) \quad (1.20)$$

Alternatively, in the Equation 1.20 is possible to choose another base power . Take into account, the arbitrary base power  $A_{base}$  we can express the Equation 1.20 as follow

$$\frac{2}{\omega_s} \sum_{i=1}^k \frac{H_i A_{nom,i}}{A_{base}} \frac{d \sum_{i=1}^k \frac{H_i A_{nom,i} \omega_i}{\sum_{i=1}^k H_i A_{nom,i}}}{dt} \cong \sum_{i=1}^k \frac{P_{i,m}}{A_{base}} - \sum_{i=1}^k \frac{P_{i,e}}{A_{base}} \quad (p.u.) \quad (1.21)$$

The COI reference transformation permits the reduction of the variables used to describe the system defining the COI angular speeds and equivalent inertia constant as [10] [20] [13]

$$\omega_{COI} \triangleq \frac{\sum_{i=1}^k H_i A_{nom,i} \omega_i}{\sum_{i=1}^k H_i A_{nom,i}} \quad (rad/s) \quad (1.22)$$

$$H_{COI} \triangleq \frac{\sum_{i=1}^k H_i A_{nom,i}}{\sum_{i=1}^k A_{nom,i}} = \frac{\sum_{i=1}^k H_i A_{nom,i}}{A_{nom,tot}} \quad (s) \quad (1.23)$$

Therefore, the equivalent motion equation of the multi-machine system expressed with respect to its COI reference is given by

$$\frac{2H_{COI}}{\omega_s} \frac{d\omega_{COI}}{dt} \cong p_{eq,m} - p_{eq,e} \quad (p.u.) \quad (1.24)$$

where:

- $p_{eq,m} = \sum_{i=1}^k \frac{P_{i,m}}{A_{base}}$
- $p_{eq,e} = \sum_{i=1}^k \frac{P_{i,e}}{A_{base}}$

The COI reference is useful to describe the response of an area of the system to external forces.

Traditionally, the main drawback of COI-based approaches is that the information about the frequency of each local bus and the inter-unit synchronizing oscillations between generators is lost. Nevertheless, different approach that permit the estimation of the local frequencies from the COI frequency are under development [7].



# 2 | Determination of the Power System Inertia

## 2.1. Sparse identification of nonlinear dynamics (SINDy)

The sparse identification of nonlinear dynamics (SINDy) algorithm is a flexible method which is used to discover linear and nonlinear dynamic system models from data.

The increase of the available data, due to the lower cost of the sensor, together with the increase of computation power and data storage of our devices allow us to obtain a proper environment for the application of the SINDy algorithm.

The SINDy algorithm bypasses the intractable combinatorial search through all possible model structures, leveraging on the fact that many dynamic systems have dynamics with only a few active terms in the space of possible righthand side functions [3].

### 2.1.1. Application of SINDy to a generic nonlinear dynamic system

If we consider a generic nonlinear dynamic system [3]

$$\frac{d}{dt} \mathbf{v}^T(t) = \dot{\mathbf{v}}^T(t) = \mathbf{f}^T(\mathbf{v}(t)) \quad (2.1)$$

$$\frac{d}{dt} \begin{bmatrix} v_1(t) & v_2(t) & \cdots & v_n(t) \end{bmatrix}_{(1 \times n)} = \begin{bmatrix} \dot{v}_1(t) & \dot{v}_2(t) & \cdots & \dot{v}_n(t) \end{bmatrix}_{(1 \times n)} \quad (2.2)$$

$$= \begin{bmatrix} f(v_1(t)) & f(v_2(t)) & \cdots & f(v_n(t)) \end{bmatrix}_{(1 \times n)} \quad (2.3)$$

The column vector  $\mathbf{v}(t) = [v_1(t) \ v_2(t) \ \dots \ v_n(t)]^T \in \mathbb{R}^n$  represents the  $n$  state of the system at time  $t$ , and the nonlinear function  $\mathbf{f}(\mathbf{v}(t))$  represents the dynamic constraints

that define the equations of motion of the system [4]. To determine the function  $\mathbf{f}$  from data, we collect a time-history of the state  $\mathbf{v}(t)$  and we either measure the derivative  $\dot{\mathbf{v}}(t)$  or approximate it numerically from  $\mathbf{v}(t)$ . The data is sampled at several times  $t_1, t_2, \dots, t_m$  and arranged into two large matrices:

$$\mathbf{V} = \begin{bmatrix} \mathbf{v}_1(t) & \mathbf{v}_2(t) & \cdots & \mathbf{v}_n(t) \end{bmatrix}_{(m \times n)} = \begin{bmatrix} v_1(t_1) & v_2(t_1) & \cdots & v_n(t_1) \\ v_1(t_2) & v_2(t_2) & \cdots & v_n(t_2) \\ \vdots & \vdots & \ddots & \vdots \\ v_1(t_m) & v_2(t_m) & \cdots & v_n(t_m) \end{bmatrix}_{(m \times n)} \quad (2.4)$$

$$\dot{\mathbf{V}} = \begin{bmatrix} \dot{\mathbf{v}}_1(t) & \dot{\mathbf{v}}_2(t) & \cdots & \dot{\mathbf{v}}_n(t) \end{bmatrix}_{(m \times n)} = \begin{bmatrix} \dot{v}_1(t_1) & \dot{v}_2(t_1) & \cdots & \dot{v}_n(t_1) \\ \dot{v}_1(t_2) & \dot{v}_2(t_2) & \cdots & \dot{v}_n(t_2) \\ \vdots & \vdots & \ddots & \vdots \\ \dot{v}_1(t_m) & \dot{v}_2(t_m) & \cdots & \dot{v}_n(t_m) \end{bmatrix}_{(m \times n)} \quad (2.5)$$

Starting from a vector of possible non linear functions defined as

$$\boldsymbol{\theta}(\mathbf{v}(t)) = [1 \ \mathbf{v}(t) \ \mathbf{v}(t)^{P_2} \ \mathbf{v}(t)^{P_3} \ \cdots \ \sin(\mathbf{v}(t)) \ \cos(\mathbf{v}(t)) \ \sin(2\mathbf{v}(t)) \ \cos(2\mathbf{v}(t))]_{(1 \times c)} \quad (2.6)$$

where  $c$  defines the number of columns of  $\boldsymbol{\theta}(\mathbf{v}(t))$  that cannot be uniquely defined, since they depends by the different nonlinear functions inserted in the vector.

A matrix  $\boldsymbol{\Theta}(\mathbf{V})$  may be constructed, considering the vector  $\boldsymbol{\theta}(\mathbf{v}(t))$  in each one of the  $m$  instants of time:

$$\begin{aligned} \boldsymbol{\Theta}(\mathbf{V}) &= \begin{bmatrix} \boldsymbol{\theta}(\mathbf{v}(t_1)) \\ \boldsymbol{\theta}(\mathbf{v}(t_2)) \\ \vdots \\ \boldsymbol{\theta}(\mathbf{v}(t_m)) \end{bmatrix}_{(m \times c)} \\ &= \begin{bmatrix} 1 & \mathbf{v}(t_1) & \mathbf{v}(t_1)^{P_2} & \mathbf{v}(t_1)^{P_3} & \cdots & \sin(\mathbf{v}(t_1)) & \cos(\mathbf{v}(t_1)) & \sin(2\mathbf{v}(t_1)) & \cos(2\mathbf{v}(t_1)) \\ 1 & \mathbf{v}(t_2) & \mathbf{v}(t_2)^{P_2} & \mathbf{v}(t_2)^{P_3} & \cdots & \sin(\mathbf{v}(t_2)) & \cos(\mathbf{v}(t_2)) & \sin(2\mathbf{v}(t_2)) & \cos(2\mathbf{v}(t_2)) \\ \vdots & \vdots & \vdots & \vdots & \vdots & \vdots & \vdots & \vdots & \vdots \\ 1 & \mathbf{v}(t_m) & \mathbf{v}(t_m)^{P_2} & \mathbf{v}(t_m)^{P_3} & \cdots & \sin(\mathbf{v}(t_m)) & \cos(\mathbf{v}(t_m)) & \sin(2\mathbf{v}(t_m)) & \cos(2\mathbf{v}(t_m)) \end{bmatrix}_{(m \times c)} \\ &= [1 \ \mathbf{V} \ \mathbf{V}^{P_2} \ \mathbf{V}^{P_3} \ \cdots \ \sin(\mathbf{V}) \ \cos(\mathbf{V}) \ \sin(2\mathbf{V}) \ \cos(2\mathbf{V})]_{(m \times c)} \end{aligned} \quad (2.7)$$

Here, higher polynomials are denoted as  $\mathbf{V}^{P_2}$ ,  $\mathbf{V}^{P_3}$ , etc., where  $\mathbf{V}^{P_2}$  denotes the quadratic nonlinearities in the state  $\mathbf{v}$ :

$$\mathbf{V}^{P_2} = \begin{bmatrix} v_1^2(t_1) & v_1(t_1)v_2(t_1) & \cdots & v_1(t_1)v_n(t_1) & v_2^2(t_1) & \cdots & v_n^2(t_1) & \cdots \\ v_1^2(t_2) & v_1(t_2)v_2(t_2) & \cdots & v_1(t_2)v_n(t_2) & v_2^2(t_2) & \cdots & v_n^2(t_2) & \cdots \\ \vdots & \vdots & \vdots & \vdots & \vdots & \ddots & \vdots & \vdots \\ v_1^2(t_m) & v_1(t_m)v_2(t_m) & \cdots & v_1(t_m)v_n(t_m) & v_2^2(t_m) & \cdots & v_n^2(t_m) & \cdots \end{bmatrix}_{(m \times (n \cdot n))} \quad (2.8)$$

while the symbol  $\mathbf{1}$  define the vector  $\mathbf{1} = \begin{bmatrix} 1 & 1 & \cdots & 1 \end{bmatrix}_{(m \times 1)}^T$ .

Each column of  $\boldsymbol{\theta}(\mathbf{v}(t))$  represents a candidate function for the right hand side of Equation 2.1. Note that  $\boldsymbol{\theta}(\mathbf{v}(t))$  is a vector of non linear functions of  $\mathbf{v}(t)$ , as opposed to  $\boldsymbol{\Theta}(\mathbf{V})$ , which is a data matrix.

The entries in the matrix  $\boldsymbol{\theta}(\mathbf{v}(t))$  are built with great freedom. Since only a few of these nonlinearities are active in each row of  $\mathbf{f}$ , it is possible to set up a sparse regression problem to define the sparse vectors of the coefficients  $\boldsymbol{\Xi} = [\boldsymbol{\xi}_1 \ \boldsymbol{\xi}_2 \ \cdots \ \boldsymbol{\xi}_n]$  that determine which nonlinearities are active.

The dynamic system in Equation 2.1 can now be represented in terms of data matrices using Equation 2.5 and Equation 2.7 as

$$\begin{aligned} \dot{\mathbf{V}} &= \boldsymbol{\Theta}(\mathbf{V}) \boldsymbol{\Xi} \\ &= \begin{bmatrix} \mathbf{1} & \mathbf{V} & \mathbf{V}^{P_2} & \mathbf{V}^{P_3} & \cdots & \sin(\mathbf{V}) & \cos(\mathbf{V}) & \sin(2\mathbf{V}) & \cos(2\mathbf{V}) \end{bmatrix}_{(m \times c)} \begin{bmatrix} \boldsymbol{\xi}_1 & \boldsymbol{\xi}_2 & \cdots & \boldsymbol{\xi}_n \end{bmatrix}_{(c \times n)} \\ &= \begin{bmatrix} \mathbf{1} & \mathbf{V} & \mathbf{V}^{P_2} & \mathbf{V}^{P_3} & \cdots & \sin(\mathbf{V}) & \cos(\mathbf{V}) & \sin(2\mathbf{V}) & \cos(2\mathbf{V}) \end{bmatrix}_{(m \times c)} \begin{bmatrix} \xi_{1,1} & \xi_{2,1} & \cdots & \xi_{n,1} \\ \xi_{1,\mathbf{V}} & \xi_{2,\mathbf{V}} & \cdots & \xi_{n,\mathbf{V}} \\ \xi_{1,\mathbf{V}^2} & \xi_{2,\mathbf{V}^2} & \cdots & \xi_{n,\mathbf{V}^2} \\ \xi_{1,\mathbf{V}^3} & \xi_{2,\mathbf{V}^3} & \cdots & \xi_{n,\mathbf{V}^3} \\ \vdots & \vdots & \vdots & \vdots \\ \xi_{1,\sin(\mathbf{V})} & \xi_{2,\sin(\mathbf{V})} & \cdots & \xi_{n,\sin(\mathbf{V})} \\ \xi_{1,\cos(\mathbf{V})} & \xi_{2,\cos(\mathbf{V})} & \cdots & \xi_{n,\cos(\mathbf{V})} \\ \xi_{1,\sin(2\mathbf{V})} & \xi_{2,\sin(2\mathbf{V})} & \cdots & \xi_{n,\sin(2\mathbf{V})} \\ \xi_{1,\cos(2\mathbf{V})} & \xi_{2,\cos(2\mathbf{V})} & \cdots & \xi_{n,\cos(2\mathbf{V})} \end{bmatrix}_{(c \times n)} \end{aligned} \quad (2.9)$$

Each column  $\boldsymbol{\xi}_k$  in  $\boldsymbol{\Xi}$  is a vector of unknowns determining the active terms in the  $k$ -th

equation of the Equation 2.1 and can be found using a convex  $l_1$ -regularized sparse regression algorithm as:

$$\boldsymbol{\xi}_k = \arg \min_{\boldsymbol{\xi}'_k} \|\dot{\mathbf{V}}_k - \Theta(\mathbf{V})\boldsymbol{\xi}'_k\|_2 + \lambda \|\boldsymbol{\xi}'_k\|_1 \quad \forall k \quad (2.10)$$

where  $\dot{\mathbf{V}}_k$  is the  $k$ -th column of  $\dot{\mathbf{V}}$ , and  $\lambda$  is called sparsity-promoting knob.

A parsimonious model will provide an accurate model fit in Equation 2.9 with as few terms as possible in  $\Xi$ . A more detailed explanation about the parsimonious model is provided in Appendix B.2. The algorithm used in SINDy for the estimation of the few active terms present in the matrix  $\Xi$  is the Sequentially thresholded least-squares algorithm (STLS) analyzed more in depth in Subsection 2.1.2.

Once  $\Xi$  has been determined, a model of each of the governing equations in the Equation 2.1 may be constructed as follows:

$$\dot{\mathbf{v}}_k = \theta(\mathbf{v}_k)\boldsymbol{\xi}_k \quad (2.11)$$

The result of the SINDy regression is a parsimonious model that includes only the most important terms required to explain the observed behaviour.

### 2.1.2. Sequentially thresholded least-squares algorithm (STLS)

The STLS, given a parameter  $\lambda$  that specifies the minimum magnitude for a coefficient in  $\Xi$ , perform a least squares fit and then zero out all coefficients with magnitude below the threshold. [5]

In particular, if we want to solve the Equation 2.9 with respect to  $\Xi$ , the result is an over-fitted matrix in which it is difficult to identify the true active terms for the reconstruction of the dynamic behaviour of the system. For this reason, we start a sequential method that allows to increase the sparsity of the matrix  $\Xi$  repeating the same procedure for  $k$  times.

In every repetition the terms of the matrix  $\Xi$  that respect this relationship  $|\xi_k| < \lambda$  are set equal to zero.

The *sparsification knob* allows to identify a threshold under which the algorithm sets the term  $\xi_k$  equal to zero.

Then, we exclude from the matrix  $\Theta(\mathbf{V})$  the term whose results is a term  $\xi_k$  considered negligible and fixed equal to zero.

Finally, the matrix  $\Xi$  is recomputed with the new matrix  $\Theta(\mathbf{V})$ .

This process of fitting and thresholding is performed until convergence.

The convergence is reached when the sparsity of the matrix does not change between two consecutive iterations. Usually, ten iterations are enough to achieve convergence.

The sparsification knob and the number of iteration achieved until convergence are the most important parameter that can be changed to modify the sparsity of the matrix  $\Xi$ . The code used to perform the sequential thresholded least squares in MATLAB is presented in Appendix B.1.

### 2.1.3. Application of SINDy for the estimation of the power system inertia

If we consider to have the possibility of measure the value over time of system variables, we can define three matrices in which each column is related to a machine of the studied electric system.

$$\mathbf{X} = \begin{bmatrix} \mathbf{x}_1(t) & \mathbf{x}_2(t) & \cdots & \mathbf{x}_n(t) \end{bmatrix}_{(m \times n)} = \begin{bmatrix} x_1(t_1) & x_2(t_1) & \cdots & x_n(t_1) \\ x_1(t_2) & x_2(t_2) & \cdots & x_n(t_2) \\ \vdots & \vdots & \ddots & \vdots \\ x_1(t_m) & x_2(t_m) & \cdots & x_n(t_m) \end{bmatrix}_{(m \times n)} \quad (2.12)$$

$$\mathbf{Y} = \begin{bmatrix} \mathbf{y}_1(t) & \mathbf{y}_2(t) & \cdots & \mathbf{y}_n(t) \end{bmatrix}_{(m \times n)} = \begin{bmatrix} y_1(t_1) & y_2(t_1) & \cdots & y_n(t_1) \\ y_1(t_2) & y_2(t_2) & \cdots & y_n(t_2) \\ \vdots & \vdots & \ddots & \vdots \\ y_1(t_m) & y_2(t_m) & \cdots & y_n(t_m) \end{bmatrix}_{(m \times n)} \quad (2.13)$$

$$\mathbf{Z} = \begin{bmatrix} \mathbf{z}_1(t) & \mathbf{z}_2(t) & \cdots & \mathbf{z}_n(t) \end{bmatrix}_{(m \times n)} = \begin{bmatrix} z_1(t_1) & z_2(t_1) & \cdots & z_n(t_1) \\ z_1(t_2) & z_2(t_2) & \cdots & z_n(t_2) \\ \vdots & \vdots & \ddots & \vdots \\ z_1(t_m) & z_2(t_m) & \cdots & z_n(t_m) \end{bmatrix}_{(m \times n)} \quad (2.14)$$

Where:

- $\mathbf{X}$  = matrix of the electromagnetic power in *MW* over the time  $t$  in each machine
- $\mathbf{Y}$  = matrix of the angular velocity of the rotor in *rad/s* over the time  $t$  in each

machine

- $\mathbf{Z}$  = matrix of the mechanical power in  $MW$  over the time  $t$  in each machine
- $n$  = number of variables measured for that specific quantity
- $m$  = number of measurement made for each specific variables

The relationship between these three matrices can be expressed using the Equation 1.15 and it results as

$$\frac{2H}{\omega_s} A_{nom} \frac{d\mathbf{Y}}{dt} \cong \mathbf{Z} - \mathbf{X} - D(\mathbf{Y} - \omega_s) \quad (MW) \quad (2.15)$$

If we elaborate the Equation 2.15, in order to obtain an equation with the same shape of Equation 2.1, the result is

$$\begin{aligned} \frac{d\mathbf{Y}}{dt} = \dot{\mathbf{Y}} &\cong \frac{\omega_s}{2H} \frac{1}{A_{nom}} (\mathbf{Z} - \mathbf{X} - D(\mathbf{Y} - \omega_s)) \quad (rad/s^2) \\ &\cong \frac{\omega_s}{2H} \frac{1}{A_{nom}} (D\omega_s - \mathbf{X} - D\mathbf{Y} + \mathbf{Z}) \quad (rad/s^2) \end{aligned} \quad (2.16)$$

Where the matrix  $\dot{\mathbf{Y}}$  is the matrix which holds time derivative computed

$$\dot{\mathbf{Y}} = \begin{bmatrix} \dot{y}_1(t) & \dot{y}_2(t) & \cdots & \dot{y}_n(t) \end{bmatrix}_{(m \times n)} = \begin{bmatrix} \dot{y}_1(t_1) & \dot{y}_2(t_1) & \cdots & \dot{y}_n(t_1) \\ \dot{y}_1(t_2) & \dot{y}_2(t_2) & \cdots & \dot{y}_n(t_2) \\ \vdots & \vdots & \ddots & \vdots \\ \dot{y}_1(t_m) & \dot{y}_2(t_m) & \cdots & \dot{y}_n(t_m) \end{bmatrix}_{(m \times n)} \quad (2.17)$$

and obtained using the fourth-order centered difference approximation. A more detailed explanation about the fourth-order centered difference approximation is present in the Appendix A.1 .

Starting from the vector of the functions present in the Equation 2.16 defined as

$$\boldsymbol{\theta}(t) = [1 \quad x_1(t) \quad x_2(t) \quad \cdots \quad x_n(t) \quad y_1(t) \quad y_2(t) \quad \cdots \quad y_n(t) \quad z_1(t) \quad z_2(t) \quad \cdots \quad z_n(t)]_{(1 \times (3n+1))} \quad (2.18)$$

A matrix  $\Theta$  is built considering the vector  $\theta(t)$  in each one of the  $m$  instants of time:

$$\begin{aligned}
\Theta(\mathbf{W}) &= \begin{bmatrix} \theta(t_1) \\ \theta(t_2) \\ \vdots \\ \theta(t_m) \end{bmatrix}_{(m \times (3n+1))} \\
&= [\mathbf{1} \quad \mathbf{x}_1(t) \quad \mathbf{x}_2(t) \quad \cdots \quad \mathbf{x}_n(t) \quad \mathbf{y}_1(t) \quad \mathbf{y}_2(t) \quad \cdots \quad \mathbf{y}_n(t) \quad \mathbf{z}_1(t) \quad \mathbf{z}_2(t) \quad \cdots \quad \mathbf{z}_n(t)]_{(m \times (3n+1))} \\
&= [\mathbf{1} \quad \mathbf{X} \quad \mathbf{Y} \quad \mathbf{Z}]_{(m \times (3n+1))} \\
&= [\mathbf{1} \quad \mathbf{W}]_{(m \times (3n+1))}
\end{aligned} \tag{2.19}$$

where the symbol  $\mathbf{W}$  defines the matrix of the measurements.

In matrix  $\Theta(\mathbf{W})$  the terms corresponding to polynomial terms with order higher than one and any other function is not considered, since they do not appear in the Equation 1.15.

The Equation 2.16 can now be represented in terms of data matrices using Equation 2.17 and Equation 2.19 as

$$\begin{aligned}
\dot{\mathbf{Y}}_{\text{est}} &= \Theta(\mathbf{Y}) \Xi \\
&= [\mathbf{1} \quad \mathbf{X} \quad \mathbf{Y} \quad \mathbf{Z}]_{(m \times (3n+1))} \begin{bmatrix} \xi_1 & \xi_2 & \cdots & \xi_n \end{bmatrix}_{(3n+1) \times n} \\
&= [\mathbf{1} \quad \mathbf{X} \quad \mathbf{Y} \quad \mathbf{Z}]_{(m \times (3n+1))} \begin{bmatrix} \xi_{1,k} & \xi_{2,k} & \cdots & \xi_{n,k} \\ \xi_{1,x_1} & \xi_{2,x_1} & \cdots & \xi_{n,x_1} \\ \xi_{1,x_2} & \xi_{2,x_2} & \cdots & \xi_{n,x_2} \\ \vdots & \vdots & \cdots & \vdots \\ \xi_{1,x_n} & \xi_{2,x_n} & \cdots & \xi_{n,x_n} \\ \xi_{1,y_1} & \xi_{2,y_1} & \cdots & \xi_{n,y_1} \\ \xi_{1,y_2} & \xi_{2,y_2} & \cdots & \xi_{n,y_2} \\ \vdots & \vdots & \cdots & \vdots \\ \xi_{1,y_n} & \xi_{2,y_n} & \cdots & \xi_{n,y_n} \\ \xi_{1,z_1} & \xi_{2,z_1} & \cdots & \xi_{n,z_1} \\ \xi_{1,z_2} & \xi_{2,z_2} & \cdots & \xi_{n,z_2} \\ \vdots & \vdots & \cdots & \vdots \\ \xi_{1,z_n} & \xi_{2,z_n} & \cdots & \xi_{n,z_n} \end{bmatrix}_{(3n+1) \times n}
\end{aligned} \tag{2.20}$$

$$\begin{aligned}
& \left[ \begin{array}{cccc} 1 & 1 & \cdots & 1 \\ x_1(t_1) & x_1(t_2) & \cdots & x_1(t_m) \\ x_2(t_1) & x_2(t_2) & \cdots & x_2(t_m) \\ \vdots & \vdots & \ddots & \vdots \\ x_n(t_1) & x_n(t_2) & \cdots & x_n(t_m) \\ y_1(t_1) & y_1(t_2) & \cdots & y_1(t_m) \\ y_2(t_1) & y_2(t_2) & \cdots & y_2(t_m) \\ \vdots & \vdots & \ddots & \vdots \\ y_n(t_1) & y_n(t_2) & \cdots & y_n(t_m) \\ z_1(t_1) & z_1(t_2) & \cdots & z_1(t_m) \\ z_2(t_1) & z_2(t_2) & \cdots & z_2(t_m) \\ \vdots & \vdots & \ddots & \vdots \\ z_n(t_1) & z_n(t_2) & \cdots & z_n(t_m) \end{array} \right]^T \\
= & \begin{array}{c} \left[ \begin{array}{cccc} \xi_{1,k} & \xi_{2,k} & \cdots & \xi_{n,k} \\ \xi_{1,x_1} & \xi_{2,x_1} & \cdots & \xi_{n,x_1} \\ \xi_{1,x_2} & \xi_{2,x_2} & \cdots & \xi_{n,x_2} \\ \vdots & \vdots & \cdots & \vdots \\ \xi_{1,x_n} & \xi_{2,x_n} & \cdots & \xi_{n,x_n} \\ \xi_{1,y_1} & \xi_{2,y_1} & \cdots & \xi_{n,y_1} \\ \xi_{1,y_2} & \xi_{2,y_2} & \cdots & \xi_{n,y_2} \\ \vdots & \vdots & \cdots & \vdots \\ \xi_{1,y_n} & \xi_{2,y_n} & \cdots & \xi_{n,y_n} \\ \xi_{1,z_1} & \xi_{2,z_1} & \cdots & \xi_{n,z_1} \\ \xi_{1,z_2} & \xi_{2,z_2} & \cdots & \xi_{n,z_2} \\ \vdots & \vdots & \cdots & \vdots \\ \xi_{1,z_n} & \xi_{2,z_n} & \cdots & \xi_{n,z_n} \end{array} \right]_{(3n+1) \times n} \end{array} \\
& \hspace{15em} \text{\scriptsize } (m \times (3n+1)) \hspace{15em} \text{\scriptsize } (3n+1) \times n
\end{aligned}$$

The non-zero elements  $\xi$  of the matrix  $\Xi$  are corresponding to the active terms of the right side of the Equation 2.16.

Each column  $\xi_k$  in  $\Xi$  is a vector of coefficients determining the active terms in the  $k$ -th differential equation in Equation 2.16 and can be found using a a convex  $l_1$ -regularized sparse regression algorithm as:

$$\boldsymbol{\xi}_k = \arg \min_{\boldsymbol{\xi}'_k} \|\dot{\mathbf{W}}_k - \boldsymbol{\Theta}(\mathbf{Y})\boldsymbol{\xi}'_k\|_2 + \lambda \|\boldsymbol{\xi}'_k\|_1 \quad (2.21)$$

Ideally, once the sparse regression problem is solved, the matrix  $\Xi$  becomes very sparse and it can be expressed as



$$\dot{\mathbf{Y}}_{\text{est}} = [\mathbf{1} \ \mathbf{X} \ \mathbf{Y} \ \mathbf{Z}]_{(m \times (3n+1))} \begin{bmatrix} \xi_{1,k} & \xi_{2,k} & \cdots & \xi_{n,k} \\ \xi_{1,x_1} & 0 & \cdots & 0 \\ 0 & \xi_{2,x_2} & \cdots & 0 \\ \vdots & \vdots & \cdots & \vdots \\ 0 & 0 & \cdots & \xi_{n,x_n} \\ \xi_{1,y_1} & 0 & \cdots & 0 \\ 0 & \xi_{2,y_2} & \cdots & 0 \\ \vdots & \vdots & \cdots & \vdots \\ 0 & 0 & \cdots & \xi_{n,y_n} \\ \xi_{1,z_1} & 0 & \cdots & 0 \\ 0 & \xi_{2,z_2} & \cdots & 0 \\ \vdots & \vdots & \cdots & \vdots \\ 0 & 0 & \cdots & \xi_{n,z_n} \end{bmatrix}_{(3n+1) \times n} \quad (2.22)$$

However, is very common obtain higher number of non-zero terms in the  $\Xi$ , due to errors during the sparse regression problem. Since the Equation 2.22 approximates the Equation 2.17, the following equality can be defined as

$$\dot{\mathbf{Y}} \cong \dot{\mathbf{Y}}_{\text{est}} \quad (2.23)$$

Then, if we only consider the terms related to the 1-st machine for the sake of simplicity, the Equation 2.23 becomes

$$\frac{\omega_s}{2H_1} \frac{1}{A_{nom,1}} [D\omega_s - \mathbf{x}_1(t) - D\mathbf{y}_1(t) + \mathbf{z}_1(t)] \cong [\mathbf{1} \ \mathbf{X} \ \mathbf{Y} \ \mathbf{Z}] \begin{bmatrix} \xi_{1,k} \\ \xi_{1,x_1} \\ 0 \\ \vdots \\ 0 \\ \xi_{1,y_1} \\ 0 \\ \vdots \\ 0 \\ \xi_{1,z_1} \\ 0 \\ \vdots \\ 0 \end{bmatrix} \quad (2.24)$$

$$\frac{\omega_s}{2H_1} \frac{1}{A_{nom}} [D\omega_s - \mathbf{x}_1(t) - D\mathbf{y}_1(t) + \mathbf{z}_1(t)] \cong \mathbf{1}\xi_{1,k} + \mathbf{x}_1(t)\xi_{1,x_1} + \mathbf{y}_1(t)\xi_{1,y_1} + \mathbf{z}_1(t)\xi_{1,z_1} \quad (2.25)$$

Then, it is possible to correlate the terms of the matrix  $\Xi$  with the constant terms that multiply the vectors  $\mathbf{x}_1(t)$ ,  $\mathbf{y}_1(t)$ ,  $\mathbf{z}_1(t)$  in the Equation 2.17

$$\xi_{1,k} = \frac{\omega_s}{2H_1} \frac{1}{A_{nom,1}} D \omega_s \quad (2.26)$$

$$\xi_{1,x_1} = -\frac{\omega_s}{2H_1} \frac{1}{A_{nom,1}} \quad (2.27)$$

$$\xi_{1,y_1} = -\frac{\omega_s}{2H_1} \frac{1}{A_{nom,1}} D \quad (2.28)$$

$$\xi_{1,z_1} = \frac{\omega_s}{2H_1} \frac{1}{A_{nom,1}} \quad (2.29)$$

The same procedure can be repeated for each machine of the system.

The estimated inertia value can be extracted from the active terms of the vector  $\xi_k$  through these computations:

$$H_1 = \frac{\omega_s}{2\xi_{1,k}} \frac{1}{A_{nom,1}} D \omega_s \quad (2.30)$$

$$H_1 = -\frac{\omega_s}{2\xi_{1,x_1}} \frac{1}{A_{nom,1}} \quad (2.31)$$

$$H_1 = -\frac{\omega_s}{2\xi_{1,y_1}} \frac{1}{A_{nom,1}} D \quad (2.32)$$

$$H_1 = \frac{\omega_s}{2\xi_{1,z_1}} \frac{1}{A_{nom,1}} \quad (2.33)$$

Theoretically, the value of  $H_1$  estimated using these last four equation must be equal. Once the inertia has been found, is possible to exploit the Equation 2.30 and Equation 2.32 to estimate the value of the damping term D.

$$D = \frac{2}{\omega_s^2} H_1 \xi_{1,k} A_{nom,1} \quad (2.34)$$

$$D = -\frac{2}{\omega_s} H_1 \xi_{1,y} A_{nom,1} \quad (2.35)$$

For the sake of completeness, a method for the estimation of the damping term is reported in Equation 2.34 and Equation 2.35. However, this concept is not faced in this thesis.

## 2.2. Division of the machine dynamics

From the Equation 2.16 and the Equation 2.19 previously defined in the Section 2.1.3 it is possible to delineate a different method in which the dynamic of a single machine is studied individually.

Considering in the Equation 2.18 the functions related to a single machine, it is possible to solve many smaller problems, instead of one large problem.

The vector  $\boldsymbol{\theta}_j(t)$  of a generic  $j$ -th machine result as

$$\boldsymbol{\theta}_j(t) = [1 \quad x_j(t) \quad y_j(t) \quad z_j(t)]_{(1 \times 4)} \quad (2.36)$$

In the same way done in previous sections, a matrix  $\Theta$  is built considering the vector  $\boldsymbol{\theta}_j(t)$  in each one of the  $m$  instants of time:

$$\begin{aligned} \Theta_j(\mathbf{w}) &= \begin{bmatrix} \boldsymbol{\theta}_j(t_1) \\ \boldsymbol{\theta}_j(t_2) \\ \vdots \\ \boldsymbol{\theta}_j(t_m) \end{bmatrix}_{(m \times 4)} \\ &= \begin{bmatrix} \mathbf{1} & \mathbf{x}_j(t) & \mathbf{y}_j(t) & \mathbf{z}_j(t) \end{bmatrix}_{(m \times 4)} \\ &= \begin{bmatrix} \mathbf{1} & \mathbf{w} \end{bmatrix}_{(m \times 4)} \end{aligned} \quad (2.37)$$

where the symbol  $\mathbf{w}$  defines the matrix of the measurements related to a single machine. Instead, the time derivative vector of a generic machine  $j$ -th can be represented considering the  $j$ -th column of in matrix  $\dot{\mathbf{Y}}$ . The dynamics of a  $j$ -th machine can be represented in term of vector product as

$$\dot{\mathbf{y}}_{j,est}(t) = \Theta_j \boldsymbol{\xi}_j = \begin{bmatrix} \mathbf{1} & \mathbf{x}_j(t) & \mathbf{y}_j(t) & \mathbf{z}_j(t) \end{bmatrix}_{(m \times 4)} \begin{bmatrix} \xi_{j,k} \\ \xi_{j,x} \\ \xi_{j,y} \\ \xi_{j,z} \end{bmatrix}_{(4 \times 1)} \quad (2.38)$$

The elements of the vector  $\boldsymbol{\xi}_j$  are the active terms corresponding to the terms of the right side of the Equation 2.16 take into account only the equation of the  $j$ -th machine .

In this case we know that each term of the vector  $\boldsymbol{\xi}_j$  must be different from zero, since all are present in the Equation 2.16 related to a generic  $j$ -th machine.

The SINDy algorithm exploit a sequential sparse regression and optimization process performing the STLS.

This process is used to increase the sparsity of the matrix  $\Xi$  providing a better estimation of active terms related to the matrix  $\Theta$  and fixing to zero the elements not present in each one of the equations studied.

Nevertheless, in this case is possible to reduce the computation burden avoiding the use of a sequential method, since we don't need to increase the sparsity of the vector  $\xi_j$ .

Therefore, the elements of the vector  $\xi_j$  can be computed using a simpler algorithm.

In this work we test some algorithm already provided by the software MATLAB such as:

- Least-Squares regression (mldivide):

```
Xi_gen=Theta_gen\dy_gen
```

- Moore-Penrose pseudoinverse

```
Xi_gen=pinv(Theta_gen)*dy_gen
```

- Fit robust linear regression

```
Xi_gen=robustfit(Theta_gen,dy_gen)
```

- Singular value decomposition

```
[U,S,V]=svd(Theta_gen,'econ');
Xi_gen=V*inv(S)*U'*dy_gen
```

- Least Absolute Shrinkage and Selection Operator (LASSO) or Elastic net regularization for linear models

```
lambda = 1e-3;
[XL1, FitInfo] = lasso(Theta_gen,dy_gen,'Lambda',lambda,
                      'CV',10,'Intercept',false);
Xi_gen = XL1(:,FitInfo.Index1SE)
```

Once the elements of the vector  $\xi_j$  are determined, taking into account that

Equation 2.38 approximates the j-th column of the matrix  $\dot{\mathbf{Y}}$ , the following equality can be defined

$$\dot{\mathbf{y}}_j(t) \cong \dot{\mathbf{y}}_{j,est}(t) \quad (2.39)$$

Then, the Equation 2.39 can be represented as

$$\frac{\omega_s}{2H_j} \frac{1}{A_{nom,j}} [D\omega_s - \mathbf{x}_j(t) - D\mathbf{y}_j(t) + \mathbf{z}_j(t)] \cong \begin{bmatrix} \mathbf{1} & \mathbf{x}_j(t) & \mathbf{y}_j(t) & \mathbf{z}_j(t) \end{bmatrix} \begin{bmatrix} \xi_{j,k} \\ \xi_{j,x} \\ \xi_{j,y} \\ \xi_{j,z} \end{bmatrix} \quad (2.40)$$

$$\frac{\omega_s}{2H_j} \frac{1}{A_{nom,j}} [D\omega_s - \mathbf{x}_j(t) - D\mathbf{y}_j(t) + \mathbf{z}_j(t)] \cong \xi_{1,k} + \mathbf{x}_j(t)\xi_{j,x} + \mathbf{y}_j(t)\xi_{j,y} + \mathbf{z}_j(t)\xi_{j,z} \quad (2.41)$$

Finally, it is possible to correlate the terms of the vector  $\xi_j$  with the constant terms that multiply the vectors  $\mathbf{x}_j(t)$ ,  $\mathbf{y}_j(t)$ ,  $\mathbf{z}_j(t)$  in right side of the Equation 2.41

$$\xi_{j,k} = \frac{\omega_s}{2H_j} \frac{1}{A_{nom,j}} D \omega_s \quad (2.42)$$

$$\xi_{j,x} = -\frac{\omega_s}{2H_j} \frac{1}{A_{nom,j}} \quad (2.43)$$

$$\xi_{j,y} = -\frac{\omega_s}{2H_j} \frac{1}{A_{nom,j}} D \quad (2.44)$$

$$\xi_{j,z} = \frac{\omega_s}{2H_j} \frac{1}{A_{nom,j}} \quad (2.45)$$

The estimated inertia value can be extracted from the active terms of the vector  $\xi_j$  through these computations:

$$H_j = \frac{\omega_s}{2\xi_{j,k}} \frac{1}{A_{nom,j}} D \omega_s \quad (2.46)$$

$$H_j = -\frac{\omega_s}{2\xi_{j,x}} \frac{1}{A_{nom,j}} \quad (2.47)$$

$$H_j = -\frac{\omega_s}{2\xi_{j,y}} \frac{1}{A_{nom,j}} D \quad (2.48)$$

$$H_j = \frac{\omega_s}{2\xi_{j,z}} \frac{1}{A_{nom,j}} \quad (2.49)$$

The same procedure can be repeated for each machine of the system.

### 2.3. Moving window method for a real time estimation

The application of this method requires the measurements of electric power and frequency and the computation of the frequency derivative. For the explanation of this method, three example variables are considered and reported in Figure 2.1

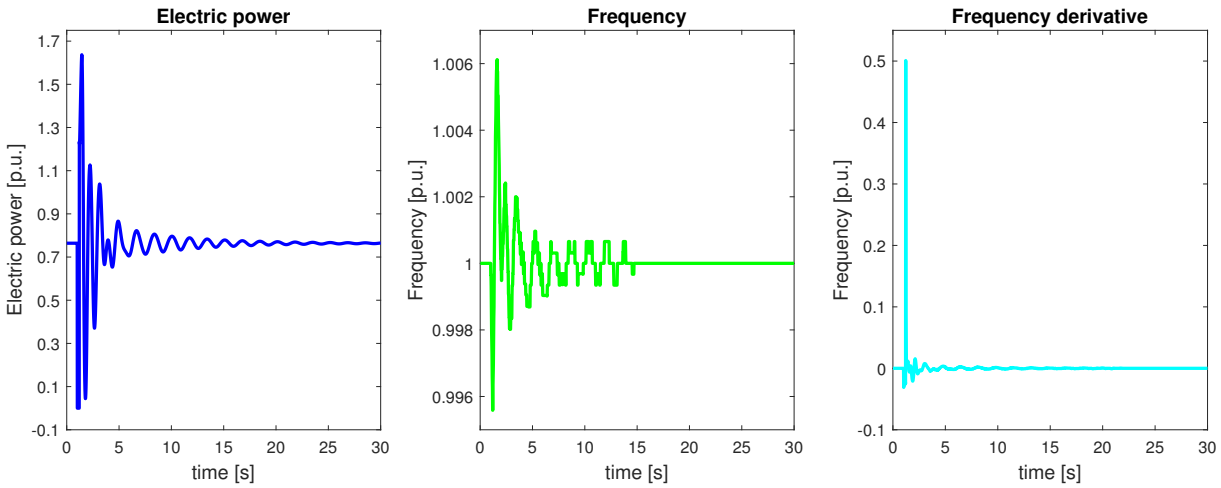


Figure 2.1: Example parameters

The following step is the identification of a time window that defines a small part of the variable trends where to apply the algorithm studied in Section 2.2 and Section 2.1.3. In this work, each time windows is assumed to be of 5 s large.

A graphic interpretation of this process, considering the first time window between 0 s - 5 s, is represented in the Figure 2.2.

Then, iterating this process moving the time window one second ahead, is possible to obtain the trend of the inertia in real-time estimated every second. An example of the result obtained considering a simulation time of 30 s is represented in Figure 2.3.

The obtained values of inertia are assigned to the end of the time window considered. For example, the inertia value estimated using the time window 0 s - 5 s is assigned to the instant 5 s.

After the red line in Figure 2.3 the value of inertia estimated are equal to infinite. This is due to a limitation of the algorithm used for the estimation of inertia, explained more in deep in Section 3.4.

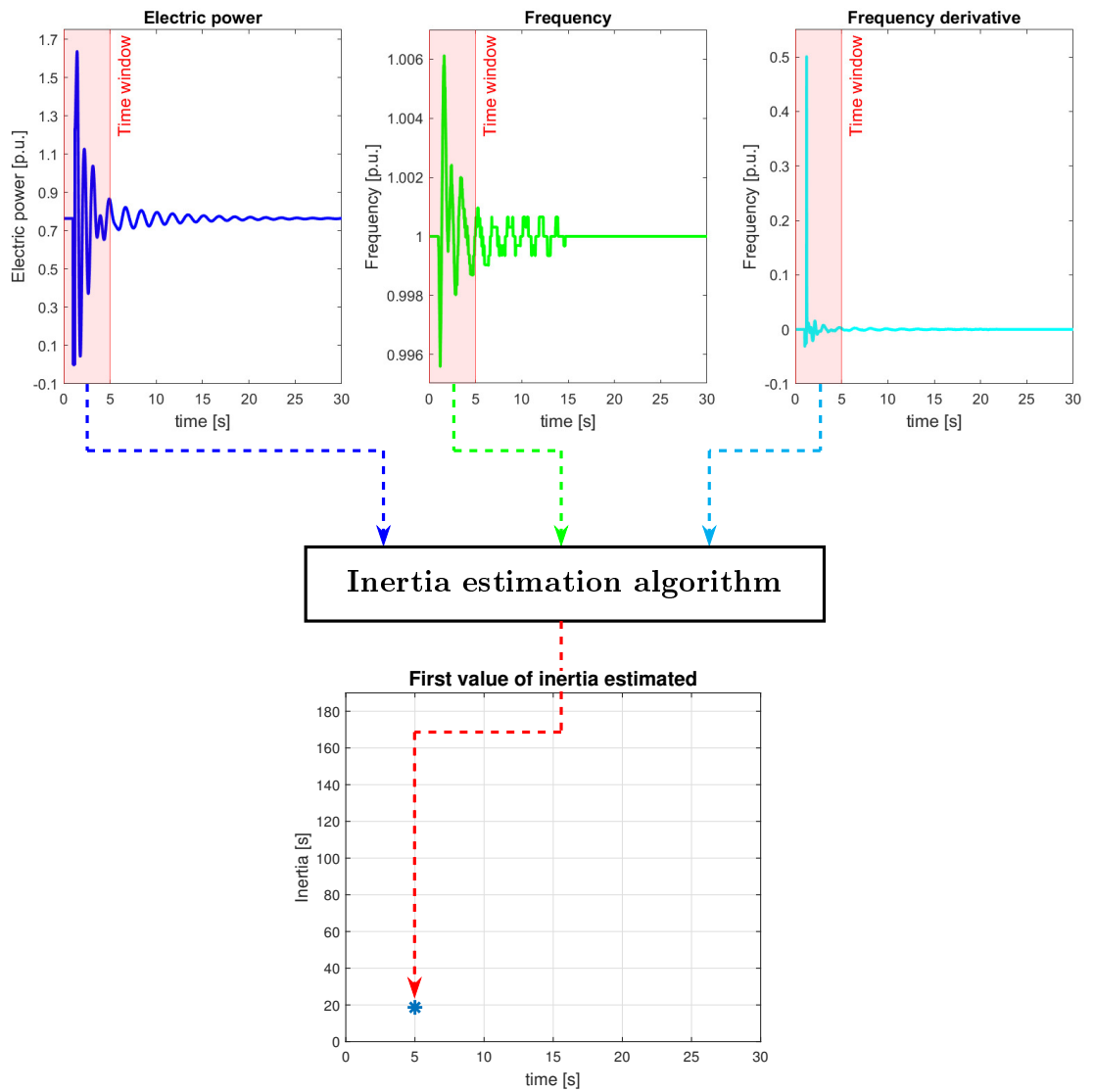


Figure 2.2: Example of the floating window method

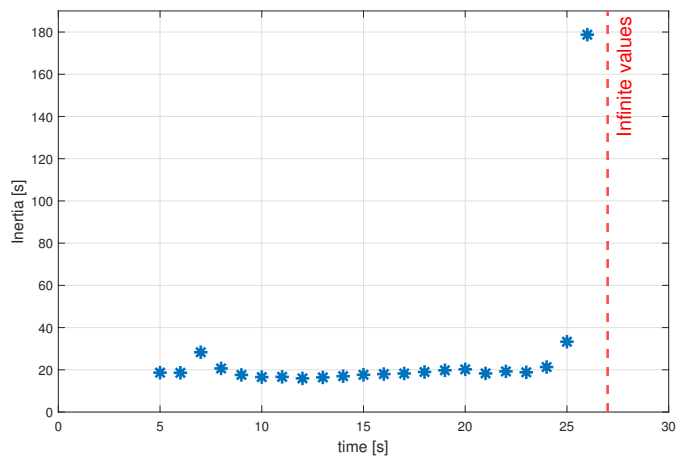


Figure 2.3: Example of inertia estimation





# 3 | Performed tests and Numerical results

In this chapter the application of the method exposed in the Chapter 2 and the numerical results obtained are reported.

In Chapter 2 the procedures to compute the inertia of the generators from the value of matrix  $\Xi$  are presented. Theoretically, the value of inertia can be computed starting from one of these variables:  $\xi_k$ ,  $\xi_x$ ,  $\xi_z$ ,  $\xi_z$ .

However, in every test of this chapter only the variable  $\xi_x$  were used for the estimation. Due to the fact that the computation using the variable  $\xi_z$  is not feasible in a real application since is impossible measure the mechanical power ( $z$ ), while the calculation using the variables  $\xi_k$  and  $\xi_y$  are affected by the variable  $D$ .

The variable  $D$  takes into account the damping effect of:

- The Governor's droop of each generators that can be easily estimated
- The effect of each machine present in the considered area (Joule losses and dampers)
- The loads that is difficult to be identified

Therefore, since we are not able to calculate in a precise way the value of the variable  $D$  also the value of the variables  $\xi_k$  and  $\xi_y$  will not be precise.

In this work we assume that the PMUs are characterized by a sensitivity of:

- 0.001 Hz: for frequency measurements
- 0.001 MW: for power measurements

Except for the last test in which is considered a sensitivity of:

- 0.00001 Hz: for frequency measurements
- 0.00001 MW: for power measurements

### 3.1. Test 1: Application of SINDy

The different simulation performed in this test are listed below:

- Simulation 1:  
SINDy algorithm is applied in an ideal condition with a single time windows of 30 s to estimate the inertia of each of machine of the system.
- Simulation 2:  
SINDy algorithm is applied for the inertia estimation in the moving window method to estimate the equivalent inertia of two areas.

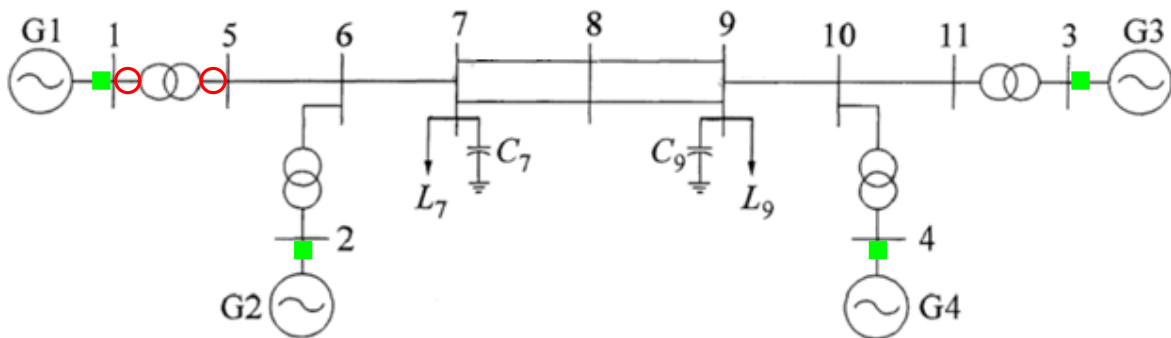
#### 3.1.1. Simulation 1

##### DETAILS OF THE SIMULATION 1

**Test system:** described in Section C.1

**Implemented in:** MATLAB

**Perturbation simulated:** Opening of the line 1



○: Opening/Reclosure    ■: PMUs location

Figure 3.1: Test 1 - Simulation 1 - Test-system

**Simulation time:** 30 s

**Sampling time:** 1 ms

**Fault time:** 1 s

**Clear time:** 1.2 s

**Governor:** ON for each generator

**PSS:** OFF for each generator

**AVR:** OFF for each generator

The true values of inertia of each machine of the system are:

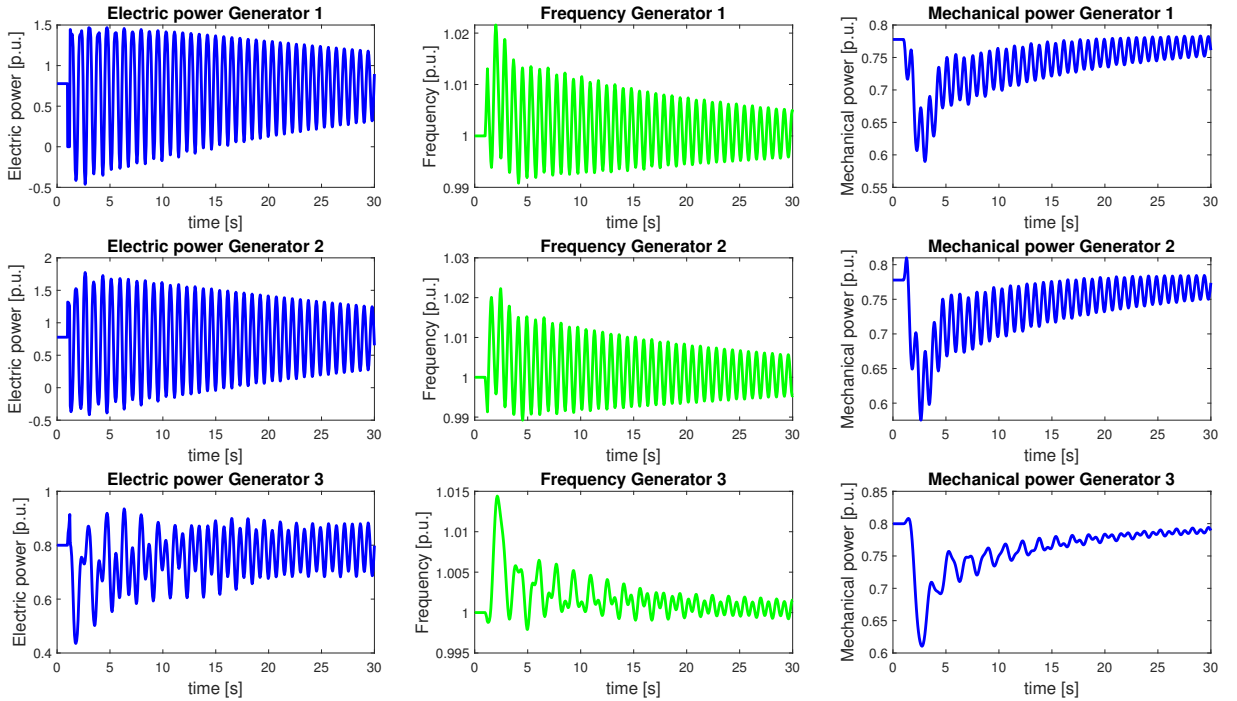
	<b>H [s]</b>
<b>Generator 1</b>	5,85
<b>Generator 2</b>	5,85
<b>Generator 3</b>	5,558
<b>Generator 4</b>	5,558

Table 3.1: Test 1 - Simulation 1 - True values of inertia

In this simulation, we apply the SINDy algorithm to estimate the inertia of the system considering a single time window of 30 s.

The methods used for these simulations are described in Section 2.1.3.

During the simulation, the generated power, mechanical power and frequency of each generator were recorded and used for the estimation of the inertia. The mechanical power is not measurable by PMUs, but in this test were recorded for testing the studied method. The trends of the generators main parameters during the simulation are reported as shown in Figure 3.2.



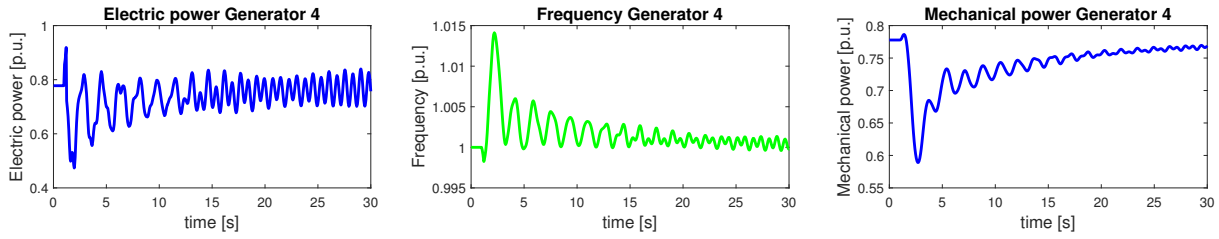


Figure 3.2: Test 1 - Simulation 1 - Main parameters of the system generators during the perturbation

As we can see after the disconnection of line 1 at 1 s and its reclosure at 1.2 s, the variables starts to oscillated and in 30 s the oscillations are not damped, since the AVR and PSS for every machine are switch off . However, the system after the perturbation is stable and seem to reach slowly a steady state condition.

The parameters used for the estimation of the inertia are variables described in Figure 3.2, plus the frequency derivatives that are computed with the method shown in Appendix A.1. The trend of the frequency derivative are represented in the following figure.

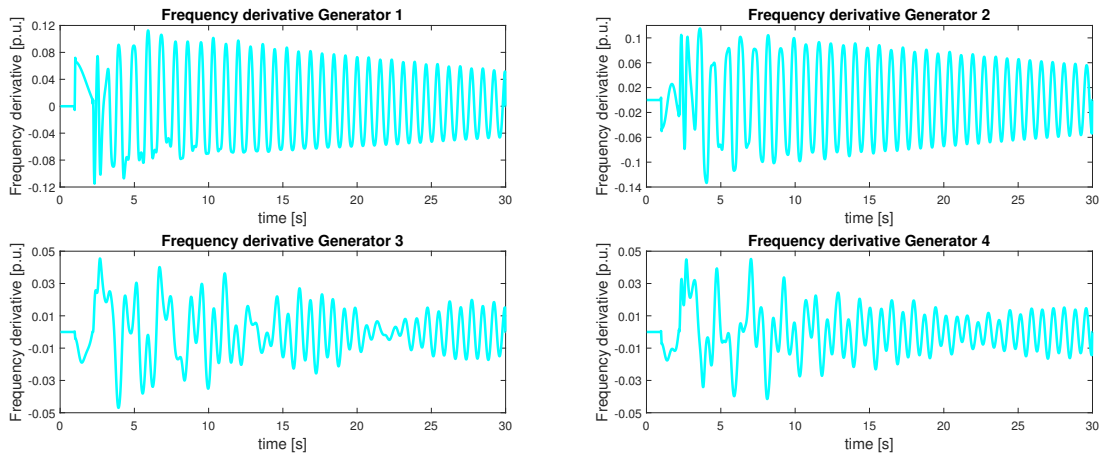


Figure 3.3: Test 1 - Simulation 1 - Frequency derivative trend

## RESULTS OF SIMULATION 1

The results obtained in this simulation are listed in the following table

	<b>H [s]</b>	<b>H<sub>estimate</sub> [s]</b>	<b>Error [%]</b>
<b>Generator 1</b>	5,85	5,848	0.03
<b>Generator 2</b>	5,85	5,851	-0.02
<b>Generator 3</b>	5,558	5,557	0.01
<b>Generator 4</b>	5,558	5,552	0.1

Table 3.2: Test 1 - Simulation 1 - Estimated values of inertia

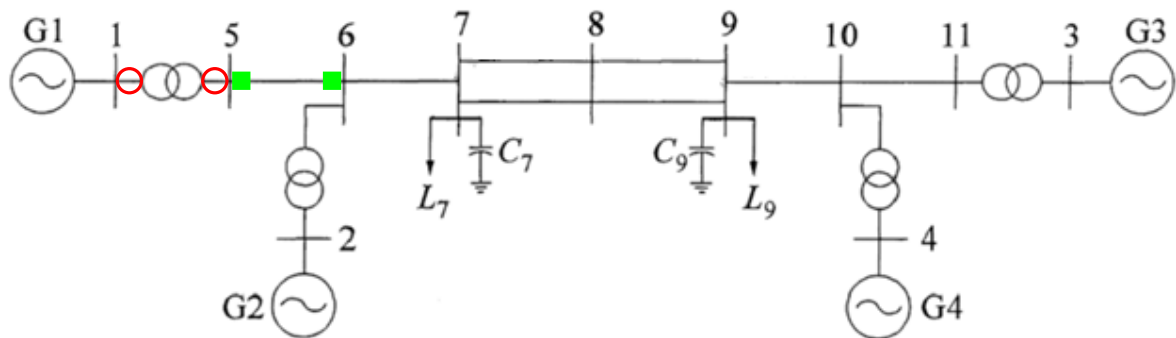
### 3.1.2. Simulation 2

#### DETAILS OF THE SIMULATION 2

**Test system:** described in Section C.1

**Implemented in:** PowerFactory

**Perturbation simulated:** Opening of the line 1



○: Opening/Reclosure    ■: PMUs location

Figure 3.4: Test 1 - Simulation 2 - Test-system

**Simulation time:** 30 s

**Governor:** ON for each generator

**Sampling time:** 20 ms

**PSS:** ON for each generator

**Fault time:** 1 s

**AVR:** ON for each generator

**Clear time:** 1.2 s

In this test the Test-system is divided in two areas each one characterized by its own inertia, as shown in Figure 3.5

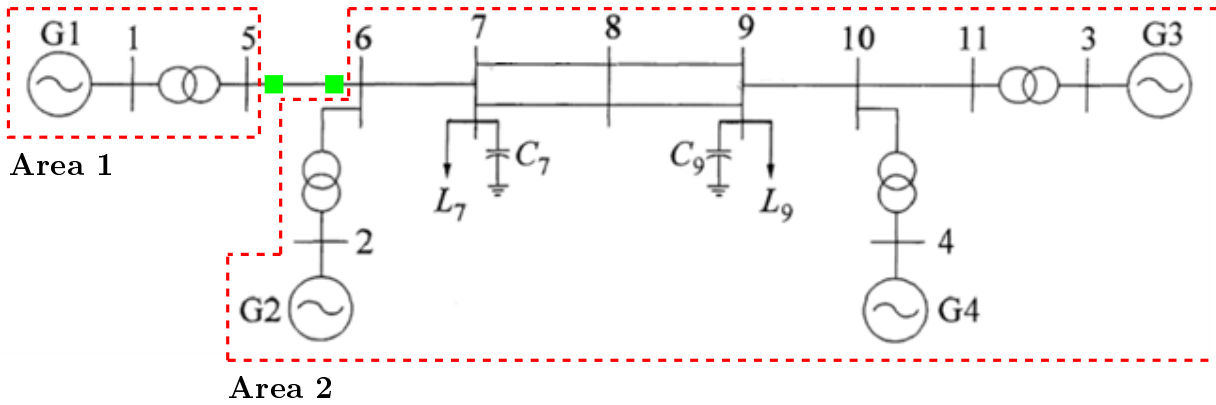


Figure 3.5: Test 1 - Simulation 2 - Areas of Test-system

The inertia of the two areas are respectively:

	<b>H [s]</b>
<b>Area1</b>	5,85
<b>Area2</b>	16,965

Table 3.3: Test 1 - Simulation 2 - Areas true values of inertia

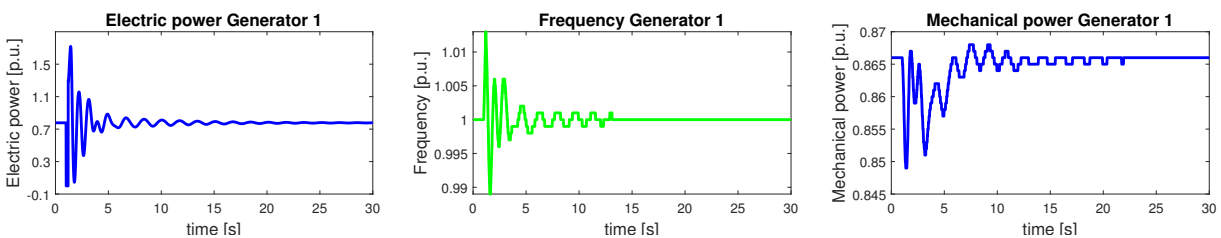
in which the inertia of Area 2 is obtained considering its COI equivalent inertia.

In this work we adopt, the method defined in Section 1.3 considering a base power equal to the nominal power of a single machine.

The perturbation considered is the same of the simulation 1, but in this case the presence of the Governor, PSS and AVR for each generator are considered.

In this simulation we test the possibility of estimating the inertia of the two equivalent areas of the system during a perturbation, assuming that PMUs are able to measure the electrical power, frequency and mechanical power. The method exploited is the moving window method described in Section 2.3, in which the estimation of the inertia is made using the SINDy algorithm.

Trends for the generators' main parameters during in the simulation, are illustrated in the following figure.



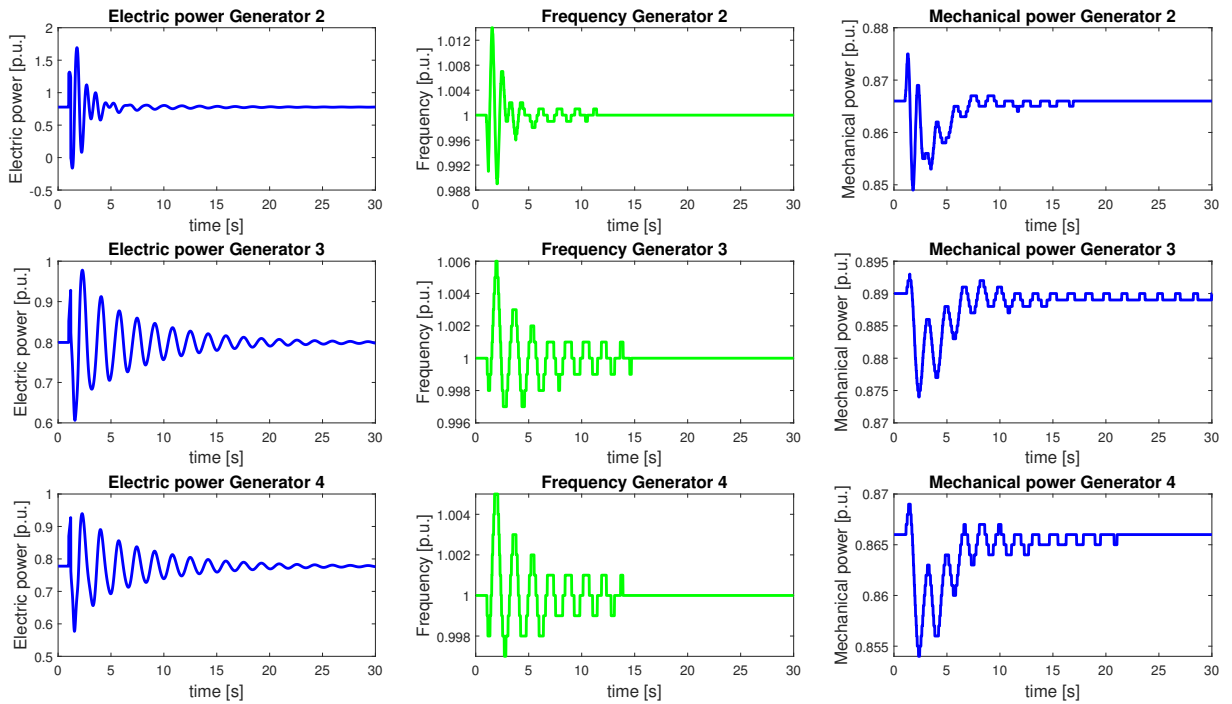


Figure 3.6: Test 1 - Simulation 2 - Main parameters of the system generators during the perturbation

To estimate inertia, the variable recorded by PMUs and the derivative of the frequency are used. The derivative of the frequency is computed using the method explained in Appendix A.1.

Figure 3.7 and Figure 3.8 display the trends of these variables.

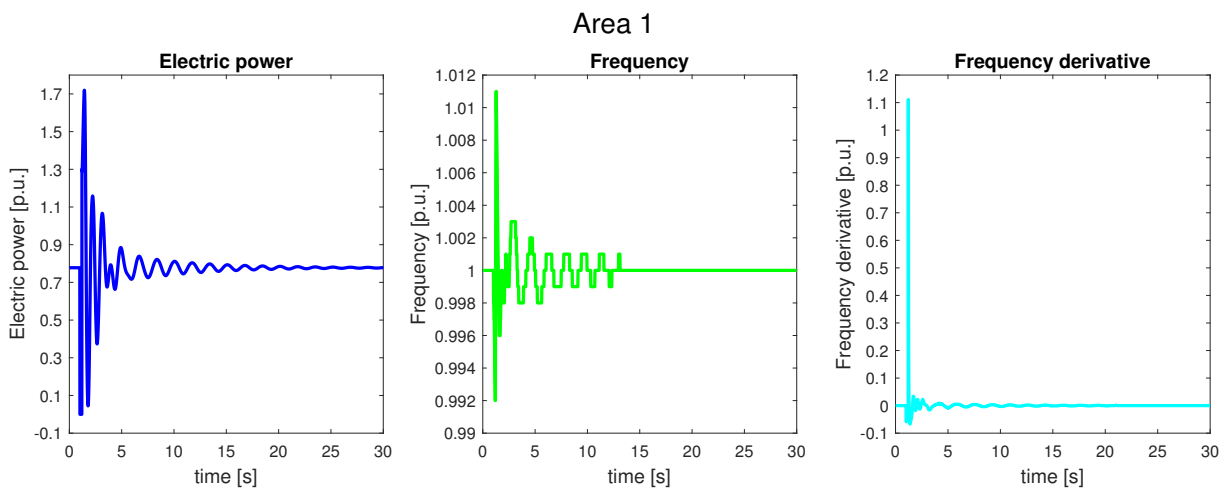


Figure 3.7: Test 1 - Simulation 2 - Area 1 measurements

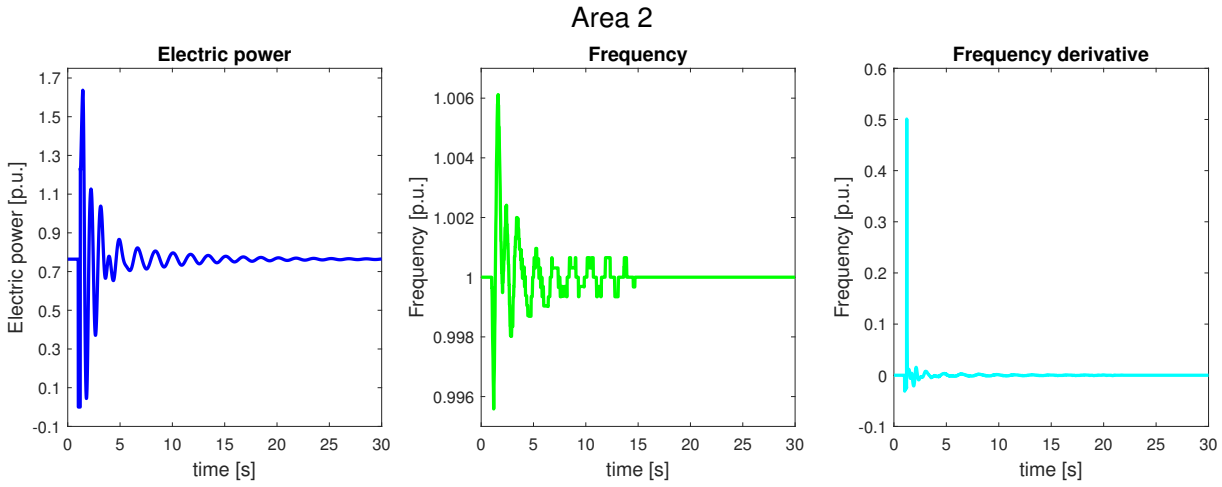


Figure 3.8: Test 1 - Simulation 2 - Area 2 measurements

## RESULTS OF SIMULATION 2

In Figure 3.9, the test's results for estimating inertia are summarized. The result is minus infinite after all the points are fixed at 27 s.

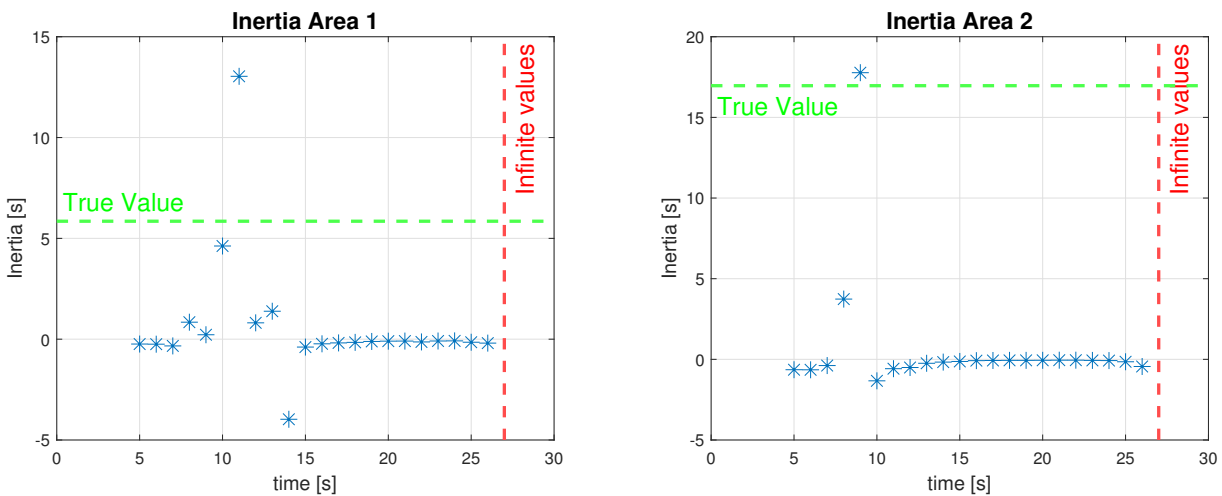


Figure 3.9: Test 1 - Simulation 2 - Inertia trend of Area 1 and Area 2

### 3.1.3. Conclusion of test 1

In Simulation 1, the SINDy algorithm perform well and the result obtained are very close to the true ones. Nevertheless, when we try to exploit SINDy algorithm with the moving window method the result converge to a completely wrong value with many points very far from the point of convergence. These huge different between the results of these two simulations is due to:



- **Availability of the measurements:** in Simulation 1 we were supposed to have one PMU at the terminal of each generator, which nowadays, is not feasible in real-case applications, while in Simulation 2 we suppose a more realistic case of two PMUs that monitor two Areas.
- **Simulation time:** to give these precise results shown in 3.2 in Simulation 1 we perform the SINDy algorithm considering a time window of 30s, instead in Simulation 2 SINDy algorithm is applied considering a time window of 5 s.
- **Sampling time:** this parameter is fundamental for a good inertia estimation. Since increasing the sampling time the step between the different measurements decreases and the computation of the frequency time derivative improves. In Simulation 1 we assume a sampling time of 1 ms that is not realistic for the actual technology, while in Simulation 2 we assume a more realistic sampling time of 20 ms.

## 3.2. Test 2: Removal of mechanical power

The different simulation performed in this test are listed below:

- Simulation 1:  
Comparison of the application of the moving window method considering or not the mechanical power variables in the inertia estimation, during the opening of the line 1.
- Simulation 2:  
Comparison of the application of the moving window method considering or not the mechanical power variables in the inertia estimation, during the opening of the line 8.

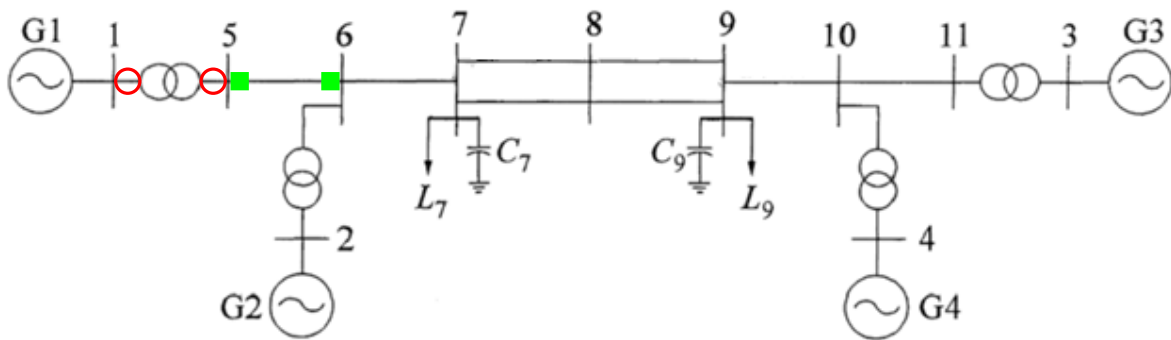
### 3.2.1. Simulation 1

#### DETAILS OF THE SIMULATION 1

**Test system:** described in Section C.1

**Implemented in:** PowerFactory

**Perturbation simulated:** Opening of the line 1



○: Opening/Reclosure    ■: PMUs location

Figure 3.10: Test 2 - Simulation 1 - Test-system

**Simulation time:** 30 s

**Governor:** ON for each generator

**Sampling time:** 20 ms

**PSS:** ON for each generator

**Fault time:** 1 s

**AVR:** ON for each generator

**Clear time:** 1.2 s

The Test-system is divided in two areas, characterized by their own inertia, separated in the same way done in Figure 3.5 and with the same value of the Table 3.3.

This simulation is useful to understand the impact, in the inertia estimation, of the mechanical power. The mechanical power is not measurable using the PMUs, so defining a method that works using the measurements of electric power, frequency and mechanical power cannot be implemented in a real application.

For this reason, in this simulation, we perform a comparison between the moving window method with and without the knowledge of mechanical power measurements.

The inertia trend is estimated considering the moving window method in which the inertia is estimated using the *mldivide* algorithm described in Section 2.2.

The trend of main parameters of the generators during the simulation are the same of the Figure 3.6. The trend of the variable used for the estimation of the inertia represented in Figure 3.11 and Figure 3.12 are the same of the Figure 3.7 and Figure 3.8 considering also the trend of the mechanical power. For sake of simplicity the figures are reported in the following:

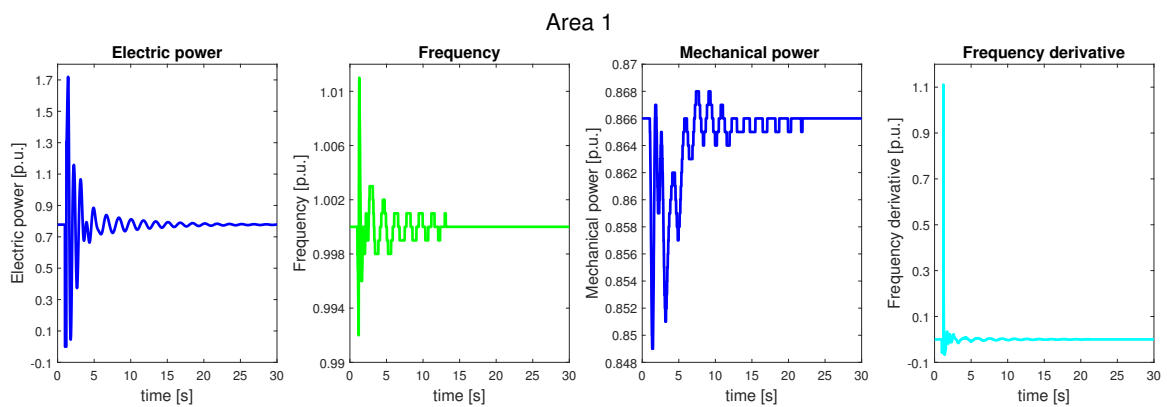


Figure 3.11: Test 2 - Simulation 1 - Area 1 measurements

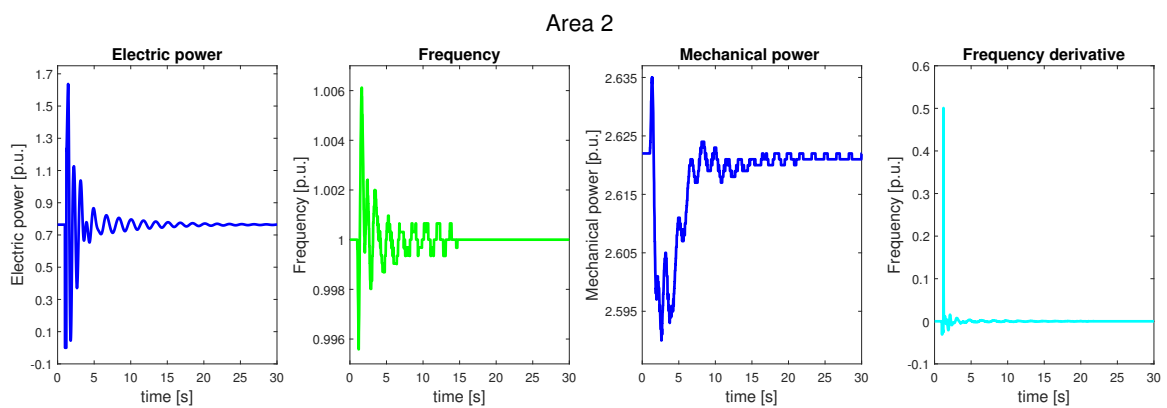


Figure 3.12: Test 2 - Simulation 1 - Area 2 measurements

The considered variables are that one recorded by PMUs, the mechanical power and the derivative of the frequency, that is computed using the method explained in Appendix A.1.

### RESULTS OF SIMULATION 1

The result of this test, in the estimation of the inertia, are summarized in Figure 3.13.

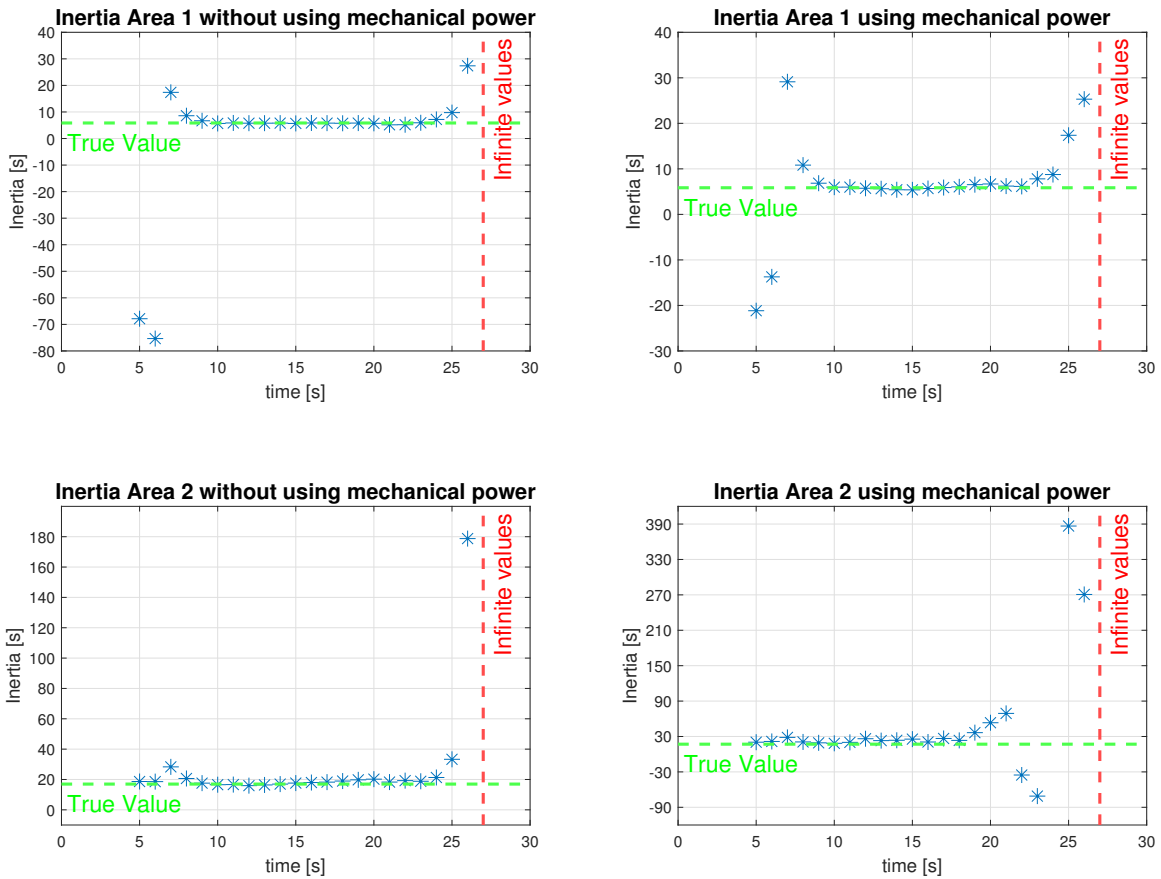


Figure 3.13: Test 2 - Simulation 1 - Inertia trend of Area 1 and Area 2

All the points, after the red line fixed at 27 s, give as result infinite.

By analysing the trend of the inertia in both cases, it is apparent that there is a time period when it seems to converge to a specific value.

### 3.2.2. Simulation 2

#### DETAILS OF THE SIMULATION 2

**Test system:** described in Section C.1

**Implemented in:** PowerFactory

**Perturbation simulated:** Opening and reclosure of line 8

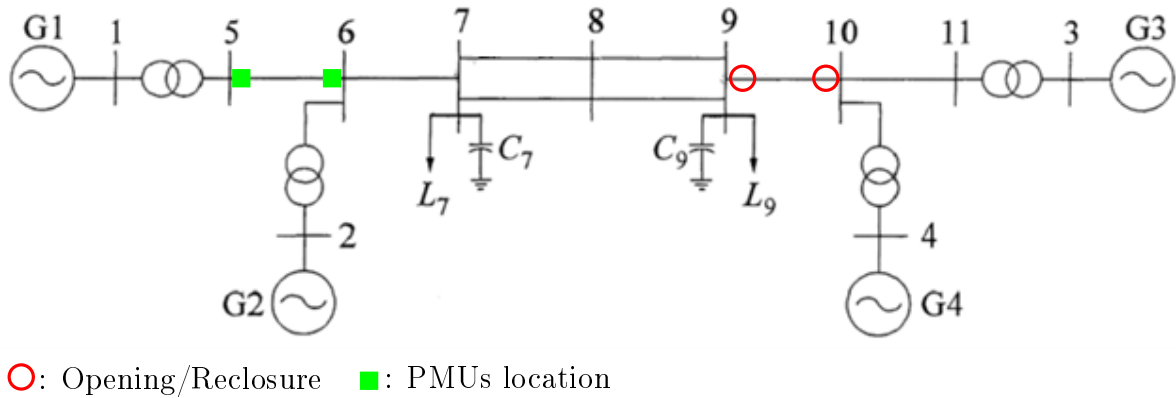


Figure 3.14: Test 2 - Simulation 2 - Test-system

**Simulation time:** 30 s

**Governor:** ON for each generator

**Sampling time:** 20 ms

**PSS:** ON for each generator

**Fault time:** 1 s

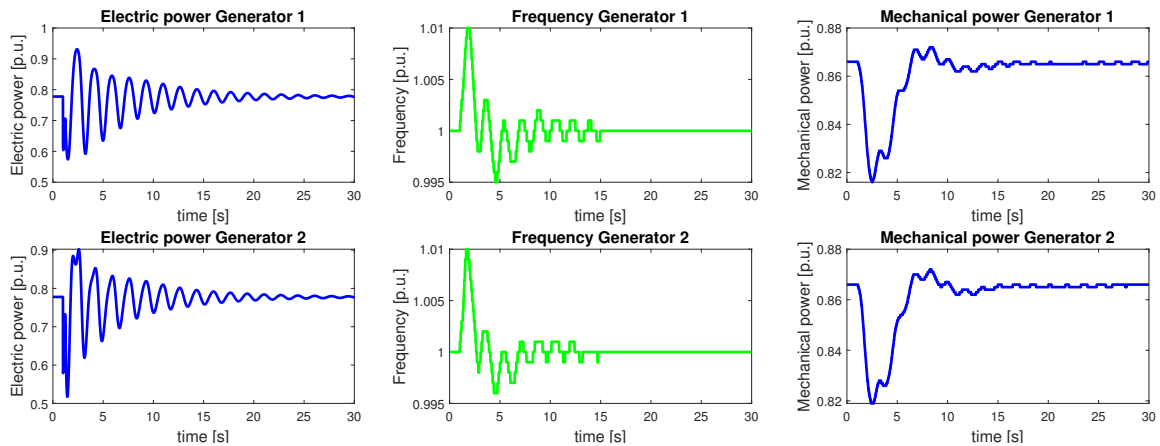
**AVR:** ON for each generator

**Clear time:** 1.2 s

The Test-system is divided in two areas, characterized by its own inertia, separated in the same way done in Figure 3.5 and with the same value of the Table 3.3.

In this simulation we perform the same computation of the previous one considering the opening and reclosure of line 8.

The trends of the generators main parameters during the simulation are reported as shown in Figure 3.2.



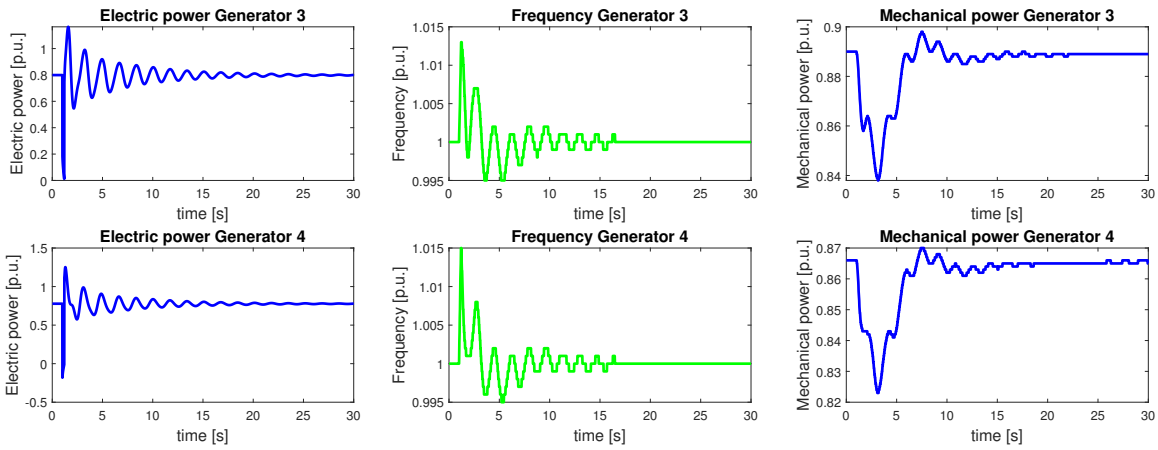


Figure 3.15: Test 2 - Simulation 2 - Main parameters of the system generators during the perturbation

The trends of the variables recorded by the PMUs are shown in Figure 3.7 and Figure 3.8

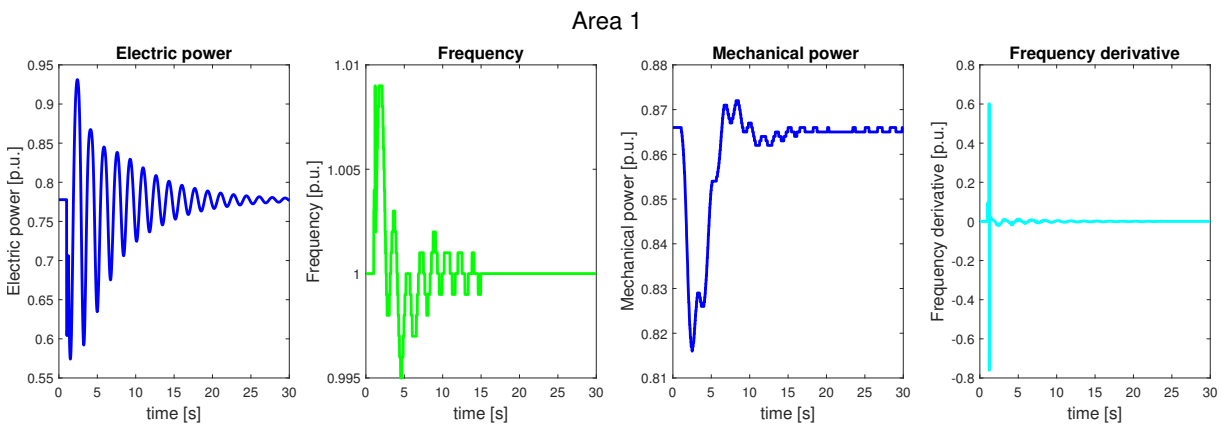


Figure 3.16: Test 2 - Simulation 2 - Area 1 measurements

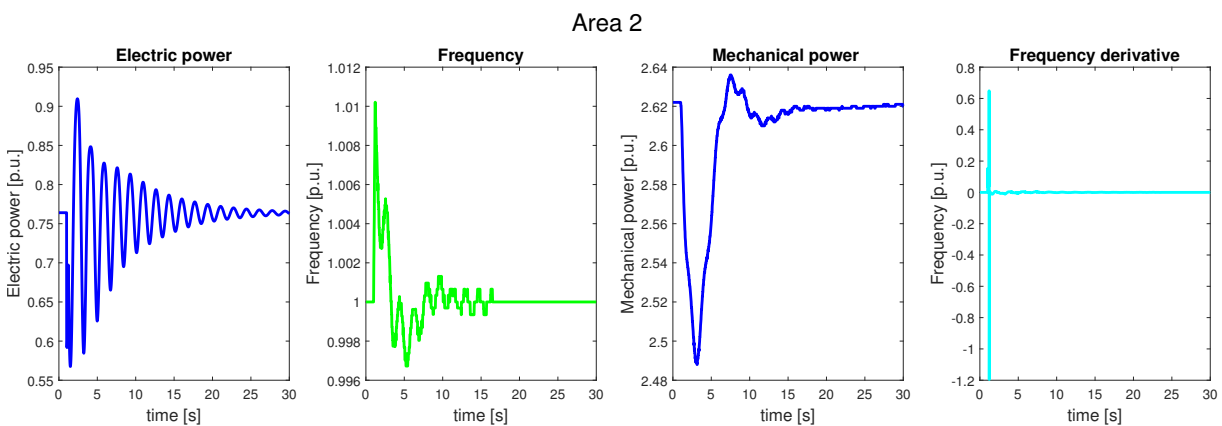


Figure 3.17: Test 2 - Simulation 2 - Area 2 measurements

## RESULTS OF SIMULATION 2

The result of this test, in the estimation of the inertia, are summarized in Figure 3.18. All the points, after the red line fixed at 29 s, give as result infinite.

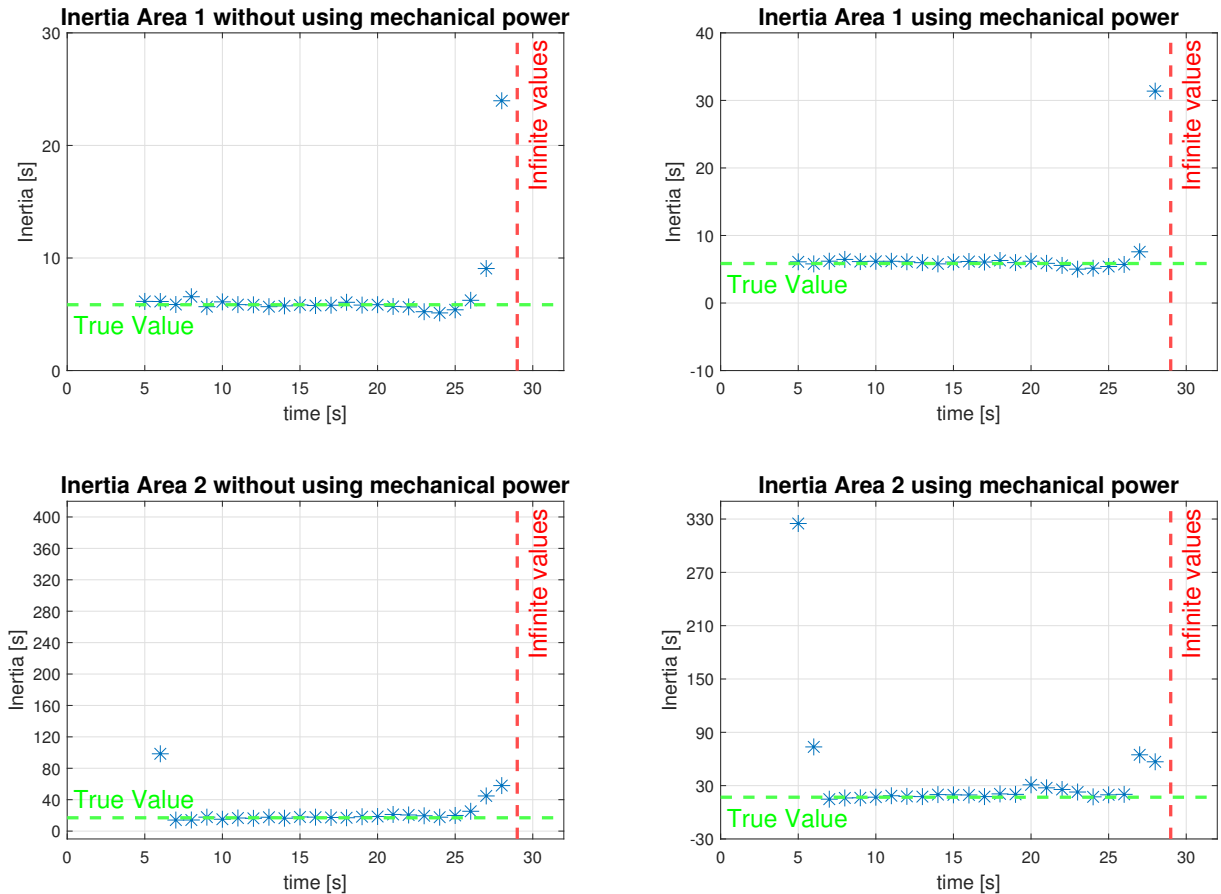


Figure 3.18: Test 2 - Simulation 2 - Inertia trend of Area 1 and Area 2

### 3.2.3. Conclusion of test 2

The results of the two simulations highlight that the presence of the mechanical power variables in the estimation of the inertia is not so relevant. Indeed, in both simulations, the algorithm can converge close to the true value without using the mechanical power variables in the computations. For this reason, in the following tests, the mechanical power variables are excluded by the estimation of the inertia. In this way, we obtain the same result, but a more realistic condition is considered since all the other variables used can be measured or calculated from the ones measured.

### 3.3. Test 3: MATLAB algorithms comparison

The different simulation performed in this test are listed below:

- Simulation 1:  
The algorithms listed in Section 2.2 are applied to estimate the inertia of each machine of the system, considering an ideal condition with a single time windows of 30 s.
- Simulation 2:  
The algorithms listed in Section 2.2 are applied for the inertia estimation in the moving window method to estimate the equivalent inertia of two areas.

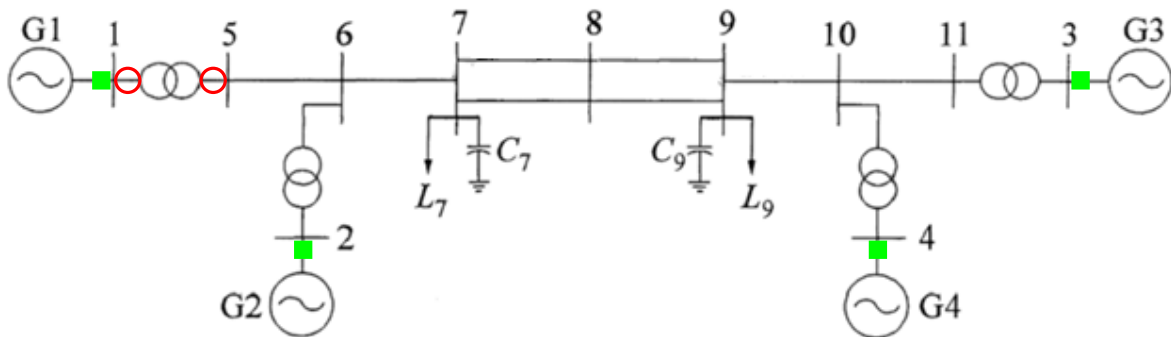
#### 3.3.1. Simulation 1

##### DETAILS OF THE SIMULATION 1

**Test system:** described in Section C.1

**Implemented in:** MATLAB

**Perturbation simulated:** Opening of the line 1



○: Opening/Reclosure    ■: PMUs location

Figure 3.19: Test 3 - Simulation 1 - Test-system

**Simulation time:** 30 s

**Governor:** ON for each generator

**Sampling time:** 20 ms

**PSS:** OFF for each generator

**Fault time:** 1 s

**AVR:** OFF for each generator

**Clear time:** 1.2 s

In this test, the algorithms listed in Section 2.2 are compared to define which of these work best in the estimation of the inertia.

In particular, the algorithm compared are:



- Least-Squares regression (mldivide)
- Moore-Penrose pseudoinverse (pinv)
- Fit robust linear regression (rfit)
- Singular value decomposition (SVD)
- Least Absolute Shrinkage and Selection Operator (LASSO)

The variables recorded in this simulation are the generated power and frequency of each generator. The trends of the generators's main parameters during the simulation are reported in Figure 3.2. The parameters used for the estimation of the inertia are the electric power and the frequency described in Figure 3.2, plus the frequency derivatives that are computed with the method shown in Appendix A.1. The trend of the frequency derivative are represented in Figure 3.3.

The true values of inertia of each machine of the system are:

	<b>H [s]</b>
<b>Generator 1</b>	5,85
<b>Generator 2</b>	5,85
<b>Generator 3</b>	5,558
<b>Generator 4</b>	5,558

Table 3.4: Test 3 - Simulation 1 - True values of inertia

## RESULTS OF SIMULATION 1

The estimation results, using the different algorithm, are listed in the Table 3.5.

	<b>mldivide</b>		<b>pinv</b>		<b>SVD</b>	
	<b>H [s]</b>	<b>Error [%]</b>	<b>H [s]</b>	<b>Error [%]</b>	<b>H [s]</b>	<b>Error [%]</b>
<b>Generator 1</b>	5,756	-1,601	5,756	-1,601	5,756	-1,601
<b>Generator 2</b>	5,7	-2,577	5,7	-2,577	5,7	-2,577
<b>Generator 3</b>	5,228	-5,936	5,228	-5,936	5,228	-5,936
<b>Generator 4</b>	5,254	-5,461	5,254	-5,461	5,254	-5,461
	<b>rfit</b>		<b>LASSO</b>			
	<b>H [s]</b>	<b>Error [%]</b>	<b>H [s]</b>	<b>Error [%]</b>		
<b>Generator 1</b>	5,753	-1,651	5,965	1,967		
<b>Generator 2</b>	5,726	-2,115	5,754	-1,638		
<b>Generator 3</b>	5,341	-3,899	5,922	6,561		
<b>Generator 4</b>	5,452	-1,893	6,088	9,542		

Table 3.5: Test 3 - Simulation 1 - Estimation of inertia

As we can see from the Table 3.5 the result obtained using the first three algorithm are the same. The LASSO algorithm is characterized by the highest percentage error in the estimation and the Fit robust linear regression is the algorithm that gives the best result with the lower percentage error. Another parameter very important in the comparison is the computation time of these algorithms. In the Table the time requested by each algorithm to obtain the result in Table 3.5 is reported.

	<b>mldivide</b>	<b>pinv</b>	<b>SVD</b>	<b>rfit</b>	<b>LASSO</b>
<b>Simulation time</b>	23 ms	14 ms	10 ms	84 ms	21,585 s

Table 3.6: Test 3 - Simulation 1 - Computation times of the considered algorithm

Analysing the result is possible to state that the quicker algorithm is the SVD and that the time requested by the LASSO algorithm is huge compared to the other one.

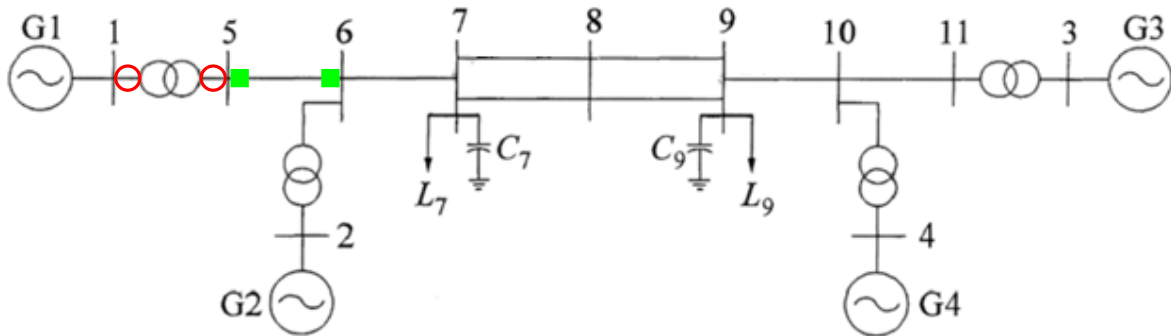
### 3.3.2. Simulation 2

#### DETAILS OF THE SIMULATION 2

**Test system:** described in Section C.1

**Implemented in:** PowerFactory

**Perturbation simulated:** Opening and reclosure of line 1



○: Opening/Reclosure    ■: PMUs location

Figure 3.20: Test 3 - Simulation 2 - Test-system

**Simulation time:** 30 s

**Sampling time:** 20 ms

**Fault time:** 1 s

**Clear time:** 1.2 s

**Governor:** ON for each generator

**PSS:** ON for each generator

**AVR:** ON for each generator

In this simulation each of the algorithm compared in the previous simulation is exploited in the moving window method.

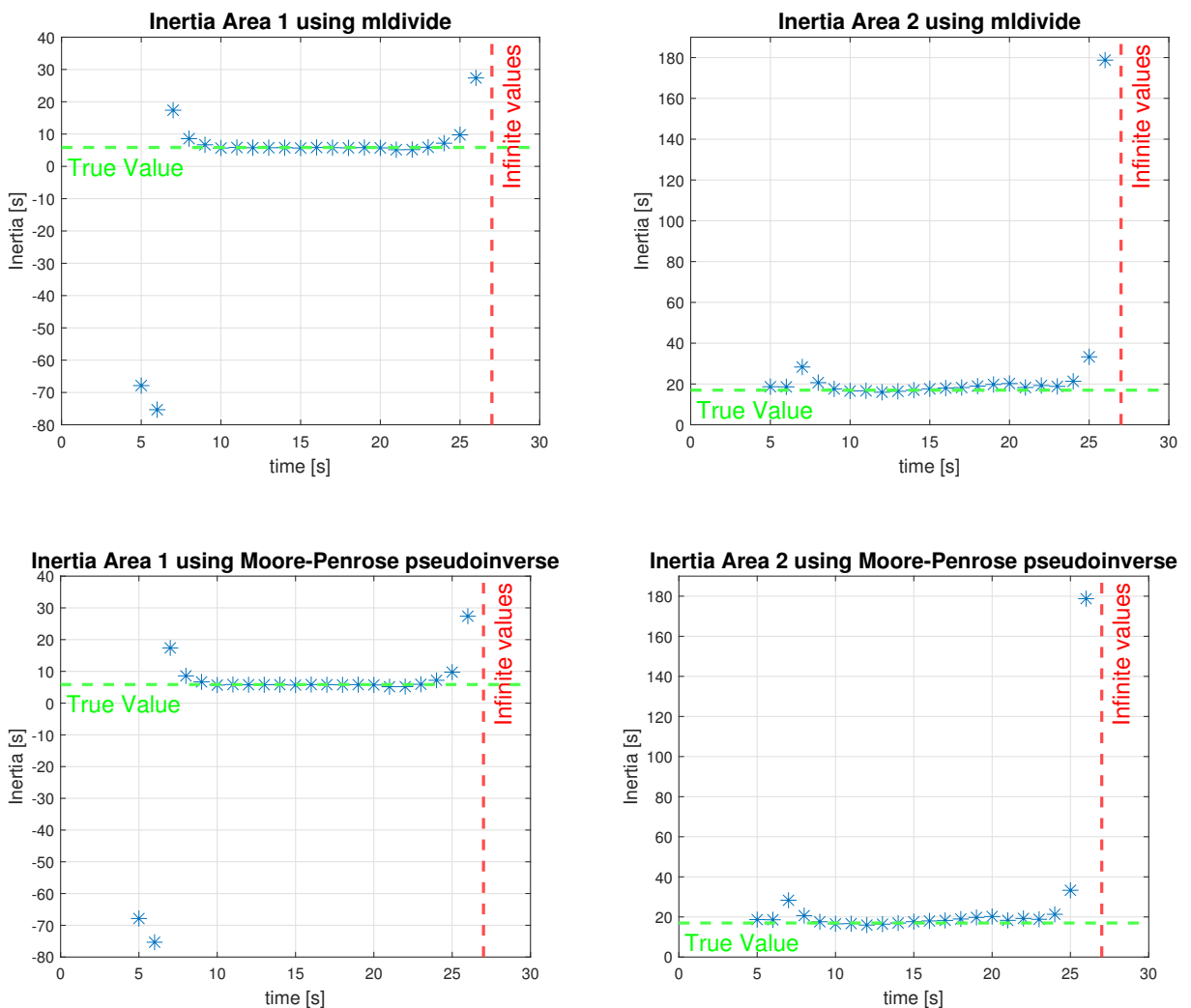
The Test-system is divided in two areas, characterized by its own inertia, separated in the same way done in Figure 3.5 and with the same value of the Table 3.3.

The trend of the main parameters of the generators, the recorded variable by the PMUs and the time derivative of the frequency during the simulation are the same of Figure 3.6, Figure 3.7 and Figure 3.8.

### RESULTS OF SIMULATION 2

The comparison between the different algorithm tested in the estimation of the inertia are summarized in Figure 3.21

All the points, after the red line fixed, give as result infinite.



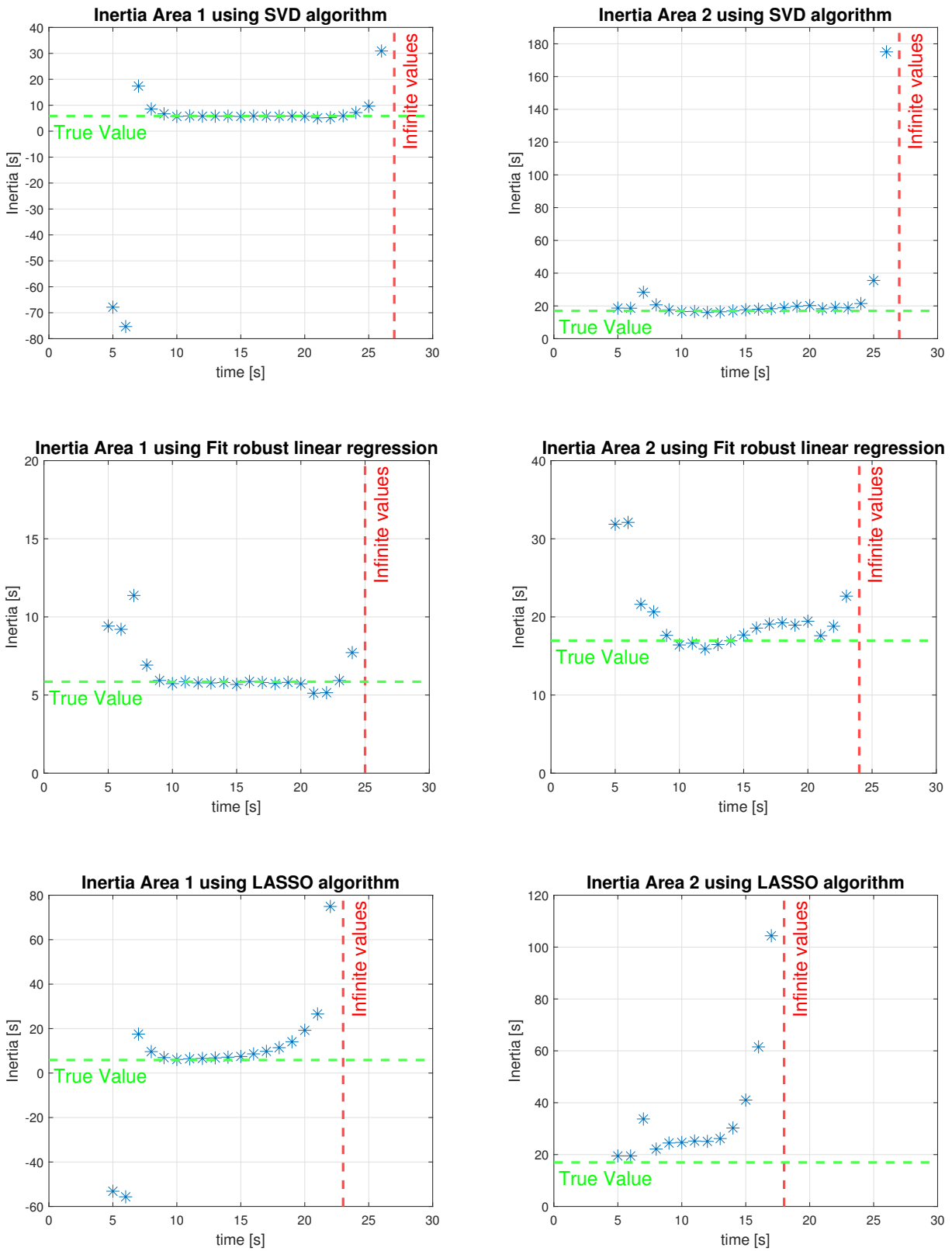


Figure 3.21: Test 3 - Simulation 2 - Inertia trend of Area 1 and Area 2 using different algorithm

In each case, there is an interval of time in which the inertia seems to converge to a specific value. The results of the first three tested algorithms are the same, while the ones of the Fit robust linear regression and LASSO algorithm are different.

The main differences between the two last algorithms tested respect the other ones are:

- **Fit robust linear regression:** is slightly more precise concerning the other algorithms, especially during the perturbation. Nevertheless, its result tends to be infinite, when the transient is close to the end, sooner than in `mldivide`, Moore-Penrose pseudoinverse and SVD algorithm.
- **LASSO algorithm:** using this algorithm the convergence is less evident, especially in the Area 2 result. Furthermore, as found for the Fit robust linear regression algorithm, the values tend to be infinite sooner than in the first three algorithms exposed.

### 3.3.3. Conclusion of test 3

Simulation 1 permits a more conscious choice of the algorithm to use for the inertia estimation and highlights the strengths and weaknesses of each algorithm. The LASSO algorithm since its low precision and its very high running time is outclassed by all the other algorithms. The Fit robust linear regression is the algorithm with the highest precision, but its computational burden is much higher than the first three algorithms analyzed. Therefore, for the analysis of a very large amount of data we need to consider that its computational burden will be very higher. Finally, the `mldivide`, Moore-Penrose pseudoinverse and SVD algorithm merged the necessity of a precise result and low simulation time. Regarding simulation 2, we have the confirmation that even using the moving window method, the results of the Least-Squares regression, Moore-Penrose pseudoinverse and SVD algorithm are the same. If the computational burden is not so high a good alternative for this algorithm is the Fit robust linear regression. Instead, after these two simulations we can state that due to its lower precision and higher running time, the LASSO algorithm is the last in terms of performance with respect to the other ones.

### 3.4. Test 4: Opening of a line

The different simulation performed in this test are listed below:

- Simulation 1:  
Moving window method to estimate the inertia trend during the opening of the line 1 is applied.
- Simulation 2:  
Moving window method to estimate the inertia trend during the opening of the line 8 is applied.

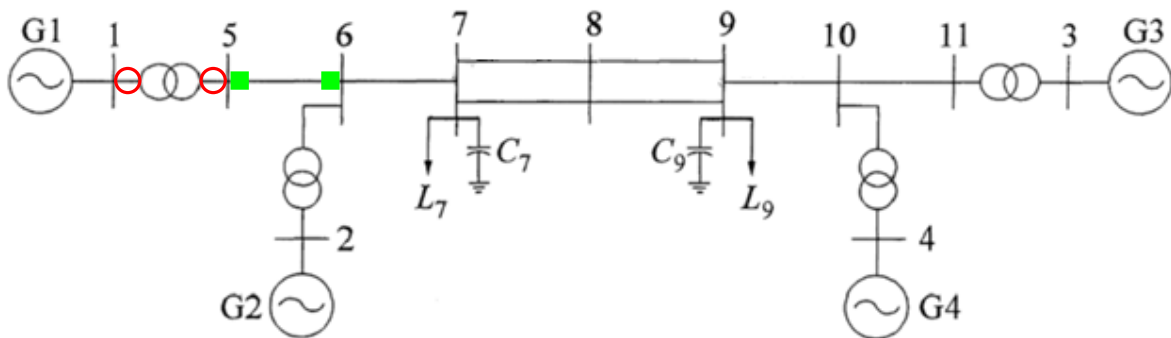
#### 3.4.1. Simulation 1

##### DETAILS OF THE SIMULATION 1

**Test system:** described in Section C.1

**Implemented in:** PowerFactory

**Perturbation simulated:** Opening and reclosure of line 1



○: Opening/Reclosure    ■: PMUs location

Figure 3.22: Test 4 - Simulation 1 - Test-system

**Simulation time:** 30 s

**Governor:** ON for each generator

**Sampling time:** 20 ms

**PSS:** ON for each generator

**Fault time:** 1 s

**AVR:** ON for each generator

**Clear time:** 1.2 s

The Test-system is divided in two areas, characterized by their own inertia, separated in the same way done in Figure 3.5 and with the same value of the Table 3.3.

This section tests the possibility of estimating the inertia of the two equivalent areas of the system, during a perturbation, using only the measurements of the electric power and

frequency recorded by the PMUs.

The inertia trend is estimated considering the moving window method in which the inertia is estimated using the *mldivide* algorithm described in Section 2.2.

Trends for the generators main parameters during in the simulation, are illustrated in Figure 3.6.

As we can see after the disconnection of line 1 at 1 s and its reclosure at 1.2 s, the frequency and the electric power of each machine start to oscillate. After about 25 s the oscillations are damped and the system returns in a steady state.

The inputs useful for the inertia estimation are the variables recorded by the PMUs and the derivative of the frequency that is computed using the method explained in Appendix A.1. The trends of this variables are shown in Figure 3.7 and Figure 3.8.

### RESULTS OF SIMULATION 1

The result of this test, in the estimation of the inertia, are summarized in Figure 3.23

All the points, after the red line fixed at 27 s, give as result infinite.

By analysing the trend of the inertia we can see that in each case there is an interval of time in which the inertia seems to converge to a specific value.

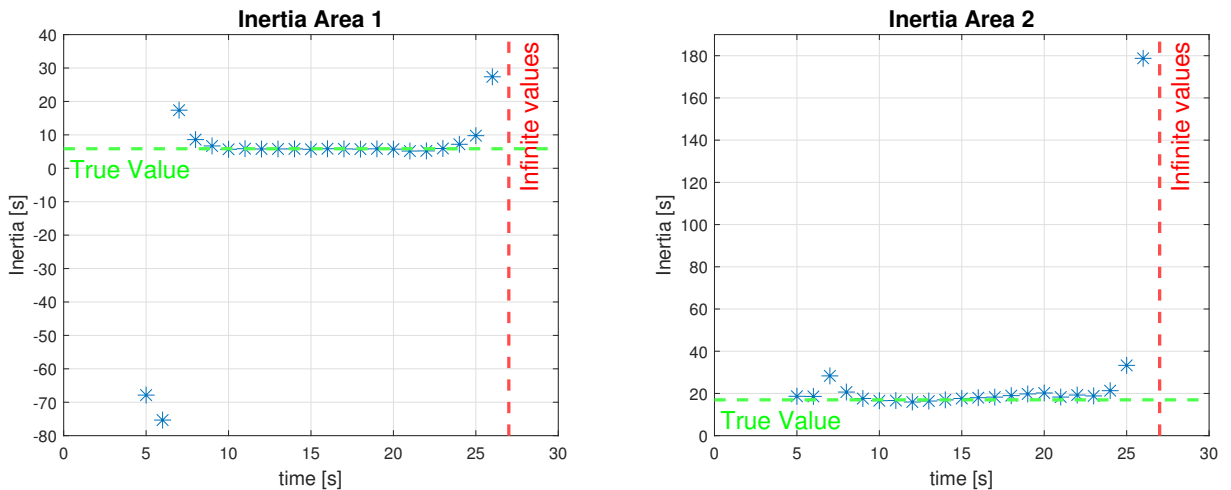


Figure 3.23: Test 4 - Simulation 1 - Inertia trend of Area 1 and Area 2

Studying more in deep the points very far from the convergence point it is interesting to delineate the limits of the method used in this test.

A first limit can be defined when the transient tends to end and the variables become more and more flat. In particular, when the frequency derivative tends to zero, the value of inertia tends to increase till becomes infinite.

Indeed, comparing three different values in different time intervals this increase is visible:

<b>Area 1</b>	<b>Point 18</b>	<b>Point 22</b>	<b>Point 23</b>
<b>H [s]</b>	5,2	27,377	-Inf
<b>Time Interval [s]</b>	17-22	21-26	22-27
<b>Area 2</b>	<b>Point 19</b>	<b>Point 22</b>	<b>Point 23</b>
<b>H [s]</b>	18,822	178.759	-Inf
<b>Time Interval [s]</b>	18-23	21-26	22-27

Table 3.7: Test 4 - Simulation 1 - Last increasing values of inertia of Area 1 and Area 2

After points 18 and 19 the estimated values start to increase till infinite. If we represent graphically, in Figure 3.24, the parameters used for the estimation of the inertia we can easily confirm their flattening.

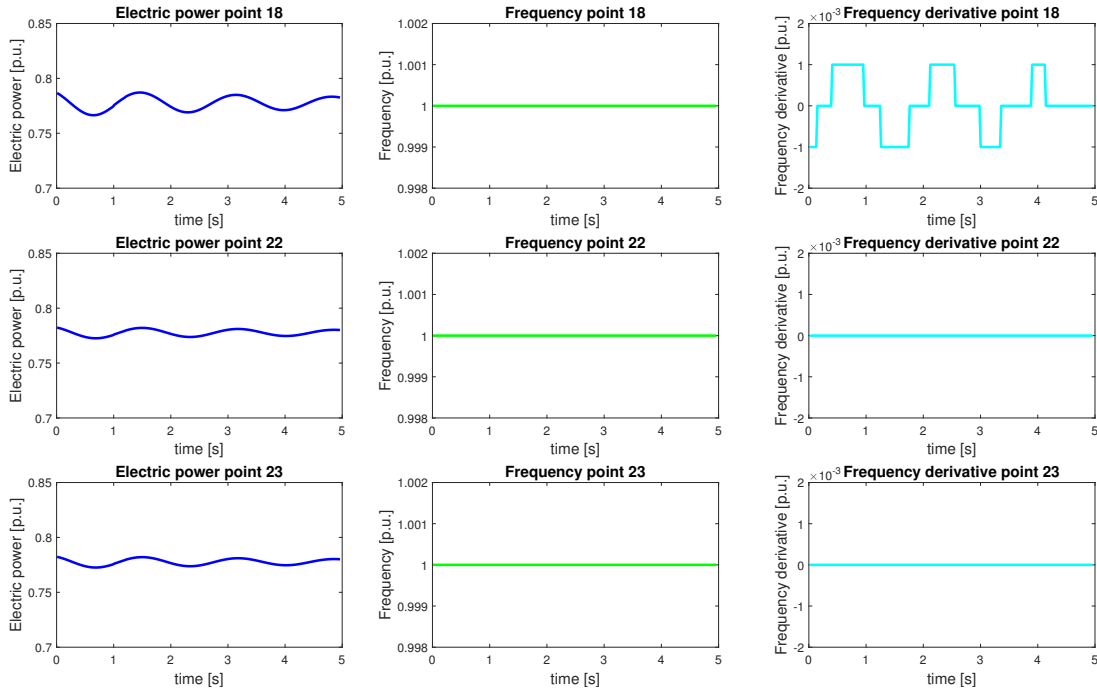


Figure 3.24: Test 4 - Simulation 1 - Increasing value of inertia of Area 1 and Area 2

Another limit is that in the area where the fault occurs, the algorithm takes some seconds to converge. To study better this aspect we consider the first values computed that are described more in deep in Table 3.8 .

<b>Area 1</b>	<b>Point 1</b>	<b>Point 2</b>	<b>Point 3</b>	<b>Point 4</b>	<b>Point 5</b>
<b>H [s]</b>	-67,863	-75,336	17,386	8,584	6,682
<b>Time Interval [s]</b>	0-5	1-6	2-7	3-8	4-9

Table 3.8: Test 4 - Simulation 1 - First increasing value of inertia of Area 1 and Area 2



We can analyse the reason behind this time span before reaching convergence considering the trend of the variable used to compute the first values of inertia of Area 1. The variables trend of the points 1 and 2 are shown in the following figure:

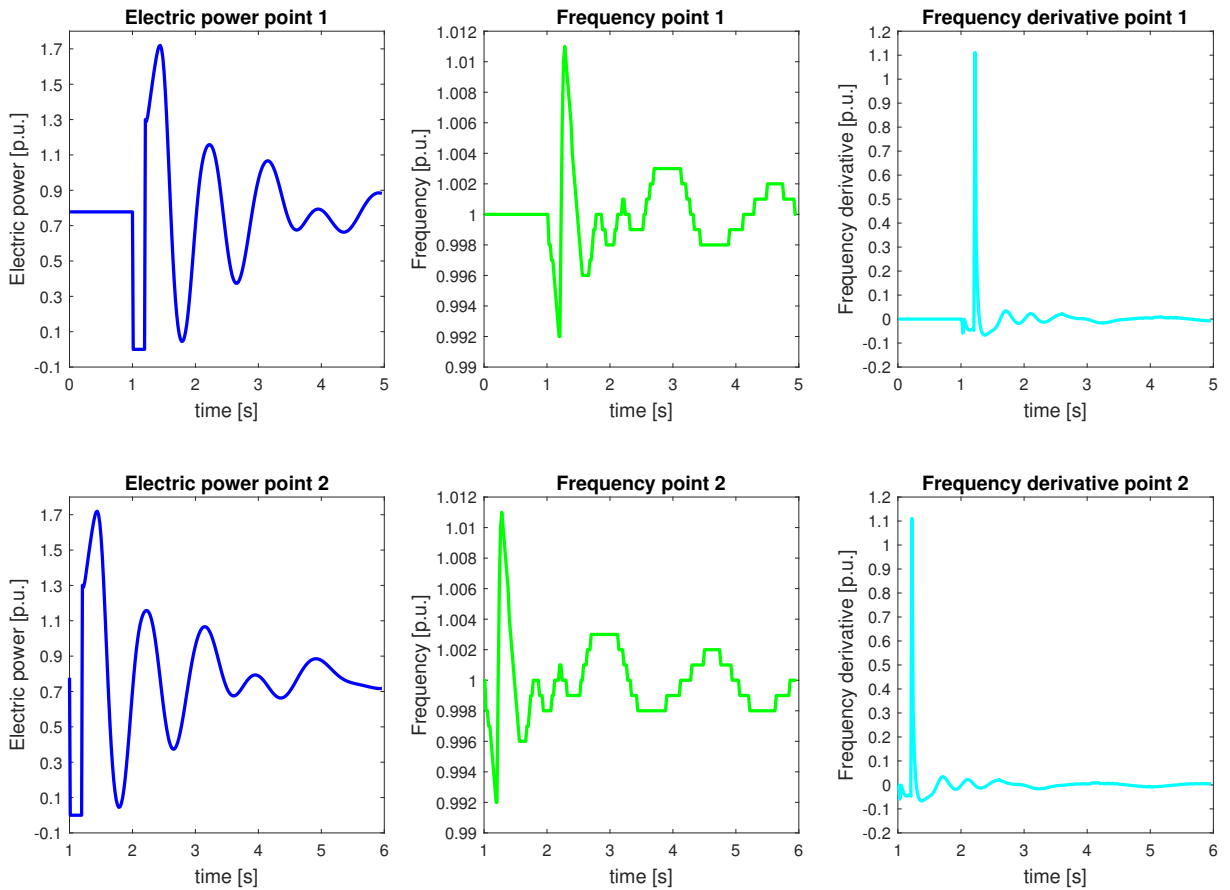


Figure 3.25: Test 4 - Simulation 1 - Variable trend Point 1 and Point 2

In the time interval of these two points, the fault occurs and that leads to a huge error in the inertia estimation.

While in points 3,4 and 5 the algorithm starts to converge, however, these points are far from the value of convergence. The variable trend in the correspondent time interval is shown in Figure 3.26.

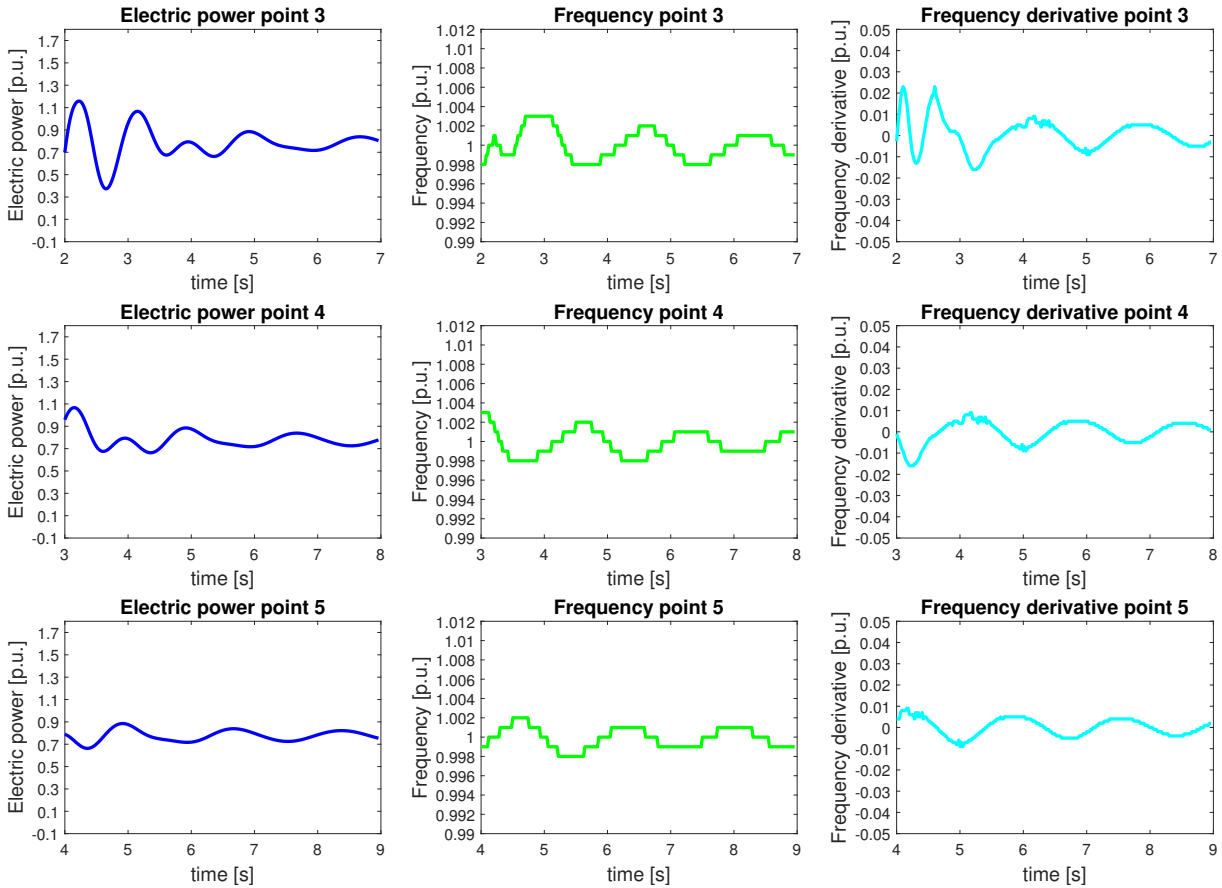


Figure 3.26: Test 4 - Simulation 1 - Variable's trend Point 3,4 and 5

Comparing the Figure 3.26 with Figure 3.27, in which is represented the trend of the variables of point 10, we can obtain important information about the limits of the inertia estimation.

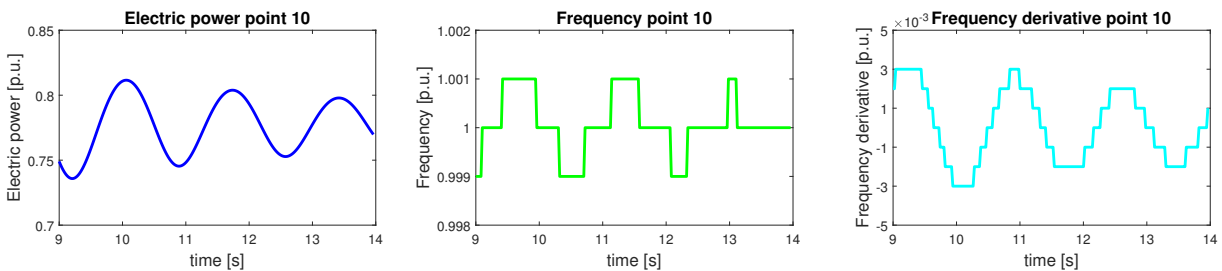


Figure 3.27: Test 4 - Simulation 1 - Variable's trend Point 10

Point 10 is very close to the true value and is one of the points used for the estimation of the mean inertia. As shown in Figure 3.27, in the variables used for the computation of point 10 the oscillations amplitude are lower, but they are more regular.

Therefore, we can reasonably assume that when the oscillations of the trend variables become more regular and sinusoidal the estimation improves.

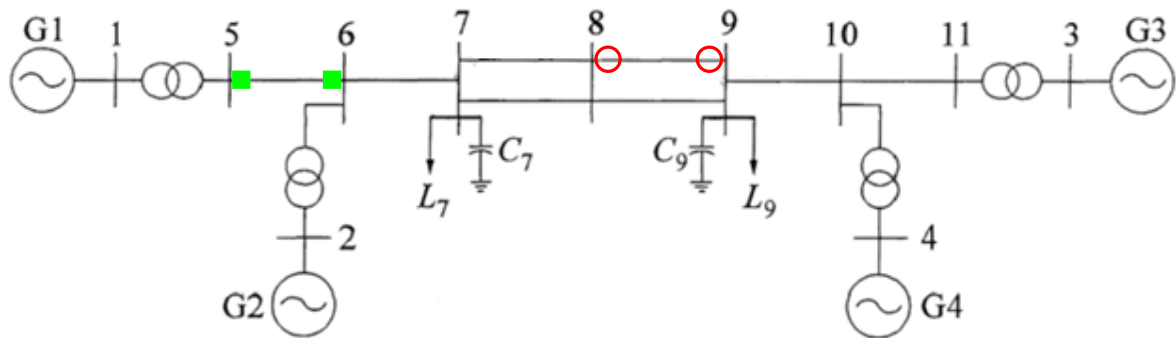
### 3.4.2. Simulation 2

#### DETAILS OF THE SIMULATION 2

**Test system:** described in Section C.1

**Implemented in:** PowerFactory

**Perturbation simulated:** Opening and reclosure of line 10



○: Opening/Reclosure    ■: PMUs location

Figure 3.28: Test 4 - Simulation 2 - Test-system

**Simulation time:** 30 s

**Governor:** ON for each generator

**Sampling time:** 20 ms

**PSS:** ON for each generator

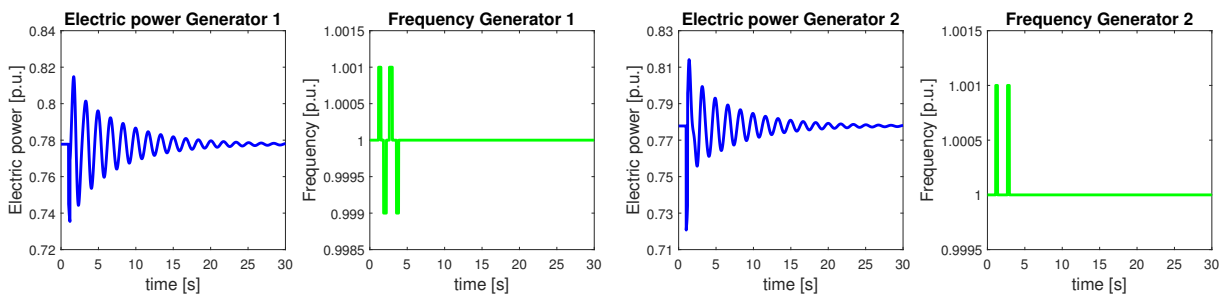
**Fault time:** 1 s

**AVR:** ON for each generator

**Clear time:** 1.2 s

The Test-system is divided in two areas, characterized by its own inertia, separated in the same way done in Figure 3.5 and with the same value of the Table 3.3.

In this simulation we perform the same computation of the previous one considering the opening and reclosure of line 10. The trends of the generator main parameters during the simulation are reported as shown in Figure 3.29.



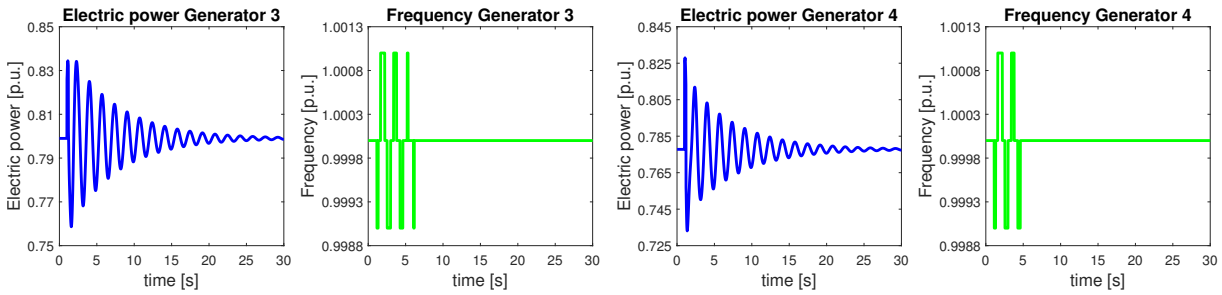


Figure 3.29: Test 4 - Simulation 2 - Main parameters of the system generators during the perturbation

The trends of the variables recorded by the PMUs are shown in Figure 3.30 and Figure 3.31

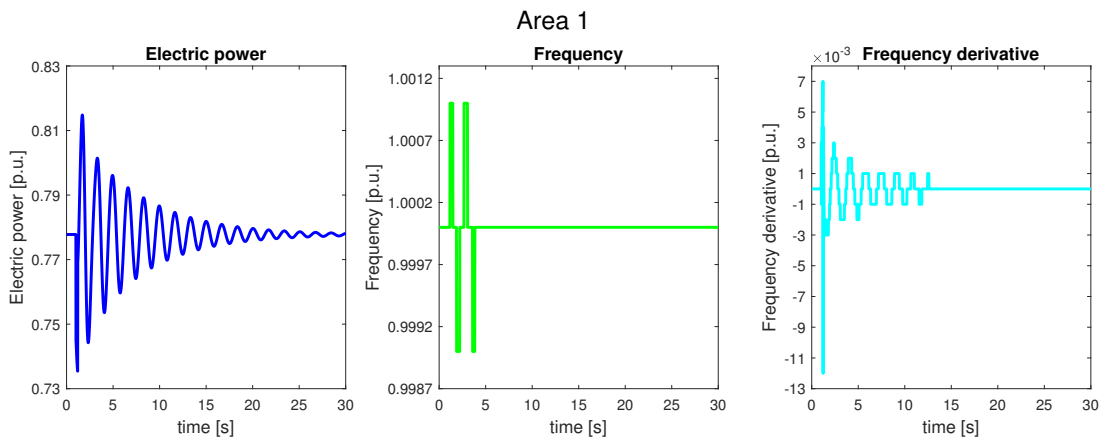


Figure 3.30: Test 4 - Simulation 2 - Area 1 measurements

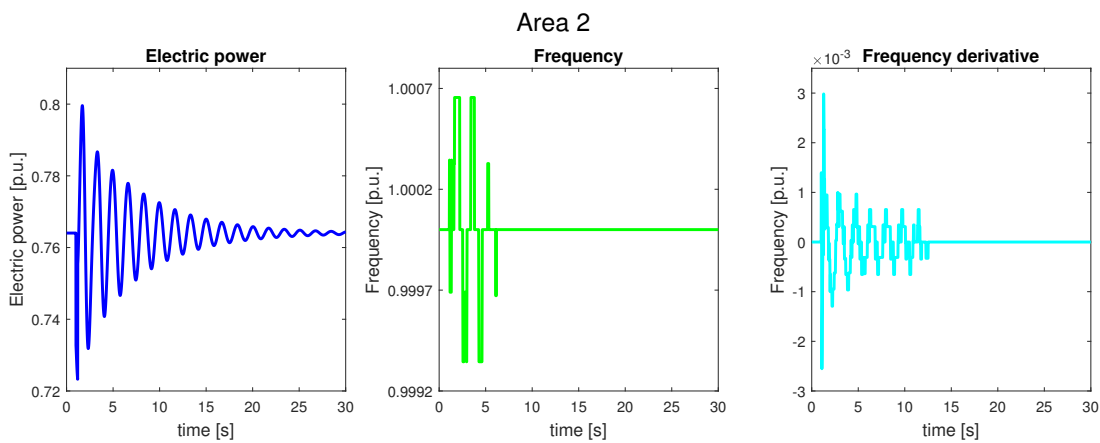


Figure 3.31: Test 4 - Simulation 2 - Area 2 measurements

## RESULTS OF SIMULATION 2

The result of this test, in the estimation of the inertia, are summarized in Figure 3.32. All the points, after the red line fixed at 18 s, give as result infinite.

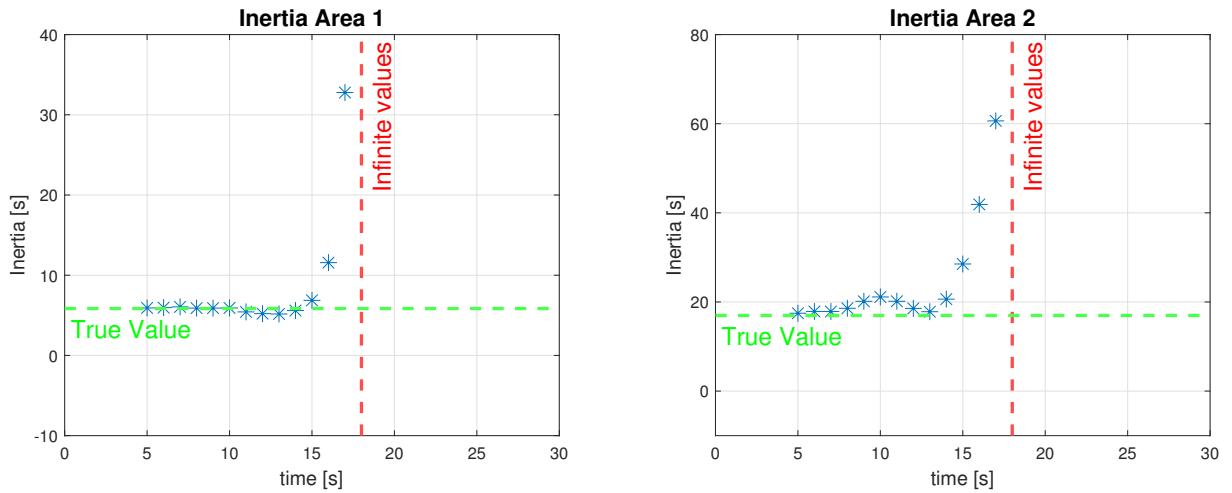


Figure 3.32: Test 4 - Simulation 2 - Inertia trend of Area 1 and Area 2

### 3.4.3. Conclusion of test 4

This test proves that using the Moving window method is possible to identify a convergence point of the inertia after a perturbation as the opening of a line.

Moreover, we show that this method fails in the estimation of the inertia when:

- The variables have large oscillations or peaks in their developments, in particular during the perturbation
- The transient ends and the variables trend becomes flat

### 3.5. Test 5: Trig of a load

The different simulation performed in this test are listed below:

- Simulation 1:  
Moving window method to estimate the inertia trend during the trig and reclosure of load 7 is applied.
- Simulation 2:  
Moving window method to estimate the inertia trend during the trig and reclosure of load 9 is applied.

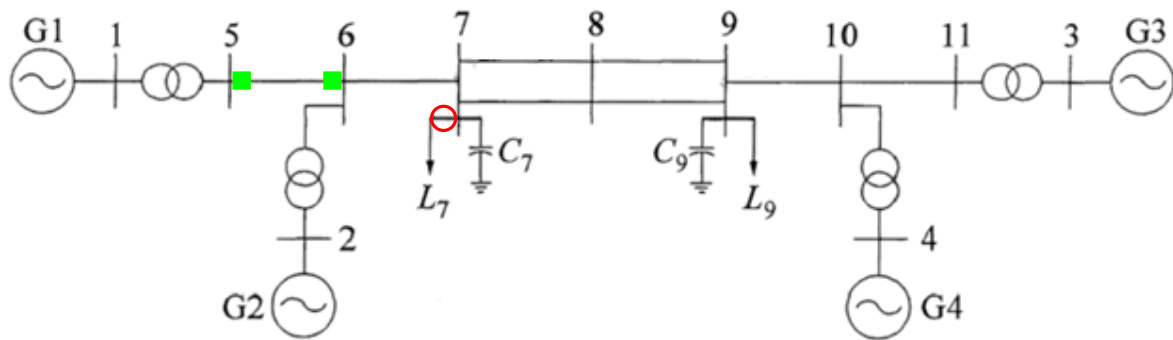
#### 3.5.1. Simulation 1

##### DETAILS OF THE SIMULATION 1

**Test system:** described in Section C.1

**Implemented in:** PowerFactory

**Perturbation simulated:** Trig and reclosure of load 7



○ : Trig/Reclosure      ■ : PMUs location

Figure 3.33: Test 5 - Simulation 1 - Test-system

**Simulation time:** 30 s

**Governor:** ON for each generator

**Sampling time:** 20 ms

**PSS:** ON for each generator

**Fault time:** 1 s

**AVR:** ON for each generator

**Clear time:** 1.2 s

The Test-system is divided in two areas, characterized by its own inertia, separated in the same way done in Figure 3.5 and with the same value of the Table 3.3.

In this test, we study the feasibility of estimating the equivalent area inertia of the system

during the disconnection and the reclosure of the load connected at the bus 7. The trends of the generator main parameters during the simulation are reported as shown in Figure 3.34.

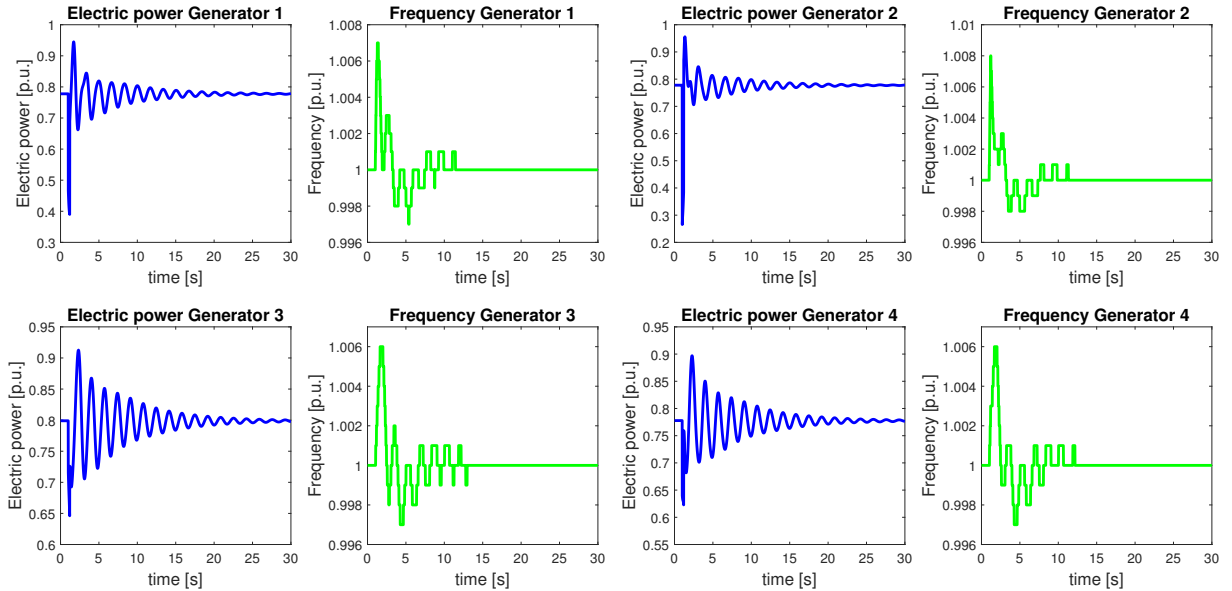


Figure 3.34: Test 5 - Simulation 1 - Main parameters of the system generators during the perturbation

The disconnection of the load and its reclosure start the oscillation of the generator variables. In the Figure 3.34 we can see that the oscillations are damped about 15-20 s after the perturbation. The parameters useful for the inertia estimation are the variables recorded by the PMUs and the derivative of the frequency that is computed using the method explained in Appendix A.1. The trends of this variables are shown in Figure 3.35 and Figure 3.36.

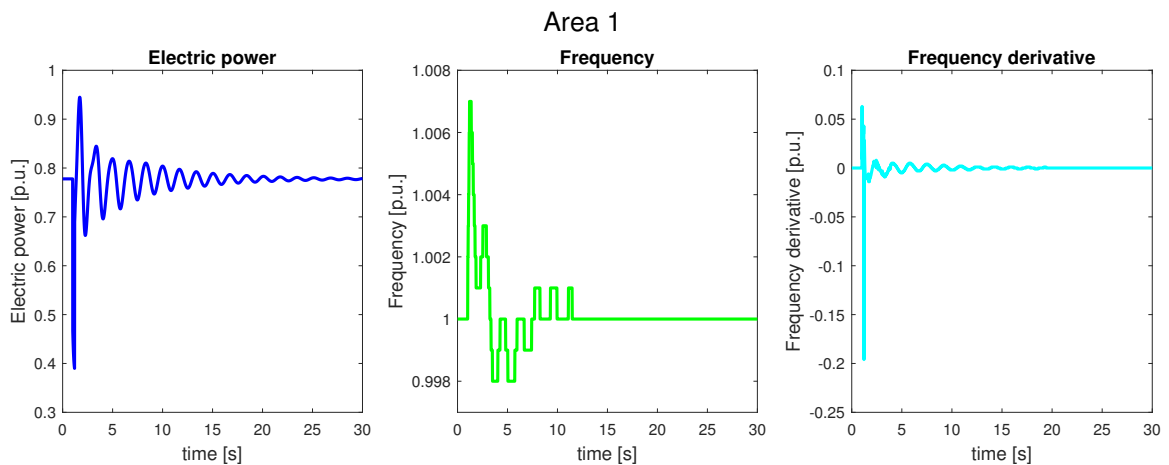


Figure 3.35: Test 5 - Simulation 1 - Area 1 parameters

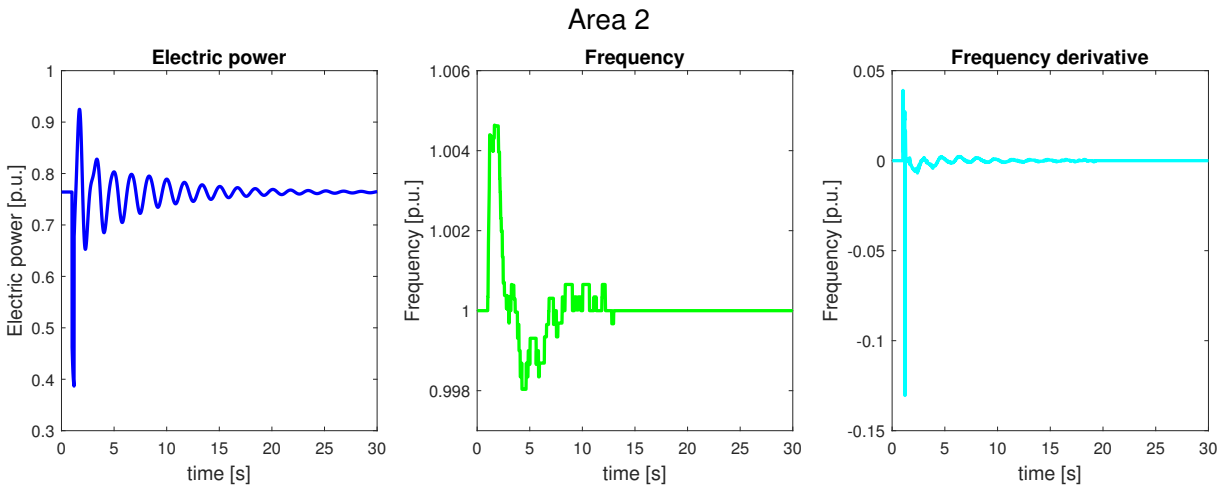


Figure 3.36: Test 5 - Simulation 1 - Area 2 parameters

## RESULTS OF SIMULATION 1

The result of this test, in the estimation of the inertia, are summarized in Figure 3.37.

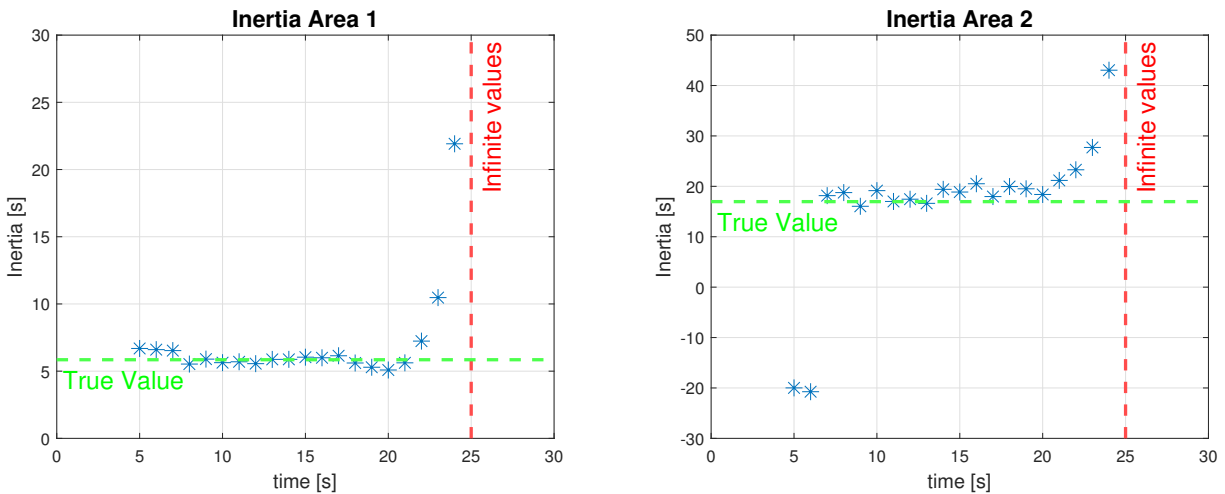


Figure 3.37: Test 5 - Simulation 1 - Inertia trend of Area 1 and Area 2

All the points, after the red line fixed at 25 s, give as result infinite.

Analysing the inertia's trend reveals that there is a time interval when it seems to converge to a specific value.

In the inertia trend of Area 2 we can distinguish:

- **Fault phase**: the inertia estimated is negative
- **Convergence phase**: the method start to converge to a precise value



- **End of the transient:** the inertia starts to increase since the oscillations becomes more and more damped

### 3.5.2. Simulation 2

#### DETAILS OF THE SIMULATION 2

**Test system:** described in Section C.1

**Implemented in:** PowerFactory

**Perturbation simulated:** Trig and reclosure of load 9

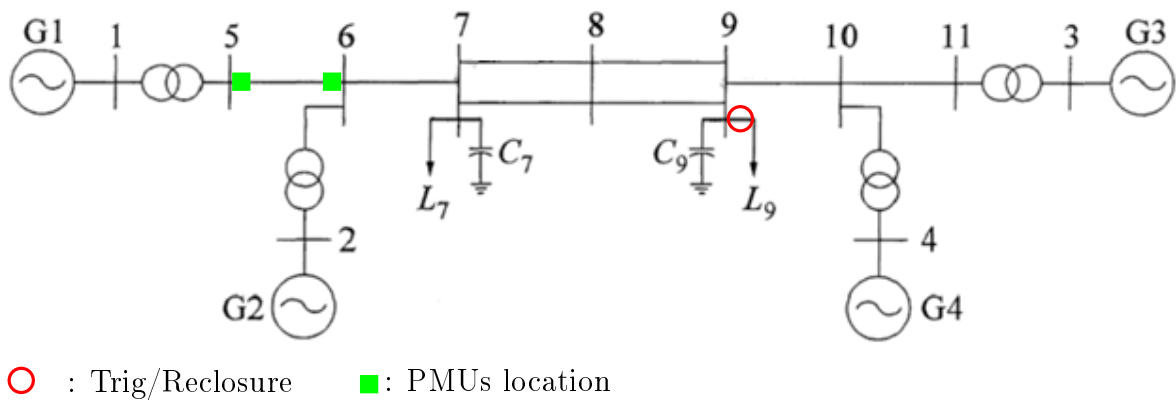


Figure 3.38: Test 5 - Simulation 2 - Test-system

**Simulation time:** 30 s

**Governor:** ON for each generator

**Sampling time:** 20 ms

**PSS:** ON for each generator

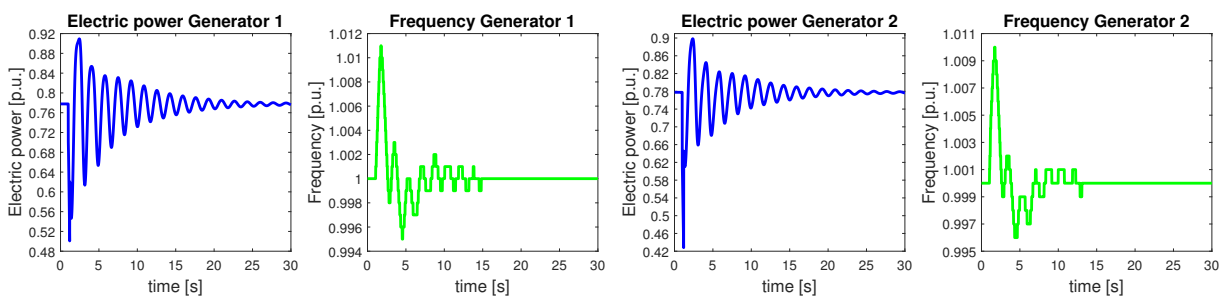
**Fault time:** 1 s

**AVR:** ON for each generator

**Clear time:** 1.2 s

The Test-system is divided in two areas, characterized by its own inertia, separated in the same way done in Figure 3.5 and with the same value of the Table 3.3.

In this simulation we perform the same computation of the previous one considering the disconnection and the reclosure of the load connected at the bus 10. Trends for the generators' main parameters during in the simulation, are illustrated in the next figure.



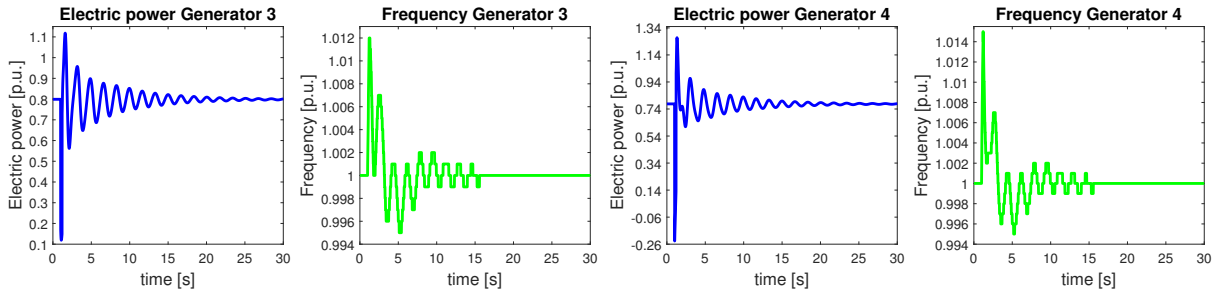


Figure 3.39: Test 5 - Simulation 2 - Main parameters of the system generators during the perturbation

The trends of the variables recorded by the PMUs are shown in Figure 3.40 and Figure 3.41.

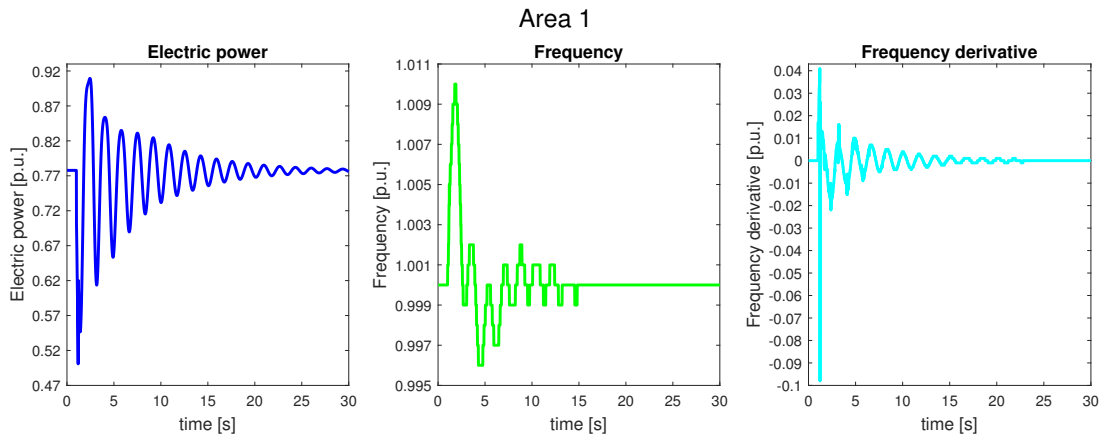


Figure 3.40: Test 5 - Simulation 2 - Area 1 measurements

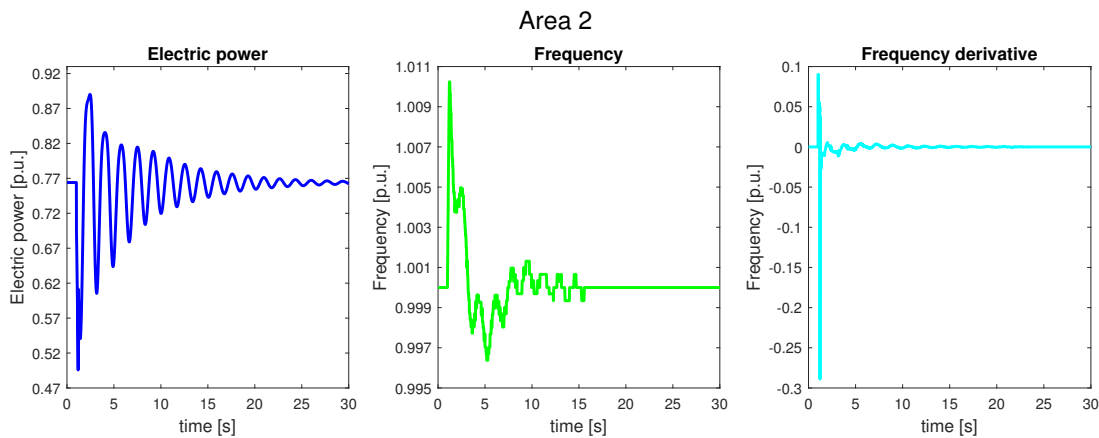


Figure 3.41: Test 5 - Simulation 2 - Area 2 measurements

## RESULTS OF SIMULATION 2

The result of this test, in the estimation of the inertia, are summarized in Figure 3.42. All the points, after the red line fixed at 28 s, give as result infinite.

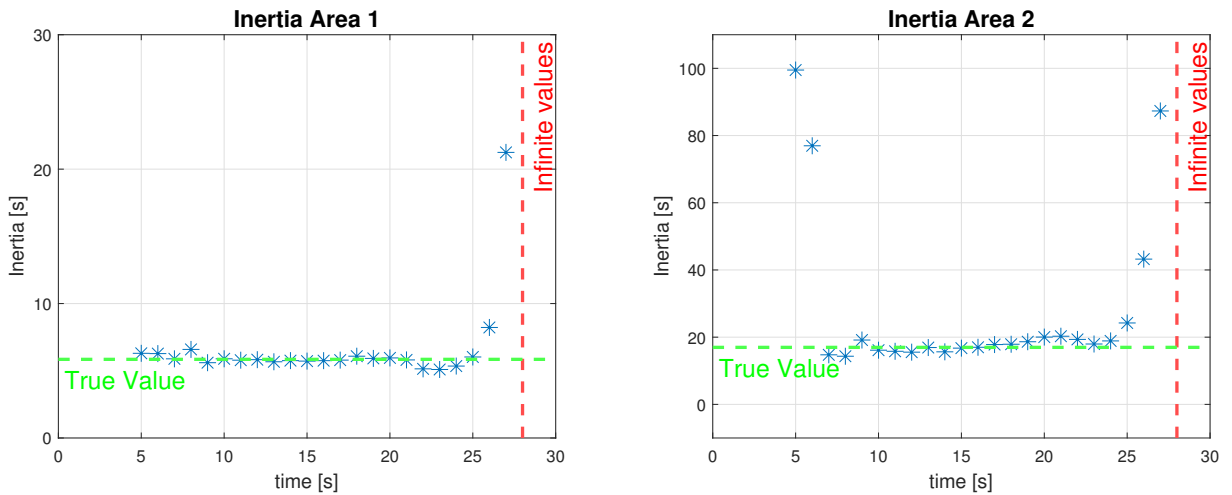


Figure 3.42: Test 5 - Simulation 2 - Inertia trend of Area 1 and Area 2

### 3.5.3. Conclusion of test 5

The results of this test prove that the Floating window method can estimate the inertia of an Area during the trig and reclosure of a load connected to a bus of the system. Also in this case are present the same limits in the estimation of the inertia exposed in the previous chapter.

### 3.6. Test 6: Short-circuit at a bus

The different simulation performed in this test are listed below:

- Simulation 1:  
Moving window method to estimate the inertia trend during a short-circuit at the bus 5 is applied.
- Simulation 2:  
Moving window method to estimate the inertia trend during a short-circuit at the bus 10 is applied.

#### 3.6.1. Simulation 1

##### DETAILS OF THE SIMULATION 1

**Test system:** described in Section C.1

**Implemented in:** PowerFactory

**Perturbation simulated:** Short-circuit at the bus 5

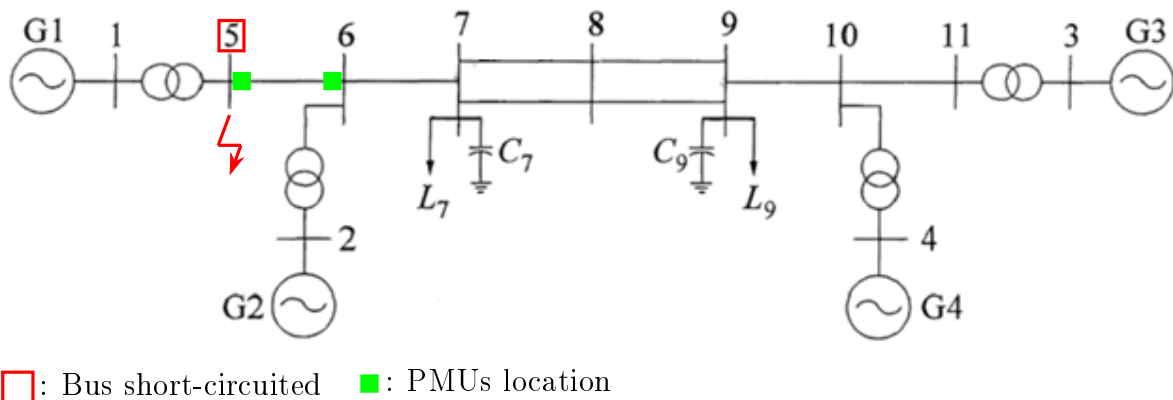


Figure 3.43: Test 6 - Simulation 1 - Test-system

**Simulation time:** 30 s

**Governor:** ON for each generator

**Sampling time:** 20 ms

**PSS:** ON for each generator

**Fault time:** 1 s

**AVR:** ON for each generator

**Clear time:** 1.2 s

The Test-system is divided in two areas, characterized by its own inertia, separated in the same way done in Figure 3.5 and with the same value of the Table 3.3.

Our objective in this test is to determine if it is possible to estimate the inertia of the equivalent areas of the system during an event of short-circuit and its subsequent clearing at the bus 5.

The trends of the generators main parameters during the simulation are reported as shown in Figure 3.44.

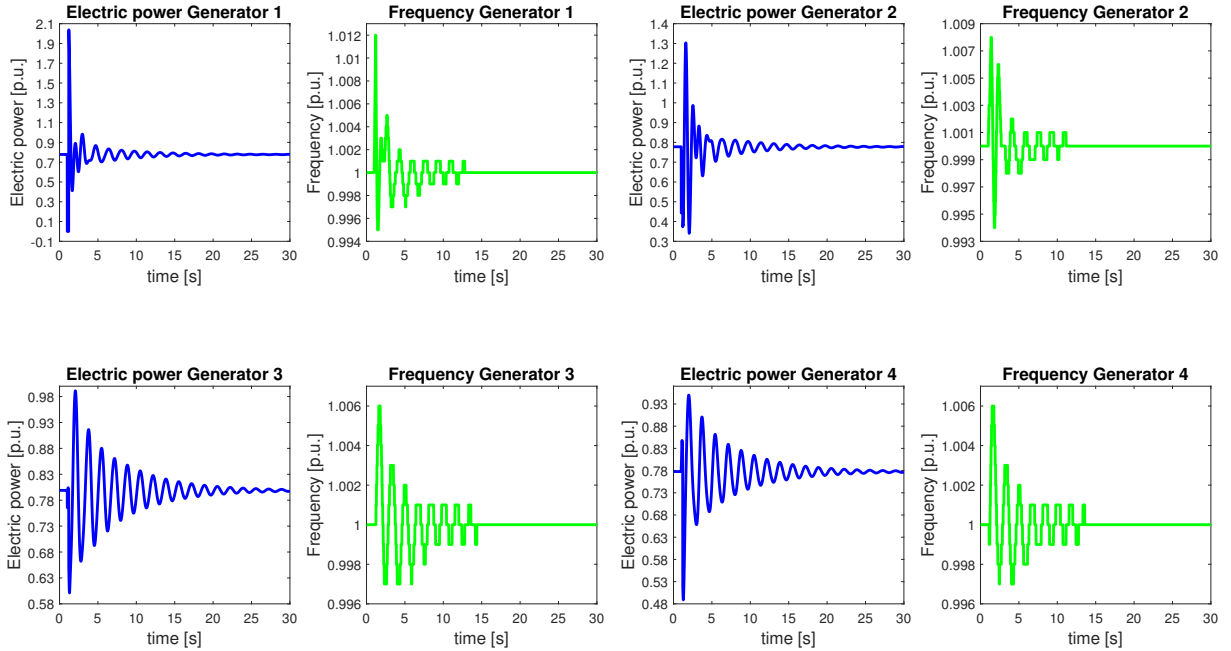


Figure 3.44: Test 6 - Simulation 1 - Main parameters of the system generators during the perturbation

The generator variables start oscillating when the shortcircuit is established and cleared. After the perturbation, the oscillations in Figure 3.44 become damped for about 20-25 seconds. The variables recorded by the PMUs and the derivative of the frequency, that is computed using the method explained in Appendix 1, are the parameters that are useful for inertia estimation. Figure 3.45 and Figure 3.46 display the trends of these variables.

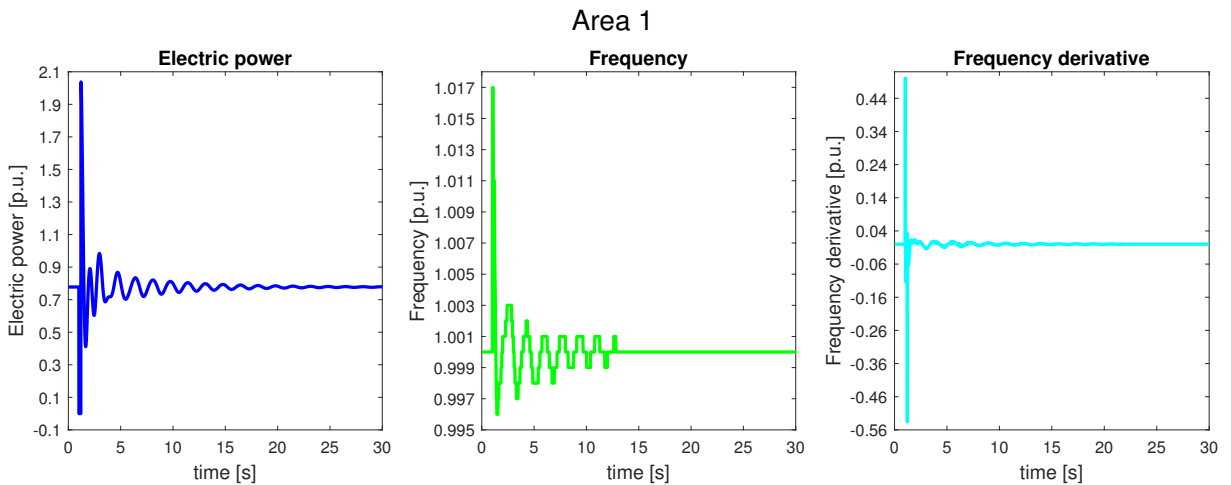


Figure 3.45: Test 6 - Simulation 1 - Area 1 parameters

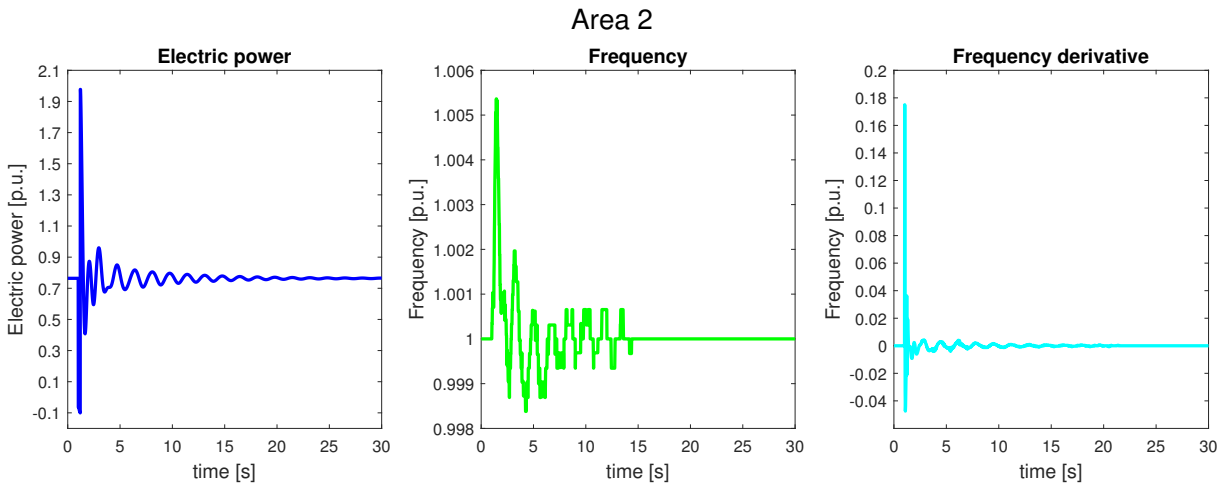


Figure 3.46: Test 6 - Simulation 1 - Area 2 parameters

### RESULTS OF SIMULATION 1

The result of this test, in the estimation of the inertia, are summarized in Figure 3.47.

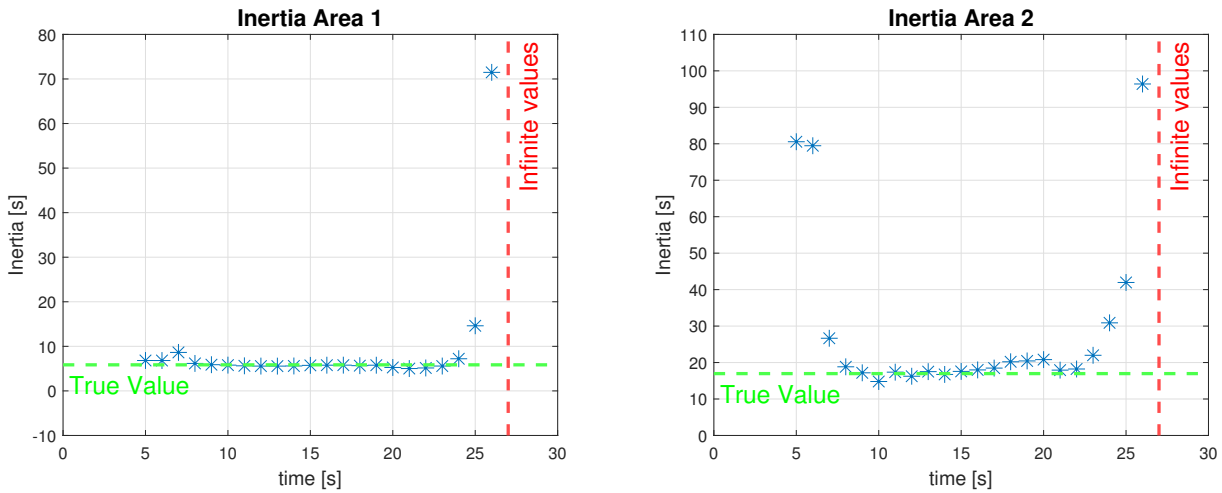


Figure 3.47: Test 6 - Simulation 1 - Inertia trend of Area 1 and Area 2

All the points, after the red line fixed at 27 s, give as result infinite.

The analysis of the inertia trend shows a time interval where it appears to converge to a specific value.

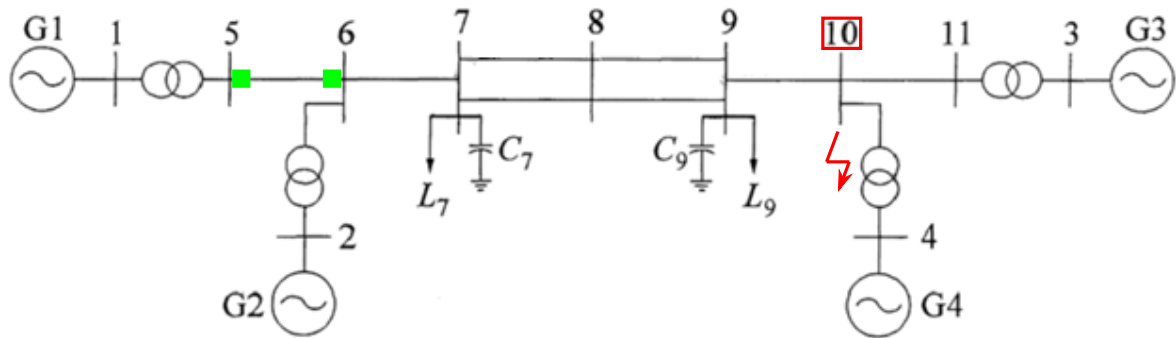
### 3.6.2. Simulation 2

#### DETAILS OF THE SIMULATION 2

**Test system:** described in Section C.1

**Implemented in:** PowerFactory

**Perturbation simulated:** Short-circuit at the bus 10



□: Bus short-circuited    ■: PMUs location

Figure 3.48: Test 6 - Simulation 2 - Test-system

**Simulation time:** 30 s

**Governor:** ON for each generator

**Sampling time:** 20 ms

**PSS:** ON for each generator

**Fault time:** 1 s

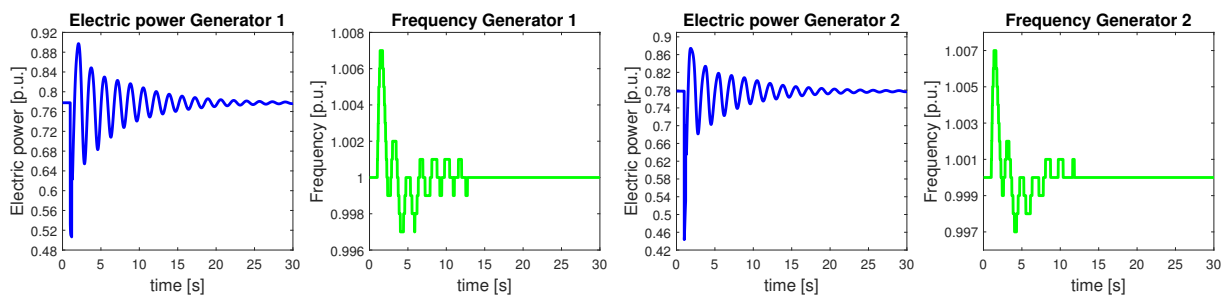
**AVR:** ON for each generator

**Clear time:** 1.2 s

The Test-system is divided in two areas, characterized by its own inertia, separated in the same way done in Figure 3.5 and with the same value of the Table 3.3.

In this simulation we perform the same computation of the previous one considering an event of short-circuit and its subsequent clearing at the bus 10.

Trends for the generators' main parameters during in the simulation, are illustrated in Figure 3.49.



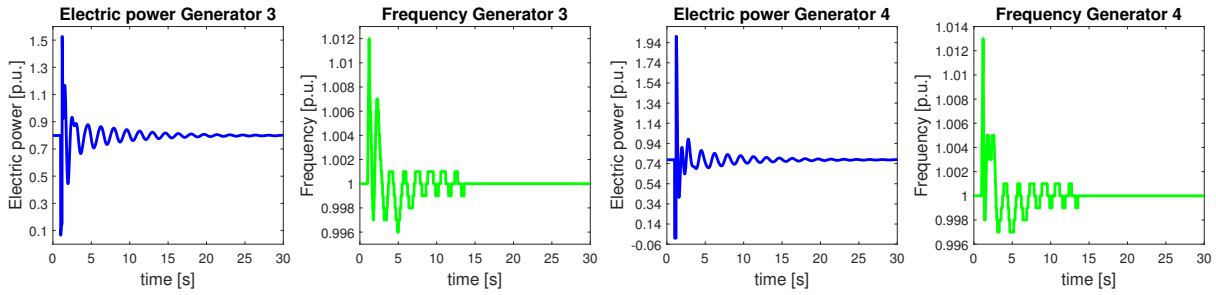


Figure 3.49: Test 6 - Simulation 2 - Main parameters of the system generators during the perturbation

The trends of the variables recorded by the PMUs are shown in Figure 3.50 and Figure 3.51

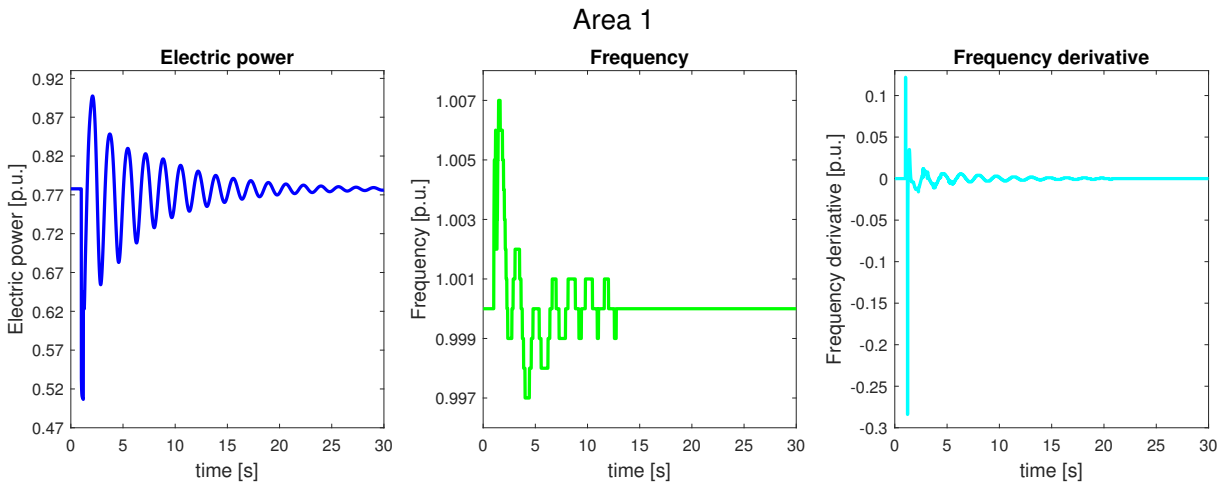


Figure 3.50: Test 6 - Simulation 2 - Area 1 measurements

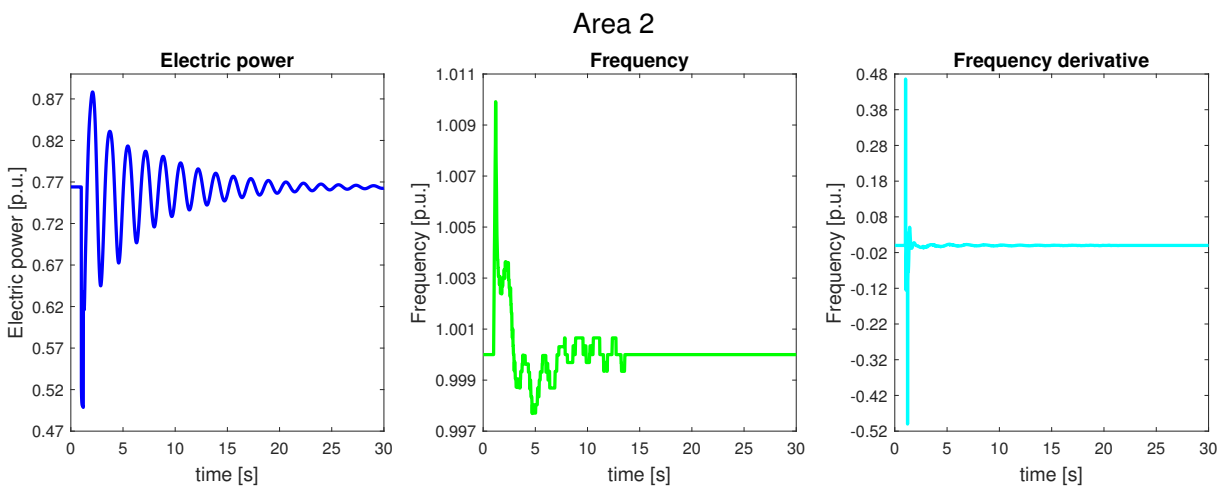


Figure 3.51: Test 6 - Simulation 2 - Area 2 measurements



## RESULTS OF SIMULATION 2

The result of this test, in the estimation of the inertia, are summarized in Figure 3.52. All the points, after the red line, give as result infinite.

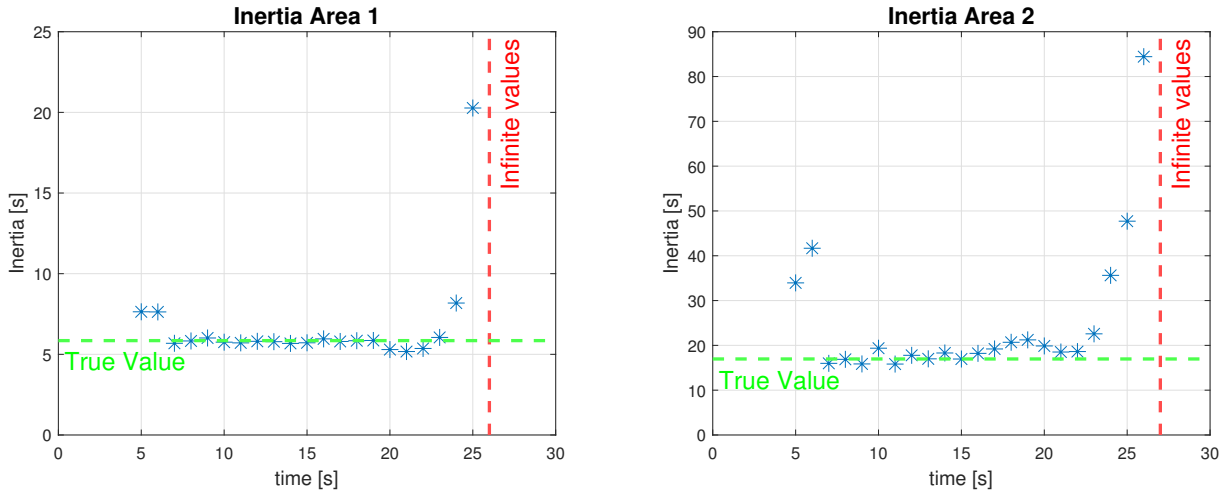


Figure 3.52: Test 6 - Simulation 2 - Inertia trend of Area 1 and Area 2

### 3.6.3. Conclusion of test 6

This test proves that using the Floating window method is possible to identify a convergence point of the inertia after a short-circuit cleared in 200 ms. Moreover, identify the same limits delineated in the previous tests.

### 3.7. Test 7: Increased sensitivity of the PMUs

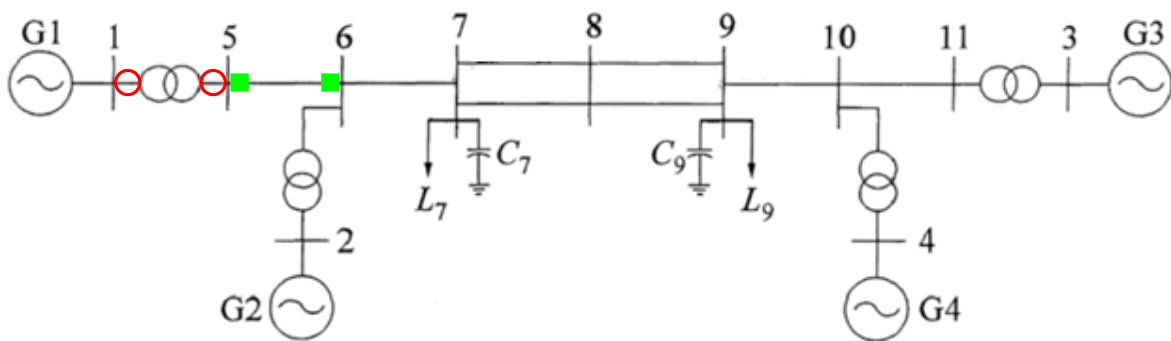
In this test, we perform a single simulation in which the same computation of Test 4 are performed increasing the sensitivity of the PMUs.

#### DETAILS OF THE TEST

**Test system:** described in Section C.1

**Implemented in:** PowerFactory

**Perturbation simulated:** Opening and reclosure of line 1



○: Opening/Reclosure    ■: PMUs location

Figure 3.53: Test 7 - Test-system

**Simulation time:** 60 s

**Governor:** ON for each generator

**Sampling time:** 20 ms

**PSS:** ON for each generator

**Fault time:** 1 s

**AVR:** ON for each generator

**Clear time:** 1.2 s

In this test we investigate about the impact of the PMUs sensitivity in the estimation of the inertia.

All the other test performed in this work are done considering that the PMUs are characterized by a sensitivity of 0.001 Hz and 0.001 MW, since is the condition closer to the reality. Nevertheless, is interesting studying more in deep which is the effect in the estimation increasing the sensitivity of the PMUs.

To do that we perform the same computation made in Section 3.4, assuming a PMUs sensitivity of 0.00001 Hz and 0.00001 MW.

The main parameters trends of the generators during the simulation are reported in Figure 3.54.

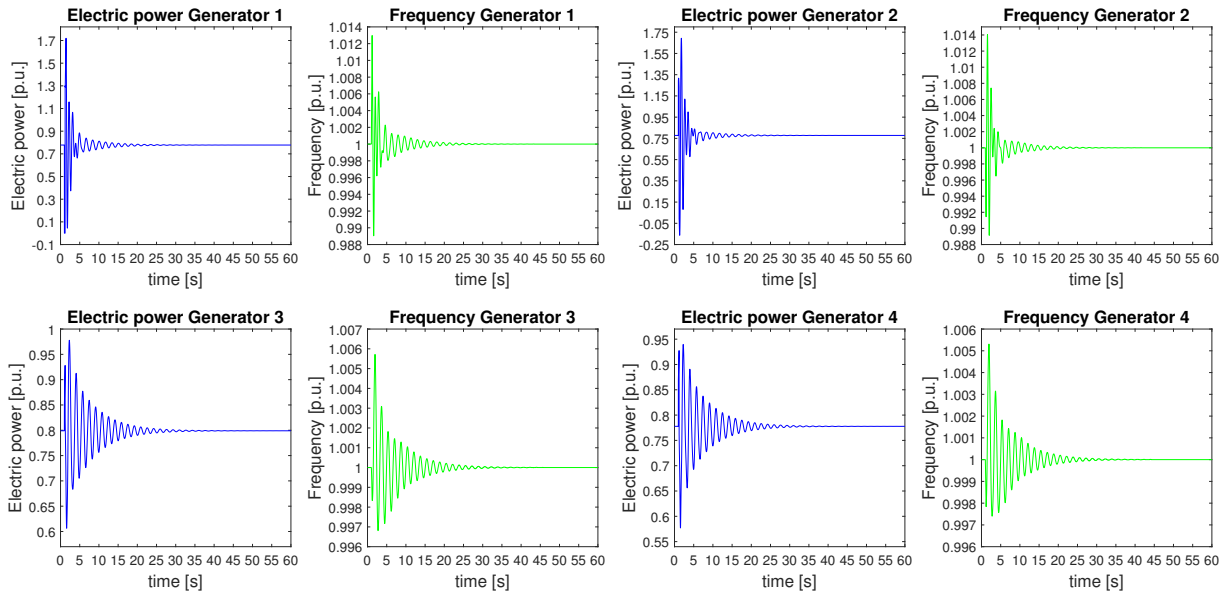


Figure 3.54: Test 7 - Main parameters of the system generators during the perturbation

The trend of the variables recorded by the PMUs and of the derivative of the frequency, used for the inertia estimation, are shown in Figure 3.55 and Figure 3.56

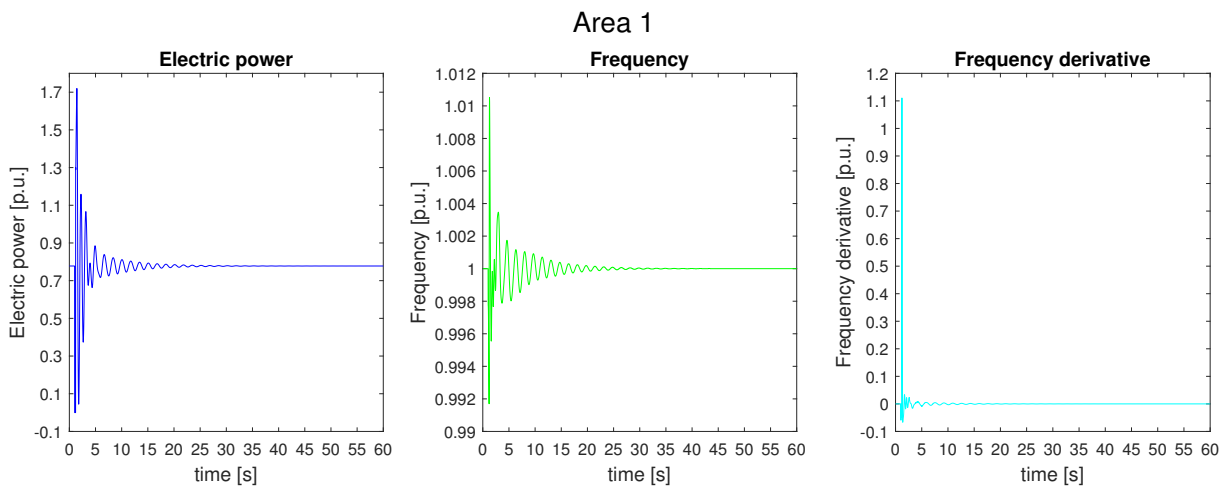


Figure 3.55: Test 7 - Area 1 measurements

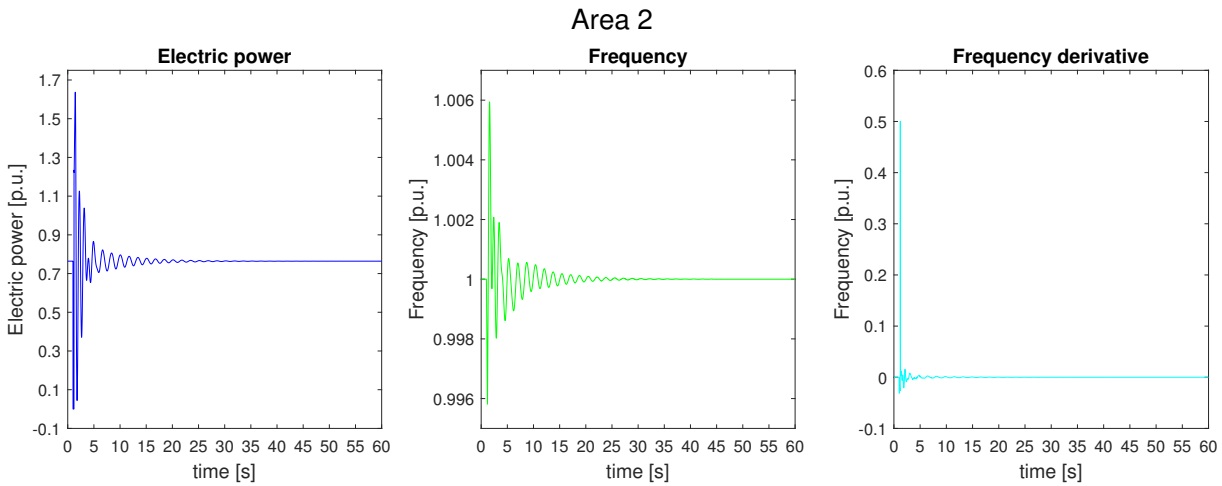


Figure 3.56: Test 7 - Area 2 measurements

Comparing the trend considering a sensitivity of 0.001 Hz and 0.001 MW in Figure 3.6, Figure 3.7 and Figure 3.8 with that ones that use a sensitivity of 0.00001 Hz and 0.00001 MW in Figure 3.54, Figure 3.55 and Figure 3.56 it is possible to identify some significant difference.

The most evident is that using measurements with a greater sensitivity the trends are more continuous, without steps, that instead characterize the trends constructed using measurements with a lower sensitivity. This concept is clearly visible in the frequency trend and in the frequency time derivative trend.

## RESULTS OF THE TEST

The result of this test, in the estimation of the inertia, are summarized in Figure 3.57

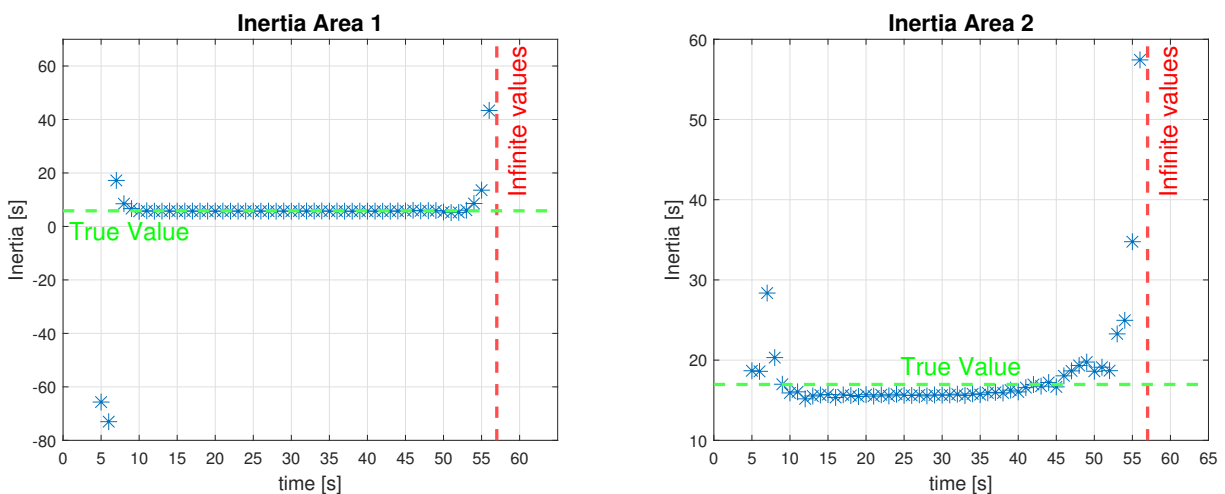


Figure 3.57: Test 7 - Inertia trend of Area 1 and Area 2

Compared to the case that exploits measurements with a sensitivity of 0.001 Hz and 0.001 MW, in this case, the trend of inertia converge for a longer time. For this reason, we need to double the simulation time to find the instant of time at which the trends tend to increase, since at 30 s the trends still converge to the true values.

### **3.7.1. Conclusion of test 7**

In this test, we prove that the sensitivity of the PMU measurements is fundamental for a real-time inertia estimation. In particular, increasing the sensitivity of the PMUs increases the precision of the results at the end of the perturbation when the trend of the variables becomes more and more flat.



# 4 | Conclusions and future developments

In the last years, the equivalent inertia of the system has continued to decrease due to the increasing penetration of RES. Moreover, this phenomenon could be worse if we consider the increase of the HVDC links. Hence, an efficient way to monitor in real-time the equivalent inertia of the system is important to schedule appropriate actions in case of system disturbances.

The possibility of estimating the inertia in real-time allow a more effective reaction by the TSO, so the risk of frequency instability decrease and better operation condition can be guaranteed for the customers. For example, the reduction of the event of load shedding. Currently, there is no definitive method for inertia estimation that has been developed. The results obtained, the challenges identified, and the needs for future studies are highlighted in this chapter, which presents and discusses conclusions about the methods and cases studied.

## 4.1. Conclusion

This thesis proposed a moving windows method exploiting different algorithms to estimate the inertia of the system, with the final goal of increasing system awareness.

The first three tests are preliminary tests in which we identify the algorithm most suitable and the necessary variables for our purpose.

In the first test, we highlight the limit of the SINDy algorithm, using it for the inertia estimation in the moving windows method. The result that was found is that the SINDy algorithm is not suitable for a real-time inertia estimation.

In the following test, we prove that the impact of the measurement of the mechanical power is not so important for a good result in the estimation. For this reason, all the other tests are performed using only the measurements of frequency and electric power.

The last of the preliminary tests allows us to understand the strengths and weaknesses of each algorithm proposed. In this test, we identify that one of the best algorithms, in

terms of precision and computational burden, for the inertia estimation in the moving windows method is the *mldivide*. This algorithm is the one used for all the other tests proposed.

In Test 4, Test 5 and Test 6 we apply the selected method considering different perturbations, in particular, we simulate: the opening of a line, the trig of a load and a short-circuit at a bus. The results obtained in these three test is similar and permit to identify a value of convergence, after the perturbation, very close to the true one. Also, the same limits of this method can be identified in these three tests, which can be briefly summarized in:

- The inertia estimations tend to be infinite when the variables tend to become flat
- The inertia estimations are not precise if the time window considered includes data during the perturbation

Therefore, the conclusion highlighted in these tests is that is possible to identify the inertia of the system immediately after a perturbation, for a brief period, before the estimation tends to infinite.

A possibility to increase the time in which the inertia converges to the true value is to increase the PMUs sensitivity. This concept is faced in the last test which studies more deeply the impact of the PMUs sensitivity in the inertia estimation and proves that the role of the PMUs in the real application of this method is fundamental.

## 4.2. Future development

This thesis studies a possible solution of a small part of the great goal to be able to estimate the inertia of the system in every instant of time. To reach this goal there are many aspects still to study such as:

- **Real measurement:**  
The measurements used for the application of the exposed method are ideal. The real measurement is characterized by measurement errors and noise that can negatively impact the estimation.
- **Increase of the equivalent area considered:**  
The increase of the equivalent area considered could be problematic. Since, as the size of the equivalent area increases, the frequency oscillation after a perturbation decreases. When the oscillation of frequency becomes less than the sensitivity of the PMUs the changes in the system are not detected by the PMUs.
- **Synthetic inertia monitoring:**



The estimating system should consider also the presence of the synthetic inertia

- **Better algorithm for the estimation:**

The study around new data-driven algorithms are several and many of these are not been tested for the inertia estimation. An algorithm more robust and with a less computational burden always improves the real-time estimation performance.

The reaching of all these goals opens a serious possibility to permit the estimation of the inertia of the system during every perturbation of the system.



## Bibliography

- [1] *IEEE* guide for synchronous generator modeling practices and applications in power system stability analyses. *IEEE Std 1110-2002 (Revision of IEEE Std 1110-1991)*, pages 1–80, 2003. doi: 10.1109/IEEESTD.2003.94408.
- [2] M. A. Abdulgalil, M. Khalid, and F. Alismail. Optimizing a distributed wind-storage system under critical uncertainties using benders decomposition. *IEEE Access*, PP: 1–1, 06 2019. doi: 10.1109/ACCESS.2019.2922619.
- [3] S. L. Brunton and J. N. Kutz. *Data Driven Science & Engineering Machine Learning, Dynamical Systems, and Control*. Cambridge University Press, 2019.
- [4] S. L. Brunton, J. L. Proctor, and J. N. Kutz. Discovering governing equations from data by sparse identification of nonlinear dynamical systems. *Proceedings of the National Academy*, 113(15):3932–3937, 2016.
- [5] K. Champion, P. Zheng, A. Y. Aravkin, S. L. Brunton, and J. N. Kutz. A unified sparse optimization framework to learn parsimonious physics-informed models from data. *IEEE Access*, 8:169259–169271, 2020.
- [6] A. D. Femine, D. Gallo, C. Landi, and M. Luiso. The design of a low cost phasor measurement unit. *Energies*, 12:2648, 2019.
- [7] H. Golpîra and A. R. Messina. A center-of-gravity-based approach to estimate slow power and frequency variations. *IEEE Transactions on Power Systems*, 33(1):1026–1035, 2018. doi: 10.1109/TPWRS.2017.2710187.
- [8] N. Hatziargyriou, J. Milanovic, C. Rahmann, V. Ajjarapu, C. Canizares, I. Erlich, D. Hill, I. Hiskens, I. Kamwa, B. Pal, P. Pourbeik, J. Sanchez-Gasca, A. Stankovic, T. Van Cutsem, V. Vittal, and C. Vournas. Definition and classification of power system stability – revisited & extended. *IEEE Transactions on Power Systems*, 36(4):3271–3281, 2021. doi: 10.1109/TPWRS.2020.3041774.
- [9] G. S. M. J. Stiasny and S. Chatzivasileiadis. Physics-informed neural networks for

- non-linear system identification applied to power system dynamics. *IEEE Transactions on Power Systems*, 04 2020. doi: <https://arxiv.org/abs/2004.04026>.
- [10] S. C. Johnson, D. J. Papageorgiou, D. S. Mallapragada, T. A. Deetjen, J. D. Rhodes, and M. E. Webber. Evaluating rotational inertia as a component of grid reliability with high penetrations of variable renewable energy. *Energy*, 180:258–271, 2019. ISSN 0360-5442. doi: <https://doi.org/10.1016/j.energy.2019.04.216>. URL <https://www.sciencedirect.com/science/article/pii/S0360544219308564>.
- [11] P. Kundur. *Power System Stability and Control*. McGraw-Hill, 1994.
- [12] S. Lakshminarayana, S. Sthapit, and C. Maple. A comparison of data-driven techniques for power grid parameter estimation, 2021.
- [13] P. Sauer and M. Pai. *Power System Dynamics and Stability*. Prentice Hall, 1998. ISBN 9780136788300. URL <https://books.google.it/books?id=d00eAQAAIAAJ>.
- [14] Y. Susuki, R. Hamasaki, and A. Ishigame. Estimation of power system inertia using nonlinear koopman modes. In *2018 IEEE Power & Energy Society General Meeting (PESGM)*, pages 1–5, 2018. doi: 10.1109/PESGM.2018.8586007.
- [15] E. Taibi, T. Nikolakakis, L. Gutierrez, C. Fernandez, J. Kiviluoma, T. J. Lindroos, and S. Rissanen. Power system flexibility for the energy transition, part 1: Overview for policy makers. Technical report, International Renewable Energy Agency, Abu Dhabi, 2018.
- [16] *International Renewable Energy Agency*. Renewables - energy system - iea, 2023. URL <https://www.iea.org/energy-system/renewables>.
- [17] *International Renewable Energy Agency*. Share of cumulative power capacity by technology, 2010-2027, 2023. URL <https://www.iea.org/data-and-statistics/charts/share-of-cumulative-power-capacity-by-technology-2010-2027>.
- [18] *Smart Grid Investment Grant Program*. Factor affecting pmu installation costs. Technical report, U.S. Department of Energy’s Office of Electricity Delivery and Energy Reliability, Washington, 2014.
- [19] R. Tibshirani. Regression shrinkage and selection via the lasso. *Journal of the Royal Statistical Society. Series B (Methodological)*, 58(1):267–288, 1996. ISSN 00359246. URL <http://www.jstor.org/stable/2346178>.
- [20] P. Tielens and D. Van Hertem. The relevance of inertia in power systems. *Renewable and Sustainable Energy Reviews*, 55:999–1009, 2016. ISSN 1364-0321. doi:

- <https://doi.org/10.1016/j.rser.2015.11.016>. URL <https://www.sciencedirect.com/science/article/pii/S136403211501268X>.
- [21] S. Tiwari, R. Naresh, and R. Jha. Comparative study of backpropagation algorithms in neural network based identification of power system. *International Journal of Computer Science and Information Technology*, 5:93–107, 08 2013. doi: 10.5121/ijcsit.2013.5407.
- [22] L. Vanfretti, M. Baudette, and A. D. White. *Renewable Energy Integration*. Elsevier, 2017.
- [23] A. Whiteman, D. Akande, N. Elhassan, G. Escamilla, and I. Ahmed. Renewable energy statistics 2023. Technical report, International Renewable Energy Agency, Abu Dhabi, 2023.
- [24] A. C. Yew. Numerical differentiation: finite differences, 2011. URL <https://www.dam.brown.edu/people/alcyew/handouts/numdiff.pdf>.
- [25] L. G. Zhang S. Robust data-driven discovery of governing physical laws with error bars. *Proc. R. Soc. A.*, 474, 09 2018. doi: <https://doi.org/10.1098/rspa.2018.0305>.
- [26] J. Zhao, A. Gomez-Exposito, M. Netto, L. Mili, A. Abur, V. Terzija, I. Kamwa, B. Pal, A. K. Singh, J. Qi, Z. Huang, and A. Meliopoulos. Power system dynamic state estimation: Motivations, definitions, methodologies and future work. *IEEE Transactions on Power Systems*, 34:3188–3198, 07 2019. doi: 10.1109/TPWRS.2019.2894769.
- [27] P. Zheng, T. Askham, S. L. Brunton, J. N. Kutz, and A. Y. Aravkin. A unified framework for sparse relaxed regularized regression: Sr3. *IEEE Access*, 7:1404–1423, 2019. doi: 10.1109/ACCESS.2018.2886528.



# A | Appendix A

## A.1. Numerical differentiation: finite differences

The derivative of a function  $f$  at the point  $x$  is defined as the limit of a difference quotient [24]:

$$f'(x) = \lim_{h \rightarrow 0} \frac{f(x+h) - f(x)}{h}$$

The approximation of the derivative  $f'(x)$  gets better as  $h$  gets smaller. The previous assumption can be proved considering the Taylor's theorem with remainder that gives the Taylor series expansion

$$f(x+h) = f(x) + hf'(x) + h^2 \frac{f''(\xi)}{2!}$$

where  $\xi$  is some number between  $x$  and  $x+h$ .

Rearranging gives

$$\frac{f(x+h) - f(x)}{h} - f'(x) = \frac{f''(\xi)}{2!}$$

which tell us that the error is proportional to  $h$ .

If  $h > 0$ , say  $h = \Delta x$  where  $\Delta x$  is a finite positive number, then

$$\frac{f(x + \Delta x) - f(x)}{\Delta x}$$

is called the first-order or  $O(\Delta x)$  *forward difference* approximation of  $f'(x)$ .

If  $h < 0$ , say  $h = -\Delta x$  where  $\Delta x > 0$ , then

$$\frac{f(x+h) - f(x)}{h} = \frac{f(x) - f(x + \Delta x)}{\Delta x}$$

is called the first-order or  $O(\Delta x)$  *backward difference* approximation of  $f'(x)$ .

By combining different Taylor series expansions, we can obtain approximations of  $f'(x)$  of various orders.

For instance, subtracting the two expansions

$$\begin{aligned} f(x + \Delta x) &= f(x) + \Delta x f'(x) + \Delta x^2 \frac{f''(x)}{2!} + \Delta x^3 \frac{f'''(\xi_1)}{3!}, & \xi_1 \in (x, x + \Delta x) \\ f(x - \Delta x) &= f(x) - \Delta x f'(x) + \Delta x^2 \frac{f''(x)}{2!} - \Delta x^3 \frac{f'''(\xi_2)}{3!}, & \xi_2 \in (x - \Delta x, x) \end{aligned}$$

gives

$$f(x + \Delta x) - f(x - \Delta x) = 2\Delta x f'(x) + \Delta x^3 \frac{(f'''(\xi_1) + f'''(\xi_2))}{6}$$

$$\frac{f(x + \Delta x) - f(x - \Delta x)}{2\Delta x} - f'(x) = \Delta x^2 \frac{(f'''(\xi_1) + f'''(\xi_2))}{12}$$

Hence  $\frac{f(x+\Delta x)-f(x-\Delta x)}{2\Delta x}$  is an approximation of  $f'(x)$  whose error is proportional to  $\Delta x^2$ .

It is called the second-order or  $O(\Delta x^2)$  *centered difference* approximation of  $f'(x)$ .

If we use expansions with more terms, higher-order approximations can be derived. An example is the fourth-order “finite difference” formula for approximating first derivatives that can be expressed as

$$f'(x) \approx \frac{-f(x + 2\Delta x) + 8f(x + \Delta x) - 8f(x - \Delta x) + f(x - 2\Delta x)}{12\Delta x}$$



# B | Appendix B

## B.1. STLS code

The MATLAB code of the STLS algorithm is:

```
function Xi = sparsifyDynamics(Theta,dXdt,lambda,n)
% Copyright 2015, All Rights Reserved
% Code by Steven L. Brunton
% For Paper, "Discovering Governing Equations from Data:
% Sparse Identification of Nonlinear Dynamical Systems"
% by S. L. Brunton, J. L. Proctor, and J. N. Kutz

% compute Sparse regression: sequential least squares
Xi = Theta\dXdt; % initial guess: Least-squares

% lambda is our sparsification knob.
for k=1:10
    smallinds = (abs(Xi)<lambda); % find small coefficients
    Xi(smallinds)=0; % and threshold
    for ind = 1:n % n is state dimension
        biginds = ~smallinds(:,ind);
        % Regress dynamics onto remaining terms to find
        % sparse Xi
        Xi(biginds,ind) = Theta(:,biginds)\dXdt(:,ind);
    end
end
end
```

## B.2. Parsimonious modelling

The parsimonious modelling, essentially, means getting the minimal model that describes the data, without considering trivial solution. The entire SINDy procedure is a generalized

linear regression, in which we follow these principal steps:

- We collect the measurements data represented by the matrix  $\mathbf{V}$
- We compute the measurements derivatives defined in the matrix  $\dot{\mathbf{V}}$
- We build a library of candidate terms  $\Theta(\mathbf{V})$
- We solve the equation for some unknown variables  $\Xi$

Regarding the column of the matrix  $\Xi$ , we want those to be as sparse as possible and still fit the data. The remaining terms in the columns of the matrix  $\Xi$  are the active term in that differential equation.

Applying the least square regression to compute the terms of the matrix  $\Xi$ , it is obtained that all the terms of the matrix result different from zero.

In this way you obtain a good fit for the system of differential equation  $\dot{\mathbf{V}} = \Theta(\mathbf{V})\Xi$ , but it is reasonable to think that the training data are overfitted, as it is unlikely that the true model will be described by a very large number of candidate terms.

Therefore, we want a sparsity penalized regression that still does a good fit, but permit to obtain the columns of the matrix  $\Xi$  sparse as much as possible. There are a lot of algorithms you could use to solve the sparse regression problem, in SINDy algorithm is used the Sequential Threshold Least Squares algorithm, exposed more in depth in Section 2.1.2.

This regression procedure can be described by the Equation 2.10, in which we're constantly balancing the *model error*  $\arg \min_{\xi'_k} \|\dot{\mathbf{V}}_k - \Theta(\mathbf{V})\xi'_k\|_2$  with the terms  $\lambda \|\xi'_k\|_1$ , that defines the sparsity of the model measured determining how many terms are nonzero.

The sparsity of the model is controlled by the sparsification knob  $\lambda$ , in particular:

- **Increasing  $\lambda$** : increase the sparsity, so the complexity of the differential equation decrease, but the model error increase. In this case the model is **underfit**.
- **Decreasing  $\lambda$** : decrease the sparsity, so the complexity of the differential equation increase, but the model error decrease. In this case the model is overfit and the obtained solution are the same of the **least square regression**.

It is possible to state that the complexity of the model is inversely proportional to  $\lambda$ . Changing the sparsification knob we translate the threshold of our terms, finding a family of models from the underfit to the overfit model. A graphical interpretation of these concepts are show in Figure B.2.

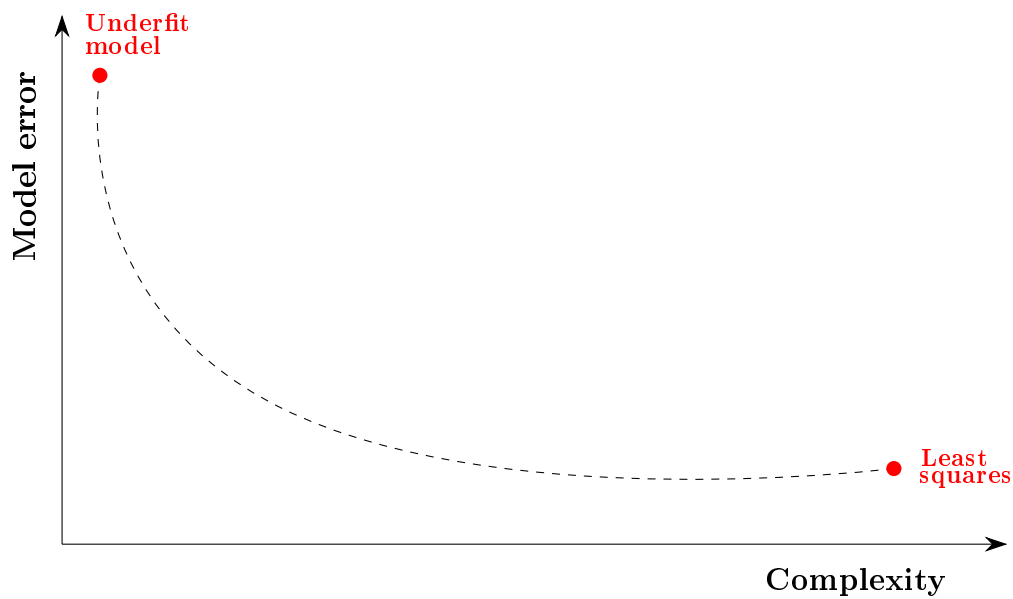


Figure B.1: Graphical interpretation of the parsimonious modelling

Increasing the complexity of the system is possible that the least square regression works well with a the training data, but it is not going to perform nearly as well on the validation data, because you're overfitting to the training data. For these reason in Figure B.2 we can identify a kind of elbow that is a Pareto optimal area in which we avoid the overfitting problem and we identify a model with a good compromise between complexity and precision.

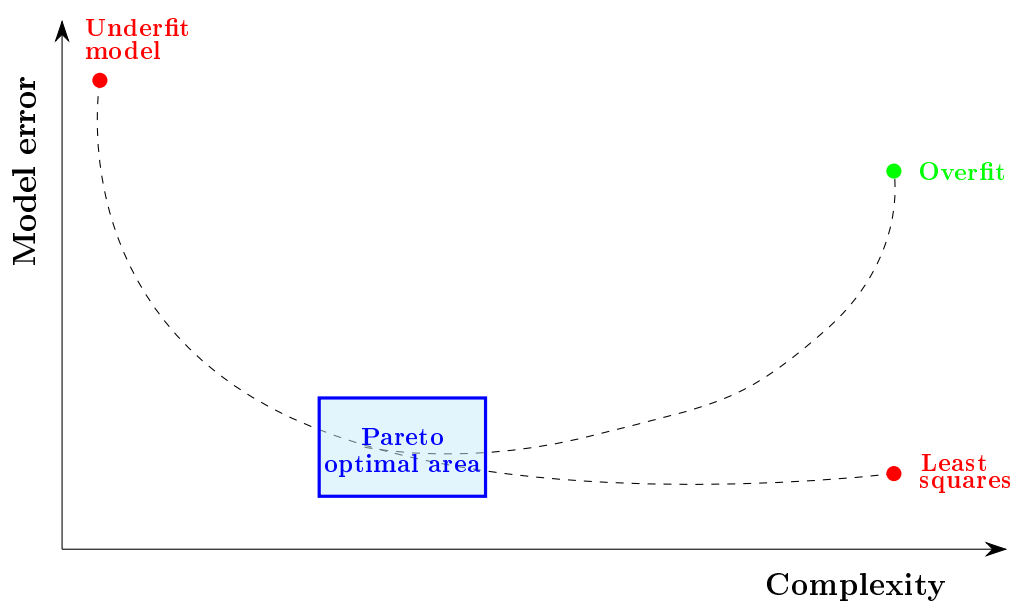


Figure B.2: Parsimonious modelling with overfitting problem



# C | Appendix C

## C.1. Test-system

Electrical scheme:

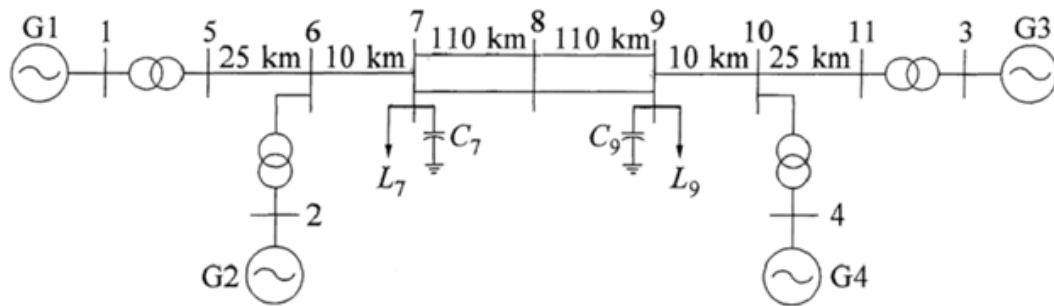


Figure C.1: Test-system [11].

Machine parameters						
Gen.	H [s]	S [MVA]	$N_g$ (*)			
$G_1$	5.850	900	1			
$G_2$	5.850	900	1			
$G_3$	5.558	900	1			
$G_4$	5.557	900	1			
Load parameters						
Bus	V [kV]	$P_L$ [p.u.]	$Q_L$ [p.u.]			
7	230	100	9.67			
9	230	100	17.67			
Transformer parameters						
Line	V [kV]	S [MVA]	$r$ [p.u. $\Omega$ /km]	$x$ [p.u.H/km]	From	To
1	20/230	900	0	0.017	1	5
2	20/230	900	0	0.017	2	6
3	20/230	900	0	0.017	3	11

4	20/230	900	0	0.017	4	10	
Line parameters							
Line	V [kV]	I [kA]	r [p.u. $\Omega$ /km]	x [p.u.H/km]	b [p.u.F/km]	From	To
5	230	0.435	0.003	0.025	0.044	5	6
6	230	0.435	0.001	0.01	0.018	6	7
7	230	0.435	0.003	0.025	0.044	11	10
8	230	0.435	0.001	0.01	0.018	10	9
9	230	0.435	0.011	0.11	0.193	9	8
10	230	0.435	0.011	0.11	0.193	9	8
11	230	0.435	0.011	0.11	0.193	7	8
12	230	0.435	0.011	0.11	0.193	7	8

Table C.1: Test-system parameters.

## List of Figures

1	World total capacity. . . . .	1
2	World total production. . . . .	2
3	Share of cumulative power capacity by technology, 2010-2027 [17]. . . . .	3
4	Technical options to increase system flexibility [15]. . . . .	4
1.1	Schematic of centralized and distributed systems [2]. . . . .	8
1.2	Classification of power system stability [8]. . . . .	10
2.1	Example parameters . . . . .	28
2.2	Example of the floating window method . . . . .	29
2.3	Example of inertia estimation . . . . .	29
3.1	Test 1 - Simulation 1 - Test-system . . . . .	32
3.2	Test 1 - Simulation 1 - Main parameters of the system generators during the perturbation . . . . .	34
3.3	Test 1 - Simulation 1 - Frequency derivative trend . . . . .	34
3.4	Test 1 - Simulation 2 - Test-system . . . . .	35
3.5	Test 1 - Simulation 2 - Areas of Test-system . . . . .	36
3.6	Test 1 - Simulation 2 - Main parameters of the system generators during the perturbation . . . . .	37
3.7	Test 1 - Simulation 2 - Area 1 measurements . . . . .	37
3.8	Test 1 - Simulation 2 - Area 2 measurements . . . . .	38
3.9	Test 1 - Simulation 2 - Inertia trend of Area 1 and Area 2 . . . . .	38
3.10	Test 2 - Simulation 1 - Test-system . . . . .	40
3.11	Test 2 - Simulation 1 - Area 1 measurements . . . . .	41
3.12	Test 2 - Simulation 1 - Area 2 measurements . . . . .	41
3.13	Test 2 - Simulation 1 - Inertia trend of Area 1 and Area 2 . . . . .	42
3.14	Test 2 - Simulation 2 - Test-system . . . . .	43
3.15	Test 2 - Simulation 2 - Main parameters of the system generators during the perturbation . . . . .	44
3.16	Test 2 - Simulation 2 - Area 1 measurements . . . . .	44

3.17	Test 2 - Simulation 2 - Area 2 measurements . . . . .	44
3.18	Test 2 - Simulation 2 - Inertia trend of Area 1 and Area 2 . . . . .	45
3.19	Test 3 - Simulation 1 - Test-system . . . . .	46
3.20	Test 3 - Simulation 2 - Test-system . . . . .	48
3.21	Test 3 - Simulation 2 - Inertia trend of Area 1 and Area 2 using different algorithm . . . . .	50
3.22	Test 4 - Simulation 1 - Test-system . . . . .	52
3.23	Test 4 - Simulation 1 - Inertia trend of Area 1 and Area 2 . . . . .	53
3.24	Test 4 - Simulation 1 - Increasing value of inertia of Area 1 and Area 2 . . . . .	54
3.25	Test 4 - Simulation 1 - Variable trend Point 1 and Point 2 . . . . .	55
3.26	Test 4 - Simulation 1 - Variable's trend Point 3,4 and 5 . . . . .	56
3.27	Test 4 - Simulation 1 - Variable's trend Point 10 . . . . .	56
3.28	Test 4 - Simulation 2 - Test-system . . . . .	57
3.29	Test 4 - Simulation 2 - Main parameters of the system generators during the perturbation . . . . .	58
3.30	Test 4 - Simulation 2 - Area 1 measurements . . . . .	58
3.31	Test 4 - Simulation 2 - Area 2 measurements . . . . .	58
3.32	Test 4 - Simulation 2 - Inertia trend of Area 1 and Area 2 . . . . .	59
3.33	Test 5 - Simulation 1 - Test-system . . . . .	60
3.34	Test 5 - Simulation 1 - Main parameters of the system generators during the perturbation . . . . .	61
3.35	Test 5 - Simulation 1 - Area 1 parameters . . . . .	61
3.36	Test 5 - Simulation 1 - Area 2 parameters . . . . .	62
3.37	Test 5 - Simulation 1 - Inertia trend of Area 1 and Area 2 . . . . .	62
3.38	Test 5 - Simulation 2 - Test-system . . . . .	63
3.39	Test 5 - Simulation 2 - Main parameters of the system generators during the perturbation . . . . .	64
3.40	Test 5 - Simulation 2 - Area 1 measurements . . . . .	64
3.41	Test 5 - Simulation 2 - Area 2 measurements . . . . .	64
3.42	Test 5 - Simulation 2 - Inertia trend of Area 1 and Area 2 . . . . .	65
3.43	Test 6 - Simulation 1 - Test-system . . . . .	66
3.44	Test 6 - Simulation 1 - Main parameters of the system generators during the perturbation . . . . .	67
3.45	Test 6 - Simulation 1 - Area 1 parameters . . . . .	67
3.46	Test 6 - Simulation 1 - Area 2 parameters . . . . .	68
3.47	Test 6 - Simulation 1 - Inertia trend of Area 1 and Area 2 . . . . .	68
3.48	Test 6 - Simulation 2 - Test-system . . . . .	69



3.49	Test 6 - Simulation 2 - Main parameters of the system generators during the perturbation . . . . .	70
3.50	Test 6 - Simulation 2 - Area 1 measurements . . . . .	70
3.51	Test 6 - Simulation 2 - Area 2 measurements . . . . .	70
3.52	Test 6 - Simulation 2 - Inertia trend of Area 1 and Area 2 . . . . .	71
3.53	Test 7 - Test-system . . . . .	72
3.54	Test 7 - Main parameters of the system generators during the perturbation	73
3.55	Test 7 - Area 1 measurements . . . . .	73
3.56	Test 7 - Area 2 measurements . . . . .	74
3.57	Test 7 - Inertia trend of Area 1 and Area 2 . . . . .	74
B.1	Graphical interpretation of the parsimonious modelling . . . . .	89
B.2	Parsimonious modelling with overfitting problem . . . . .	89
C.1	Test-system [11]. . . . .	91



## List of Tables

3.1	Test 1 - Simulation 1 - True values of inertia . . . . .	33
3.2	Test 1 - Simulation 1 - Estimated values of inertia . . . . .	35
3.3	Test 1 - Simulation 2 - Areas true values of inertia . . . . .	36
3.4	Test 3 - Simulation 1 - True values of inertia . . . . .	47
3.5	Test 3 - Simulation 1 - Estimation of inertia . . . . .	47
3.6	Test 3 - Simulation 1 - Computation times of the considered algorithm . .	48
3.7	Test 4 - Simulation 1 - Last increasing values of inertia of Area 1 and Area 2	54
3.8	Test 4 - Simulation 1 - First increasing value of inertia of Area 1 and Area 2	54
C.1	Test-system parameters. . . . .	92





## List of Symbols

Variable	Description	SI unit
$J$	Combined moment of inertia of the generator and turbine	$kg \cdot m^2$
$\omega_m$	Angular speed of the rotor	$\frac{mech.rad}{s}$
$T_a$	Accelerating torque	$N \cdot m$
$T_m$	Mechanical torque	$N \cdot m$
$T_e$	Electromagnetic torque	$N \cdot m$
$t$	Times	s
$\theta_m$	Angular position of the rotor at time $t$	mech. rad
$\omega_{sm}$	Synchronous speed of the rotor	$\frac{mech.rad}{s}$
$\delta_m$	Angular position of the rotor at time $t = 0$	mech. rad
$P_m$	Mechanical power	W
$P_e$	Electromagnetic power	W
$M$	Angular momentum	$kg \cdot m^2 \cdot \frac{rad}{s}$
$H$	Inertia constant	$\frac{Ws}{VA}$
$A_{nom}$	Nominal power of the synchronous machine	VA
$D$	Damping term	
$\omega_{COI}$	COI angular speed	rad/s
$H_{COI}$	COI equivalent inertia	s
$\mathbf{f}$	Nonlinear function	
$\mathbf{v}$	System's state vector	
$\mathbf{V}$	System's state matrix	
$\dot{\mathbf{V}}$	Time derivative of matrix $\mathbf{V}$	
$\boldsymbol{\theta}$	Vector of possible non linear functions	
$\Theta$	Matrix of the values of the vector $\boldsymbol{\theta}$ in each one of the $m$ instants of time	
$\Xi$	Matrix of the active terms	
$\xi$	Elements of the matrix $\Xi$	
$\lambda$	Sparsification knob	
$\mathbf{X}$	Matrix of the electromagnetic power over the time $t$ in each machine	MW

Variable	Description	SI unit
$\mathbf{Y}$	Matrix of the angular velocity of the rotor over the time $t$ in each machine	$rad/s$
$\mathbf{Z}$	Matrix of the mechanical power over the time $t$ in each machine	$MW$
$\dot{\mathbf{Y}}$	Time derivative of the matrix $\mathbf{Y}$	$\frac{rad}{s^2}$
$\dot{\mathbf{Y}}_{est}$	Estimated matrix of the time derivative of the matrix $\mathbf{Y}$	$\frac{rad}{s^2}$





## Acknowledgements

I would like to reserve this final space of my thesis for thanks to all those who have contributed, with their support, to the realization of the same. Without their help my work would not have been so complete and my path would certainly have been more difficult. A heartfelt thanks goes to my advisor Prof. Alberto Berizzi, for his valuable advice and for his availability. Thank you for giving me fundamental ideas in the writing of this work and for addressing me in moments of indecision.

I would also like to thank Andrea Vicario and Edoardo Daccò for their valuable help in the most difficult moments during the study of the different tests.

Finally, I thank my family and all the loved ones who have been close to me throughout my university career, making the heaviest moments lighter and encouraging me to give more and more.

Vorrei riservare questo spazio finale della mia tesi di laurea ai ringraziamenti verso tutti coloro che hanno contribuito, con il loro supporto, alla realizzazione della stessa. Senza il loro aiuto il mio lavoro non sarebbe stato così completo e il mio percorso sarebbe stato sicuramente più difficile.

Un sentito ringraziamento va al mio relatore prof. Alberto Berizzi, per i suoi preziosi consigli e per la sua disponibilità. Grazie per avermi fornito spunti fondamentali nella stesura di questo lavoro e per avermi indirizzato nei momenti di indecisione.

Vorrei inoltre ringraziare Andrea Vicario ed Edoardo Daccò per il loro prezioso aiuto nei momenti più difficili nello studio dei diversi casi.

Infine, ringrazio la mia famiglia e tutte le persone care che mi sono state vicino per tutta la mia carriera universitaria, rendendo più leggeri i momenti più pesanti e spronandomi a dare sempre di più.

